IN VIVO MAGNETIC RESONANCE SPECTROSCOPY OF MUSCULOSKELETAL DISORDERS

By JAMES RAY BALLINGER

A DISSERTATION PRESENTED TO THE GRADUATE SCHOOL
OF THE UNIVERSITY OF FLORIDA IN PARTIAL FULFILLMENT
OF THE REQUIREMENTS FOR THE DEGREE OF
DOCTOR OF PHILOSOPHY

UNIVERSITY OF FLORIDA

1994

ACKNOWLEDGEMENTS

I would like to express most sincere thanks for the following people who made this educational experience possible for me:

Katherine Scott, Ph.D., Chairperson of my committee, for her inspiration, skilled guidance, patience, and wisdom; Raymond Andrew, Ph.D., for his thoughtful comments on my publications and thesis; Jeffrey Fitzsimmons, Ph.D., for discussions about coils, NMR in general, and his insight into people; Richard Briggs, Ph.D., for discussions about pulse sequence techniques and pH measurements; Thomas Mareci, Ph.D., for discussions about lactate editing and localization techniques; and Haejin Kang, Ph.D., for teaching me how to use the animal spectrometer, implementing phosphorus spectroscopy of implanted tumors in mice, acquiring data, and constructing two of the phosphorus coils used in my studies. He has been an "adopted brother" to me and I will always remember my time with him.

I would also like to thank Byron Croker, M.D., for help with culturing tumor cells, planning mouse studies, and reviewing results of the tumor culture and mouse experiments; William Brey, Randy Duensing, Andrew Mitchell, fellow graduate students, who have shared time and thoughts with me; Carol Sweeney, for the cell culture work, mouse husbandry, collection and fitting of mouse data, and being a friend; Jim Scott, for construction of the in-magnet ergometer and phantoms, helping to collect exercise data,

volunteering to spend time in the magnet, and discussions ranging from RF coils to Shiitake mushrooms; Barbara Beck, for instruction on coil construction; Teresa Lyles, M.S., for her secretarial and statistical expertise, and her moral support; Christine Stopka, Ph.D., for her wonderful personality and encouragement to study claudication patients with magnetic resonance spectroscopy; Lori K. Marburger, M.S., who trained the peripheral vascular disease patients, performed the exercise tests and analyzed the data from the initial batch of patients; William Breshue, Ph.D., for referral of congestive heart failure and heart transplant patients and for stimulating discussions about phosphorus metabolism and exercise physiology; Alka Velenik, Ph.D., for setting up the transfer of exercise data from the Seimens scanner to a workstation for analysis; Michael Welsh, for coordinating spectroscopy sessions for the congestive heart failure patients and help in analyzing data; Michael Ingenio, M.D., for helping to acquire data on more recent claudication patients; Aubrey Sobczak, for help in fitting spectra and entering data; and Susan Kohler, Ph.D., for her helpful suggestions on implementing magnetic resonance spectroscopy on out patients and for writing a macro for manipulation of chemical shift imaging data.

Finally, I would like to thank Suzanne Spanier, M.D., for helpful discussions and providing pathological correlation for the musculoskeletal tumor cases; Juan Vasquez, for helping to work out "bugs" in the hardware of the whole body scanner; Drs. Mark Scarborough and Tom Nelson for referral of musculoskeletal tumor patients; Nancy Dixon, RN, for helping to coordinate the spectroscopy sessions with the tumor patients' chemotherapy

hospitalizations; Drs. Rudy Gurtner and James Seeger for referral of our peripheral vascular disease patients; Vincent Groupé, Ph.D., for encouraging me to return to Graduate School for my Ph.D., and for teaching me to ascribe any success I may have to God, and not to my own questionable superiority; Joanne Ballinger, PharmD, my wife, who has been patient with my odd hours through graduate school; and last but not least, Christopher and Jennifer, my son and daughter, for helping me to keep my sense of humor, to live one day at a time, and to enjoy my second childhood.

TABLE OF CONTENTS

LIST OF TABLES

LIST OF FIGURES

KEY TO SYMBOLS AND ABBREVIATIONS

ADP	Adenosine Diphosphate
ATP	Adenosine Triphosphate
CHESS	CHEmical Shift Selective
CHF	Congestive Heart Failure
Cho	Choline
CI	Confidence Interval
CIS	Cisplatin (cis-diamminedichloroplatinum)
Cr	Creatine/Creatinine
CT	Computed Tomography
DANTE	Delays Alternating with Nutations for Tailored Excitation
FID	Free Induction Decay
FOV	Field of View
Glu	Glutamate/Glutamine
HCCTP	hexachlorocyclotriphosphazene
IC	Intermittent Claudication
ISIS	Image-Selected In vivo Spectroscopy
Lac	Lactate
MR	Magnetic Resonance
MRI	Magnetic Resonance Imaging
MRS	Magnetic Resonance Spectroscopy
NMR	Nuclear Magnetic Resonance
PCr	Phosphocreatine
Pi	Inorganic phosphate
PME	Phosphomonoesters

PDE	Phosphodiesters
ppm	parts per million
PRESS	Point RESolved Spectroscopy
PVD	Peripheral Vascular Disease
ROC	Receiver Operating Characteristics
RF	Radio Frequency
SE	Spin Echo
S/N	Signal-to-Noise
SPARS	SPAtially Resolved Spectroscopy
STEAM	STimulated Echo Acquisition Mode
T	Tesla
TE	Echo Time
TM	Mixing Time
TR	Repetition Time
VOI	Volume of Interest

Abstract of Dissertation Presented to the Graduate School
of the University of Florida in Partial Fulfillment of the
Requirements for the Degree of Doctor of Philosophy

IN VIVO MAGNETIC RESONANCE SPECTROSCOPY OF MUSCULOSKELETAL DISORDERS

By

James Ray Ballinger

August, 1994

Chairman: Katherine N. Scott
Major Department: Nuclear Engineering Sciences

P-31 MRS is used to do the following: detect chemotherapy-resistant human osteosarcomas implanted into a nude mouse model; determine anesthetic and temperature effects on spectra in the nude mouse model; monitor the metabolic changes in skeletal muscle that occur in peripheral vascular disease (PVD) patients with claudication; and compare metabolic changes in skeletal muscle of PVD and congestive heart failure (CHF) patients with age-matched normal volunteers. Development of P-31 MRS in the therapy monitoring of patients with musculoskeletal tumors is also presented. Water suppressed, proton magnetic resonance spectroscopy is developed for use in diagnosis and monitoring of the therapy response of musculoskeletal neoplasms including osteosarcoma.

Significant changes in the phosphocreatine to inorganic phosphate ratio are found in treated and sensitive osteosarcomas in mice before change in the size of the tumors. This ratio does

not change significantly in either untreated or resistant tumors. Minimal direct anesthetic effects are seen on P-31 metabolites and pH in implanted osteosarcoma in mice. A profound effect of anesthesia is seen on the thermoregulatory ability of the mice. The changes in pH with change in temperature match those described in other animal models and humans.

Proton spectroscopy is successfully implemented in eleven musculoskeletal patients and statistically significant differences in the choline to creatine (Cho/Cr) ratio between malignant tumors and necrosis, edema, benign tumors, and normal muscle are found. Four of the patients with malignant tumors have follow-up studies. Follow up studies show a statistically significant drop in Cho/Cr ratio with treatment. In one patient, a change is seen within three days of the start of chemotherapy.

Significant increase in the post-exercise rate of recovery of the phosphorylated sugar peaks and pH is seen using P-31 MRS following low-intensity training of PVD patients. Significant differences in the rate of recovery of high energy metabolites and pH in skeletal muscle are seen between normal volunteers and PVD, CHF, and heart transplant patients.

CHAPTER 1
INTRODUCTION

The objective of this dissertation was to develop and implement magnetic resonance spectroscopy (MRS) techniques in the diagnosis, treatment monitoring, and basic understanding of the disease process of musculoskeletal disorders. The techniques used were in vivo phosphorus and proton MRS applied to a mouse model and to humans. A 2.0 Tesla small-bore and a 1.5 Tesla whole-body magnet were used for these studies. Volume-selective and surface coil techniques were used for localization. A treadmill and an in-magnet ergometer were used for the exercise studies. Bone and soft tissue tumors were examined as well as skeletal muscle in patients with congestive heart failure, peripheral vascular disease, and heart transplant.

The diagnosis and treatment monitoring of disease by clinicians utilizes the history or complaints of the patient, physical examination, and various tests or procedures. The tests range from rather invasive and sometimes risky procedures such as surgery and biopsy to relatively risk-free test such as body fluid analyses, EKG's, x-rays, and MR imaging and spectroscopy. The purpose of this dissertation is to explore several unique applications of MR spectroscopic techniques in the diagnosis, treatment monitoring, and basic understanding of musculoskeletal disorders.

Magnetic resonance spectroscopy (MRS) of intact biological tissues was first reported by two groups: Moon and Richards using P-31 MRS to examine intact red blood cells in 1973 (1), and Hoult et al. using P-31 MRS to examine excised leg muscle from the rat in 1974 (2). Since then MRS has been applied to almost every organ of the body including brain (3-7), heart (8-11), liver (8, 12-14), kidney (15-17), prostate (18-20), and extremities (21-23). MRS is useful for looking at disorders of metabolism, tumors and certain inflammatory and ischemic diseases. Most of the work with in vivo MRS in humans has been in the brain. Abnormalities have been seen, sometimes with earlier detection than for any other diagnostic procedure short of biopsy, in primary brain tumors (6, 24-31), infections such as AIDS (32, 33), demyelinating disorders such as multiple sclerosis (34), epilepsy (35), and stroke (36, 37).

Spectroscopic changes are documented in a variety of enzyme deficiencies, mitochondrial abnormalities, dystrophies, inflammatory myopathies, and thyroid disease. In muscle these diseases include phosphofructokinase deficiency, amyloglucosidase deficiency, Duchenne muscular dystrophy, Becker muscular dystrophy, dermatomyositis, polymyositis, inclusion body myositis, hypothyroidism, and congestive heart failure (CHF) (38-43).

The research presented in this dissertation deals with application of MRS to disorders of the extremities, specifically, the musculoskeletal system. These applications have been relatively neglected except unlocalized P-31 MRS of mitochondrial and enzyme abnormalities. Diseases of the musculoskeletal system for which MRS may have some value include metabolic (including ischemic) diseases and neoplasms. MRS may be useful for diagnosis,

treatment monitoring, or understanding of the basic mechanism of these diseases.

Changes in muscle function and P-31 metabolism of patients are reported with both peripheral vascular disease (44-46) and CHF (47-49). P-31 MRS data are presented in this dissertation from a unique treatment for peripheral vascular disease (PVD) patients introduced a few years ago (44). This treatment was implemented recently on PVD patients locally.

MRS of neoplastic disease involving the musculoskeletal system has not been evaluated extensively. This is probably a result of the rare occurrence of musculoskeletal tumors and the demanding technical problems. For this dissertation, several types of musculoskeletal tumors in humans and an osteosarcoma model in mice are studied with P-31 and proton (H-1) MRS. I hope that this technique will eventually allow detection of chemotherapy and radiation therapy nonresponders in humans earlier than conventional imaging procedures. This would result in reducing the delay for surgery and reducing unnecessary chemotherapy and radiation therapy costs. Our spectroscopy research group plans to extend the animal research to evaluating new drugs for reversing chemotherapy resistance. This will be applied to humans later if successful in the animal model.

The effects of temperature and anesthesia on the P-31 metabolites and pH will be examined in mice. If present, these effects could alter the results of the chemotherapy studies.

Research Hypotheses

The following are the hypotheses that will be tested in this dissertation:

Mouse P-31 Tumor Studies

The presence or absence of statistically significant differences in the rates of change of the phosphocreatine/inorganic phosphate ratio (PCr/Pi) and phosphomonoesters (PME) between a) untreated and treated mice; and b) chemotherapy-treated sensitive and resistant mice will be determined. This information will be used to calculate the sensitivity and specificity for detecting the untreated mice and the resistant mice.

Human P-31 Tumor Studies

The PCr/Pi ratio and the PME signal will be examined in spontaneous musculoskeletal tumors in humans, using localized P-31 MRS, in hopes of using this information to detect tumors that fail to respond to therapy.

Anesthetic and Temperature Dependence of P-31 Metabolites

The presence or absence of the following phenomena will be determined:

1) Anesthesia with Innovar-Vet causes loss of thermoregulation in nude mice at doses required for immobilization for MRS studies.
2) Intracellular pH in implanted osteosarcoma in the nude mouse exhibits a temperature dependency similar to that reported in other tissues and in other models, including humans.
3) Anesthesia effects may be seen in the pH and P-31 metabolites of osteosarcoma.

Animal H-1 Tumor Study

An osteosarcoma mouse model will be used to determine the following:

1) Localized H-1 MR spectra, using water suppression techniques, will be successfully acquired from osteosarcomas implanted in nude mice.

2) Proton spectra from mouse tumors will show abnormalities in the choline/creatine (Cho/Cr) ratio.

Human H-1 Tumor Study

The H-1 MRS of mice will be complemented with examination of musculoskeletal tumors in humans to evaluate the following hypotheses:

1) Localized H-1 MR spectra, using water suppression techniques, will be successfully acquired from spontaneous musculoskeletal tumors, including osteosarcomas, in humans.

2) Viable tumor tissue will be distinguished from normal muscle, edematous tissue, and necrosis by H-1 MRS in humans.

3) The response to chemotherapy of musculoskeletal tumors in humans will be detected and quantified by changes in the H-1 spectrum.

4) The localized H-1 spectral data from humans will be correlated with magnetic resonance imaging (MRI), computed tomography (CT), and histopathology of the tumors.

5) Changes in Cho/Cr ratio will be used to differentiate chemotherapy non-responders from responders and will do so earlier than with MRI or CT.

Exercise Studies

We will use P-31 MRS of leg muscle in conjunction with exercise testing to test the following:

1) Improvement in the post-exercise recovery rates of phosphorus metabolites and pH will be seen after low-intensity exercise training.

2) Significant differences will be seen in the immediate post-exercise metabolite levels and pH in the skeletal muscle of PVD patients, CHF patients, heart transplant patients, and normal volunteers.

3) Significant differences will be seen in post-exercise recovery rate of phosphorus metabolites and pH in skeletal muscle of PVD patients, CHF patients, heart transplant patients, and normal volunteers following exercise.

Specific Objectives

Mouse P-31 Tumor Studies

Phosphorus MRS data will be collected from an osteosarcoma mouse model using a 2 Tesla (T) MR spectrometer. Data will be obtained and analyzed to show any statistically significant differences in metabolite levels between untreated and treated mice and between treated sensitive and resistant tumor mice.

Human P-31 Tumor Study

1) Existing localization techniques on a 1.5 T whole body magnetic resonance (MR) scanner (Signa, General Electric Company, Milwaukee) will be evaluated and (if necessary) modified to obtain well-localized P-31 spectra. Chemical shift imaging (CSI) techniques will be evaluated with phantoms, human volunteers, and patients. Spectral data will be obtained with signal-to-noise and spectral resolution adequate to show metabolite concentration differences between normal muscle, treated tumors, and untreated tumors.

2) Localized spectra of the tumor, necrosis, and surrounding normal and edematous tissue will be compared to the MRI in the humans.

Anesthetic and Temperature Dependence of P-31 Metabolites

1) Nude mice with implanted tumors will be anesthetized with Innovar-Vet and their rectal and skin temperature measured over a two hour period to detect any loss of thermoregulation.

2) Serial P-31 spectra will be obtained from anesthetized mice that become hypothermic and from mice that are heated to maintain normal body temperature over a two-hour period. Peak areas and pH will be measured and correlated with the rectal temperature and the time from injection of anesthesia.

Animal H-1 Tumor Study

Surface coils and a Faraday shield will be used initially for localization in mice in a 2 T spectrometer/imager. Water suppression techniques will be evaluated with phantoms and mice to obtain 200+ fold suppression of water. Spectral data will have spectral resolution sufficient to resolve the Cho and Cr peaks (~0.2 ppm).

Human H-1 Study

1) Existing localization techniques on the whole-body MR scanner will be evaluated and (if necessary) modified to obtain well-localized H-1 spectra. Various water suppression techniques will be evaluated with phantoms, human volunteers, and patients to obtain 200+ fold suppression of water. Shimming and adjustment of voxel size will be done to obtain a spectral resolution sufficient to resolve the Cho and Cr peaks (~0.2 ppm).

2) Localized spectra of the tumor, necrosis, and surrounding normal and edematous tissue will be compared to the MRI in the tumor patients.

3) The prebiopsy H-1 spectral data will be correlated with MRI and CT, and the histopathology of the biopsy material in humans.

4) Changes in spectral data during and after therapy will be documented. These changes will be compared with imaging data, gross and microscopic histopathology, and tumor response to therapy. Estimates of the ability of H-1 MRS to distinguish benign from malignant tissues and therapy responders from nonresponders will be made.

Exercise Studies

1) Recovery rates will be calculated for pH and P-31 metabolite levels obtained in the whole body MR scanner following a treadmill exercise stress test of PVD patients before and after low-intensity exercise training. The data will be tested for any significant changes from pre- to posttraining.

2) P-31 metabolite levels and pH will be measured from PVD patients, CHF patients, heart transplant patients, and normal volunteers in the whole body MR scanner during and following exercise with an in-magnet ergometer. Absolute metabolite concentrations and recovery rates will be calculated. Differences in these parameters among the four groups of subjects will be determined.

Collaborations

Part of the work presented in this dissertation was done in collaboration with others. The treated and untreated mouse section and the sensitive and resistant mouse section were a joint effort

of J.R. Ballinger, H. Kang, and C.A. Sweeney. Specific details of each person's contribution are presented later. The sections on P-31 spectroscopy of musculoskeletal tumors in humans and anesthetic and temperature dependence of pH and P-31 metabolites in mice, and the chapter on H-1 spectroscopy of musculoskeletal tumors was the work of J.R. Ballinger alone. The spectroscopy results in the chapter on P-31 spectroscopy of skeletal muscle in peripheral vascular disease and congestive heart failure was the work of J.R. Ballinger, with the ancillary exercise testing performed by C. Stopka, W. Breshue, and colleagues. A. Velenik, a postdoctorate fellow at the time, set up and performed the transfer of some exercise data from the Siemens scanner to a workstation for analysis.

CHAPTER 2
TECHNIQUES

Localization Techniques

Radio Frequency Localization

In vivo MRS generally requires some degree of localization. With implanted tumors in mice, it is desirable to obtain the signal from the tumor only and not from underlying muscle. Muscle and fat are found surrounding most musculoskeletal tumors in humans. Muscle may cause signal contamination in both unlocalized P-31 and H-1 tumor spectra, and fat may cause undesirable lipid contamination in H-1 tumor spectra. Localization requirements are less strenuous in P-31 MRS of calf muscle for metabolic studies. Here too, potential problems exist without some degree of localization. Different muscle groups are used to different degrees in any given exercise (for example the soleus and the gastrocnemius in the calf). These two muscle groups also have different proportion of muscle fiber types (50). Both these factors may introduce variability in spectral data.

Surface Coil Localization

The simplest localization technique is with a surface coil. Localization with this technique relies on the limited extent of the B_1 field to define the volume of interest (51). The distance from the coil at which a 90° tip angle occurs (providing the maximum signal) may be varied by adjusting the amplitude or length

of the radio frequency (RF) pulse. This technique has been used for localizing implanted tumors in nude mice by various authors, including ourselves (18, 52, 53). Double-tuned coils to P-31 and H-1 provide proton imaging and shimming capability along with phosphorus spectroscopy (54). A Faraday shield around the base of the tumor may be used to remove additional unwanted signal from surrounding muscle and other tissues (55).

Selective Presaturation

Another localization technique involves selective saturation of the spins outside the volume of interest (VOI). Excitation and dephasing of the spins outside the VOI are immediately followed by acquisition of a free induction decay (FID), spin echo (SE), or stimulated echo from the tissue inside the VOI. This technique may be combined with selective excitation localization techniques. The VOI may be defined by saturating orthogonal slabs or cylindrical volumes (56-58).

Selective Excitation

Several localization techniques use selective excitation and detection of spins to detect the signal from within a VOI. One of the original volume excitation localization techniques is VSE (volume selective excitation) (59). More accurate localization techniques with less power deposition are used more commonly now. ISIS (Image-selected in vivo spectroscopy) localization (60) has been used frequently with P-31 MRS and has been reported at least once with H-1 MRS of the human brain (61). This technique uses three 180° inversion RF pulses with gradients to select orthogonal slabs, defining the VOI at the intersection. This is followed by a 90° excitation pulse and signal acquisition. An eight-step phase

cycling routine is used to eliminate the residual signal from outside the desired voxel. Additional spatial presaturation pulses may be necessary to eliminate additional extraneous signal from outside the VOI as the result of subtraction errors during the ISIS experiment. A multivolume ISIS technique has been described using multiple-line frequency selective pulses (62). For n volumes, 2^n experiments must be done. The number of experiments required for a small number of voxels with in vivo spectroscopy would not be a problem as we need about 256 averages for adequate signal-to-noise.

Commonly used selective excitation localization techniques for H-1 MRS include STEAM (STimulated Echo Acquisition Mode) (63, 64), PRESS (Point Resolved Spectroscopy) (65, 66), and SPARS (SPAtially Resolved Spectroscopy) (67, 68). STEAM selectively excites three orthogonal planes with two 90° RF pulses and one 180° RF pulse followed by acquisition of a stimulated echo. A localized image may be obtained to confirm proper positioning and size of the VOI. This sequence collects only one-half of the original signal but allows a short echo time (TE) (20 ms or less).

If more signal is necessary because of a small VOI or low levels of metabolites, the entire signal can be collected as a spin echo using the PRESS technique. PRESS consists of gradient localized 90°-180°-180° RF pulses. The SPARS technique consists of three sets of 90°-180°-90° RF pulses applied in the presence of gradients. SPARS localization results in significant contamination from outside the VOI unless care is taken in adjusting the 180° pulses. This problem is not seen with STEAM (22). SPARS has a greater RF load on the patient than STEAM or PRESS (67). There is

a sacrifice of a longer echo time in the PRESS and particularly the SPARS techniques resulting in T2 decay of the signal. This is rarely a problem with H-1 MRS because of the long T2 relaxation times of observable metabolites (69-71).

Chemical Shift Imaging

Chemical Shift Imaging (CSI) involves the use of stepped gradients to phase encode the spectra in one to three dimensions (72, 73). CSI has one major advantage over single volume localization methods. Spectra from multiple locations within the VOI may be sampled simultaneously (60, 74, 75). Sampling multiple areas within a tumor is desirable because of the heterogeneity of many tumors. Spectra from adjacent normal tissue are sometimes desirable.

There are two significant disadvantages of these methods. First, 45% or more of the signal from a voxel comes from bleeding from other voxels (76). This occurs because CSI uses a finite number of phase encoding steps to generate a limited series of sine and cosine functions to encode discrete and discontinuous voxels. The bleeding can be reduced with the use of selective Fourier transform localization (76, 77). With this technique, the k-space data set is weighted by a function that maximizes the signal from acquisitions with small gradients and minimizes the signal from acquisitions with strong gradients. Maximum SNR per unit time is accomplished with this technique by varying the number of averages at each phase-encoded step. Similar results may be obtained with post processing by multiplying the k-space data matrix in the spatial directions by an apodizing function, such as a Hanning, sine, Gaussian, or Fermi function. Use of a filter

causes a small drop in SNR, yielding approximately 2% less signal than a CSI acquisition without a filter. The filter decreases the contamination from outside the voxel to about 11% (76). The width of the response function in each spatial dimension increases by 1.6 times that without weighing the data. To compensate for the increase in width of the response function, the phase encoded steps may be increased by 1.6 or the field of view (FOV) may be decreased by the same factor. A modification of the selective Fourier transform CSI experiment was developed using variable flip angles at different phase encoding steps to reduce bleed and improved SNR per unit time (78). The efficiency of these techniques has been compared recently (79).

Water Suppression Techniques

The adult human is approximately 60% water by weight; skeletal muscle is approximately 79% water (80). This results in a concentration of water in skeletal muscle of about 44 M. The concentration of metabolites of interest in H-1 MRS is between 5 mM and 30 mM. This 1400+ fold difference in concentration results in a dynamic range problem for the receiver and the analog-to-digital converter of most spectroscopy systems and causes difficulty in quantitating accurately nearby peaks. It is therefore desirable to reduce or eliminate the water signal for detection and accurate quantification of metabolites.

Desirable features of a solvent suppression technique include uniform excitation of the nonsuppressed peaks of interest. Hore has summarized other desirable features for solvent suppression pulse sequences:

> (a) insensitivity to B_0 inhomogeneity and small errors in the choice of transmitter frequency; (b) wide band excitation, preferably on both sides of the solvent; (c) insensitivity to pulse imperfections (B_1 inhomogeneity, nonideal pulse shapes, off resonance effects, phase shift errors); (d) only linear phase correction required; (e) simple modification to obtain a 180° pulse; and (f) easy to program and use. (81) pp. 285-286

One of the first proposed methods for reducing the water signal in H-1 MRS was Redfield's long, weak 90 degree RF pulse (82). The pulse results in a narrow bandwidth of excitation centered off resonance from water and on the frequency of the metabolite resonance of interest. This method is sensitive to magnetic field inhomogeneity resulting in incomplete suppression of the water peak, or nonuniform excitation of the desired metabolite, or both. The length of the pulse results in T2 weighting to the signal and a rolling baseline artifact. Redfield later introduced a "2-1-4 pulse" sequence that uses alternating 180 degree phase shifts of a constant amplitude RF pulse in a timing pattern of 2-1-4-1-2 (83). This results in a sinusoidal excitation spectrum where the water resonance is at a null point. This sequence results in a 100-fold decrease in the water signal. Disadvantages of the 2-1-4 sequence include nonuniform excitation of resonances of different chemical shifts and incomplete water suppression.

Plateau and Gueron introduced a sequence of strong pulses for water suppression (84). These pulses are simpler to generate and less sensitive to errors in pulse amplitude than Redfield's soft pulses. This sequence consists of two pulses separated by a delay τ (90°, τ, -90°, acquire) with the pulses centered on the water

frequency. In the rotating frame of reference, the water magnetization vector is flipped on to the +x axis. After a period τ, the water vector has remained unchanged in position, while other resonances have undergone precession in the x-y plane. The second pulse returns the water vector to the z axis resulting in no component in the x-y plane and therefore no signal. The off resonant vectors will have a component of varying degree remaining in the x-y plane resulting in a signal. The amplitude of the signal from the other spins follows a sinusoidal pattern in the frequency domain, with maximum signal from those spins resonating at $\pm 1/(4\tau)$ Hz, $\pm 3/(4\tau)$ Hz, etc. relative to the frequency of water. In a modification of this technique by Bleich and Wilde (85) (90°, τ, +90°, acquire) the RF pulse is centered Δf Hz away from the water resonance such that the peak of interest is located $\Delta f/2$ from water. The water vector is allowed to rotate 180° in time τ at which time the second pulse returns it to the z axis. The peak of interest will remain in the x-y plane. These two hard-pulse sequences result in a 300-fold decrease in the water signal. Disadvantages of these sequences include the high sensitivity of the water suppression to phase shifts of the RF pulses and to amplitude balance in the RF channels (81).

Hore first described the binomial pulse sequences in 1983 in two papers (81, 86). The binomial pulse sequences were developed to have the following properties: 1) a broad null to accommodate widening of the water peak due to magnetic field inhomogeneity and to allow for minor errors in the setting of the transmitter frequency; 2) a wide band of excitation in the remainder of the

spectrum of interest; 3) insensitivity to imperfections in the RF pulse shape and amplitude (as may be caused by finite rise and fall times, inhomogeneous RF fields from surface coils, and off resonance effects due to the long pulse lengths needed by whole body coils); and 4) a short sequence length to allow for T1 measurements if desired.

The Fourier transformations of the binomial pulse sequences approximate the desirable features of the excitation spectrum at small flip angles. Hore chose a sinusoidal function for an excitation spectrum: $S(\omega)=\sin^n(\omega\tau/2)$. The inverse Fourier transformation of this function gives a series consisting of equally spaced delta functions with alternating signs given by the binomial coefficients (81). This series can be approximated by a series of equally spaced short pulses whose amplitudes are given by the binomial series, e.g., 1,2,1; 1,3,3,1; 1,4,6,4,1. The RF pulses alternate 180° phase shifts. The longer sequences have broader null regions and would therefore be more efficient in case of a broad water peak. The disadvantage of the longer sequences is that a large frequency dependent phase shift is introduced into the spectrum (87). The symmetric sequences (1,1; 1,3,3,1) are insensitive to minor errors in the flip angle compared to the asymmetric sequences. This is because each pulse in a symmetric sequence has an oppositely phased pulse of the same amplitude. Signal errors resulting from imperfect 180° phase shifts can be corrected with phase cycling (88). An approximately 1000-fold decrease in the water signal can be obtained with the most commonly implemented binomial sequence: 1,3,3,1. Additional sequences that may be used are 1,1,8,8,1,1 and 1,5,20,20,5,1 (87).

Water suppressed spectroscopy can also be performed using presaturation with a narrow bandwidth, frequency selective RF pulse, the so-called CHESS (CHEmical Shift Selective) technique (63, 89-93). Frahm et al. describe a combination of two CHESS pulses followed by STEAM localization (94). Greater suppression can be obtained using three CHESS pulses (95, 96), a technique we have available on our whole body scanner. Addition or substitution of a binomial sequence (81, 86), or a DANTE (Delays Alternating with Nutations for Tailored Excitation) sequence (97) are alternatives. The water suppression from T2 decay with the long TE PRESS localization technique can be supplemented with preceding CHESS pulses or an inversion pulse (98).

Lactate Editing

Lactate editing is necessary in in vivo experiments for at least two reasons. First, the peak position (1.33 ppm) overlaps that of the lipid signals (1.10-1.48 ppm) and second, the lactate signal intensity may be several times smaller than the lipid signal.

Several spectroscopic techniques may be used for lactate editing including homonuclear double-resonance difference (99, 100), double quantum coherence transfer (101-105), and zero quantum coherence (106-109). A zero quantum technique for lactate editing has been described using stimulated echo localization (106). This sequence is the only technique available to us to use on the whole-body imager at this time.

Lactate methyl protons are J-coupled to the adjacent methylene protons, resulting in phase modulation that is a

function of the TE and the mixing time (TM). The lipid protons that resonate at a similar frequency show only mild J-coupling and do not exhibit significant phase modulation (110). By acquiring two spectra with a different TM and subtracting, the lipid signal can be removed, leaving only the lactate signal. The lactate peak phase modulation alternates minima and maxima at TE = 1/2J where J is the coupling constant for lactate and equals 7.35 Hz. At 1/J = 136 ms, the lactate peak modulates with the TM with a period of 1/ Δf where f is the chemical shift between the methyl and methylene peaks of lactate. At 1.5 T, f is equal to 178.5 Hz. Best results are obtained by keeping the TE constant at 136 ms and varying the TM.

The homonuclear double-resonance difference technique requires two transmitters and subtraction of spectra. This works well with in vitro and ex vivo work in spectrometers but most whole-body imagers do not have two transmitters. Most of the double quantum coherence transfer techniques result in a 50% loss of the lactate signal and require phase cycling to help reduce the water signal. Double quantum coherence transfer techniques have been reported that require no phase cycling and might be more desirable for in vivo experiments but have not yet been implemented on whole body imagers (111, 112).

An alternative to zero and double quantum editing techniques is to take advantage of the short T1 of lipids compared to lactate by the use of a 180° inversion pulse to null the lipid signal. As a result of using this technique, 20%-30% of the lactate signal is lost. The inversion pulse has been used with a binomial spin echo sequence to obtain both water and lipid suppression (113). This

inversion pulse has been combined with two CHESS pulses for both water and lipid suppression (114) and is available now on our whole body spectrometer.

The differences in T2 between lipids and lactate were used in a mouse model to eliminate most of the lipid signal (58). This is effective when only a small amount of lipid is present and required a TE of at least 270 ms.

Quantitation of molar Concentrations of Metabolites In Vivo

Tofts and Wray have published a comprehensive review of quantitation methods (115). They include a discussion of the assumptions and problems of each technique. Buchli and Boesiger have published recently an evaluation of the accuracy and reproducibility of several techniques for quantitation of P-31 spectra (116).

Twelve factors to be considered in quantitating in vivo MR spectroscopy follow:

1) The minimum detection limits for metabolites are about 0.5 mM for P-31 and 0.1 mM for H-1.

2) "NMR invisibility" sometimes occurs when a metabolite is not mobile enough (i.e., rapidly rotating or translating) to give a narrow peak. Much of the choline and phosphomonoester, for example, is bound in cell membranes as phospholipids and is not visible in normal tissue.

3) Normal tissues and to a greater degree, tumors, are heterogeneous. The heterogeneity may be macroscopic (fat vs. muscle or tumor vs. necrosis) or microscopic (different tumor subtypes or intracellular vs. extracellular metabolites).

4) The transmitter (B_1) homogeneity and receiver sensitivity must be considered. Surface coils have quite an inhomogeneous B_1 field. Volume coils are better in terms of B_1 homogeneity.

5) Coil loading must be considered where using external standards for reference.

6) Peak ratios avoid some transmitter, receiver and coil problems. The problem with peak ratios is that changes in individual metabolites are not determined; changes may occur in both the numerator and the denominator. This is less of a problem in normal tissues where certain metabolites have relatively constant concentration (such as adenosine triphosphate (ATP) in muscle or water in brain and muscle), unlike the situation found in tumors.

7) Tissue extracts have been used to help quantitate MRS data, however, the concentrations depend on what technique is used and how efficient the technique is in extracting all of the metabolite.

8) External standards may be used for quantitation. These should experience the same B_1 field and receiver sensitivity as the tissue or corrections should be made for differences. When the external standard is used during a separate experiment from the tissue, coil loading must be considered.

9) Internal standards may be used as alluded to under (6) above. Both ATP and internal water are frequently used. In tumors or metabolic diseases, they may not be as constant as in normal tissue, adding possible error and variability to results. Exogenous standards given internally have been used primarily in animals. Their invasive and possible toxic effects are drawbacks in humans.

10) Concentration measurements require some sort of volume determination unless the volume of the tissue and the standard are the same.

11) Relaxation effects need to be considered when TR < ~5 T1 for the metabolites of interest or the standard. Also, if there is a delay of acquisition as occurs with spin echoes and stimulated echoes, T2 decay must be considered unless the TE << T2 for the metabolites and standard. Variation of the water T1 and T2 times has been found in implanted mammary adenocarcinoma in mice as a function of the age of tumor (117).

12) Various methods have been used to measure the signal magnitude in NMR spectra. These include manual measurements of peak height, triangulated peak areas, and cutting out and weighing the paper that the spectrum is drawn on. Automated methods include integrating the spectrum between two points, fitting Lorentzian or Gaussian shaped curves to the frequency-domain data, or fitting damped sinusoids to the time-domain data (118, 119). The manual methods are time consuming, and peak height and triangulation are not very accurate unless the peak line width and shape remain the same. Integration works well on well separated but not overlapping peaks. Some authors claim that fitting of the time domain data is more reproducible than fitting of the frequency domain data. Problems with time domain fitting include the need for very good SNR and the more computer intensive processing than is required for fitting frequency data.

The significant factors to consider in measuring metabolite concentrations from in vivo experiments using MRS have been

expressed in an equation by Bottomley and Hardy (120). The equation is as follows:

$$[M]=[s]\frac{S_m V_s \psi_s F_s(T1_s,\alpha_s) E_s(T2_s,T_d)}{S_s V_m \psi_m F_m(T1_m,\alpha_m) E_m(T2_m,T_d)}$$

Where:

[M] is the metabolite concentration

[s] is the standard concentration

subscripts m and s denote metabolite and standard, respectively

S is the NMR signal

V is the sample volume

ψ is the detection coil sensitivity

F is a function accounting for T1 saturation effects

α is the flip angle

E is a function accounting for T2 decay occurring during the delay time T_d

Two specific methods proposed for quantitation of in vivo MR spectra include the following: Michaelis et al. suggest the use of control spectra obtained from standard solutions in separate experiments but under identical experimental conditions including identical coil loading (121). This paper and two other abstracts report the use of the water signal present in the brain as a control or calibration standard for the quantitation of proton spectra (122, 123). This method was originally proposed by Thulborn and Ackerman (124). The water concentration in the brain is relatively constant (≈75-85%) (122).

Recently a combination technique using both an internal standard and an external standard was proposed for proton spectroscopy (125). Alger et al. use tissue water as an internal standard and a reference tube of distilled water as an external standard. The metabolite signals are referenced to the internal water signal in the same volume of tissue. This in turn is referenced to the ratio of water signal intensities of the same tissue volume and the reference standard obtained from a short TE MRI image. The concentration of pure water in the reference standard is known, and with estimates of the relaxation factors of the metabolites, tissue water and external reference standard, the metabolite concentration can be calculated. The metabolite concentration would be computed by the following equation:

$$[M] = [W_v] * \frac{M}{W} * \frac{N_u}{N_s} * \frac{2}{N_p} * C_3 * C_4$$

Where:

[M] is the metabolite concentration

M is the metabolite NMR signal

W is the unsuppressed tissue water signal

N_u is the number of acquisitions used to obtain the unsuppressed water signal

N_s is the number of acquisitions used to obtain the water suppressed spectra

N_p is the number of equivalent protons producing the metabolite's signal

$[W_v]$ is the tissue water concentration derived from the equation below:

$$[W_v]=55M*\frac{W_v}{W_r}*C_1*C_2*C_5$$

Where:

55 M is the concentration of pure water in the standard

W_v is the signal intensity of water in the region of interest from the MRI

W_r is the signal intensity of the pure water reference from the MRI

C_{1-4} are the correction factors for T1 and T2 relaxation

C_5 is a correction factor for sensitivity differences in the receiver coil for the standard and volume of interest.

This method is quite attractive for use in in vivo experiments with humans. Images are obtained to measure volume changes in the tumors or tissue of interest and to provide a localization guide for gradient localization techniques. Little additional time would be required in using this quantitation technique.

CHAPTER 3
P-31 SPECTROSCOPY OF HUMAN OSTEOSARCOMA IN A MOUSE MODEL AND IN HUMANS

Extensive literature exists describing abnormal P-31 spectra of animal and human tumors. There are fewer reports of alteration of the P-31 spectra following therapy. For a concise review see Negendank (126).

Review of the Literature

General Problem

Osteosarcoma is a relatively rare malignancy of bone occurring predominantly in teenagers and young adults with an annual incidence in the United States of approximately 2100 new cases (127, 128). Bone tumors account for about 5% of all childhood malignancies. Osteosarcomas comprise about 60% of malignant childhood bone tumors (129). The tumor consists of malignant osteoid-forming cells, i.e., those cells that form the organic matrix in which bone ossification occurs (130). These tumors occur primarily in the metaphyseal or growth regions of long bones, especially near the knee in the distal femur and proximal tibia. They have a propensity with time to extend beyond the bone into the adjacent soft tissues and joints.

Less common forms of osteosarcoma occur in older adults (usually > 50 yrs. old) associated with either a benign disease called Paget's disease or with previous radiation therapy (130).

Earlier in this century, there were two groups of patients, that we no longer see, that developed osteosarcomas. Patients with tuberculosis of the spine were once treated with irradiation; and watch-dial painters often placed their brushes containing radium-226 doped paint in their mouths. Both groups had an increased incidence of osteosarcoma (131). These less common forms have a poorer prognosis than the primary osteosarcoma in children. Osteosarcomas in children have not been directly associated with any external or environmental factors, but are usually associated with the rapid growth that occurs in this age group (129). In some cases, osteosarcomas are associated with potentially inherited and acquired genetic defects (132-135).

History of Treatment

Before 1972, the 5-year survival rate of osteosarcoma was 20%, amputation being the primary treatment method (136). Post-operative adjuvant therapy was introduced by Jaffe in 1972, reporting a 30% to 40% response rate (137). In 1977, Jaffe introduced the idea of pre-operative or neoadjuvant chemotherapy with a primary response rate of 60% (138). The 5-year survival rate for osteosarcoma in humans from three recent randomized trials, reviewed by Eiber and Rosen in 1989, was 70% (range 66% to 77%) (130). These three clinical studies used combination chemotherapy including doxorubicin, methotrexate, and cisplatin. The 30% mortality rate in this review article is from drug-resistant tumors.

Surgical management of osteosarcoma following chemotherapy currently includes amputation, disarticulation, and limb salvage procedures. Limb salvage procedures involve the replacement of the

effected segment of bone with normal donor bone. This preserves normal function of the patient's limb, unlike amputation and disarticulation. This may be possible if tumor involvement of the soft tissues and bone marrow is not extensive and if the adjacent joint is not traversed.

Monitoring of Therapy Response with Imaging Techniques

Response to chemotherapy is followed with MRI and CT; however, these modalities depend primarily on evaluating gross anatomical features such as change in tumor size. Detection of a significant response to chemotherapy with conventional clinical and imaging techniques requires a 4-6 week period. This results in a delay of either definitive surgery or change in the chemotherapy regimen if the desired response fails to occur.

A significant diagnostic problem is distinguishing soft tissue extension of tumor from surrounding edema and inflammation. Edema was present in six out of 21 osteosarcomas reported in a recent paper (139). Neither CT nor MRI (with or without enhancement) can accurately detect the difference between tumor and edema in osteosarcoma (139), chondrosarcoma (140), and soft-tissue tumors (141) and inflammation in soft-tissue tumors (142).

A 90% necrosis of the tumor on histopathological examination has a better prognostic value for patient survival than tumor size, site, and classification (143). The survival rate was 91% for patients with greater than 90% necrosis, compared to 14% survival for patients with less than 90% necrosis. Unfortunately, current imaging techniques including standard MRI fail to accurately determine the amount of necrosis in osteosarcomas and other malignant musculoskeletal tumors (142, 144-146). Two recent

papers report the use of dynamic Gd-DTPA enhanced MRI to predict the amount of necrosis following chemotherapy. The first paper was able to distinguish >90% necrosis from <90% necrosis (144). The second paper mapped six osteosarcomas into 11 to 56 regions each (147). The fraction of regions with rapid signal intensity change with time predicts the histopathological grade of the tumor, i.e., <50% necrosis, 50%-90% necrosis, >90% necrosis, and 100% necrosis. Individual regions were occasionally false positive for tumor when vascular fibrosis was present. Two recent abstracts discriminate chemotherapy responders from nonresponders based on the rate on contrast enhancement after a bolus injection of gadopentetate dimeglumine (148, 149).

P-31 Magnetic Resonance Spectroscopy

P-31 spectra of tumors and malignant cells consist mainly of peaks for phosphomonoester (PME), inorganic phosphate (Pi), phosphodiester (PDE), phosphocreatine (PCr), nucleoside triphosphate (Primarily ATP) and diphosphodiester (DPDE). The PME peak contains various sugar phosphates, phosphoryl ethanolamine (PE), and phosphoryl choline (PC). The latter two are precursors of phospholipids and are produced by choline and ethanolamine kinases (150). Phospholipids are important constituents of cell membranes and organelles involved in the synthesis of proteins and generation of energy (151). The PDE peak consists primarily of glycerolphosphoryl choline (GPC) and glycerolphosphoryl ethanolamine (GPE), which are membrane breakdown products (150).

Thus, the P-31 spectrum gives information on phospholipid synthesis (PC and PE) and degradation (GPC & GPE), cell energetics (PCr, ATP, & Pi), pH (Pi and PCr positions) (152) and

glycoprotein/glycolipid synthesis (DPDE). Actively growing cells (as in malignant tumors) have high rates of energy consumption and protein/membrane synthesis and breakdown, contributing to P-31 spectral abnormalities.

P-31 spectra of bone tumors, including osteosarcoma in humans, show increased PME, PDE, and Pi, and a decrease in PCr (153-160) relative to normal skeletal muscle. The concentration of ATP may increase, decrease, or remain unchanged, depending on the study. The pH of the tumors is also variable, depending on the type and the stage of the tumor. An elevated pH is seen in two studies (154, 155), a normal pH is seen in four studies (153, 156, 159, 161), both slightly elevated and normal values in one study (160).

Treatment Response

P-31 MR spectral changes may be seen in human osteosarcoma patients on the second day after beginning chemotherapy (153). A decrease in PME in human osteosarcomas as a response to chemotherapy is reported (160, 162, 163). An increase in the PCr/Pi ratio is reported, following treatment, in human osteosarcoma (154, 160), soft tissue sarcomas (163), and in murine osteosarcoma (164), mammary adenocarcinoma (165), RIF-1 tumors (166), and 9L gliosarcoma (167).

Subtle changes may be present in osteosarcomas and other tumors within one hour of the start of chemotherapy (154, 168). The prognostic value of these changes is uncertain. Following chemotherapy in humans, long term decrease in PDE is associated with >90% necrosis (155). An increase in the PCr/Pi ratio is correlated with a decreased transverse tumor diameter by Semmler

et al. (154). Ross et al. (153) observe a decrease in PME and ATP relative to PCr. Pi showed biphasic behavior with respect to time in his study, initially decreasing, then increasing. Wehrle et al. (166) observe biphasic behavior of Pi with respect to the chemotherapy dose in RIF-1 tumors implanted in mice. A decrease in Pi relative to α-NTP (nucleoside triphosphate) is seen at moderate doses of cyclophosphamide (150 mg/kg i.p., LD_{10} or less). At high doses (200 mg/kg, approximately LD_{50} dose), they observe an increase in Pi relative to α-NTP. Wehrle also observes a decrease in PME and an alkaline shift in pH. Koutcher showed a significant increase in PDE/PME in malignant fibrous histiocytomas that responded to chemotherapy compared to a slight decrease or no change with nonresponders (163). The responders also had a significantly lower PDE/PME before chemotherapy compared to nonresponders. Redmond et al. showed a significant decrease in PME in human osteosarcomas (160). A recent abstract found that the PCr/Pi and PCr/ATP ratios discriminate between chemotherapy responders and nonresponders (169).

pH Changes

Alkaline shifts in tumor pH following treatment have been seen for a variety of tumors including non-Hodgkin's lymphoma (170). The pH in three osteosarcomas following chemotherapy failed to change significantly (160).

Advantages of P-31 MRS

1) The high energy phosphates so important to tumor metabolism, i.e., PCr and ATP, are readily seen at 1.5 T. ATP is important as the immediate source of energy for most metabolic

processes. Decreased levels are found in tumors with reversal following effective treatment. ATP is identified and quantified by H-1 MRS in human skeletal muscle at 4.1 T (171) but not at 1.5 T. Total creatine can be resolved with H-1 MRS, however PCr and Cr cannot be separated at 1.5 T.

(2) The different phosphoesters, PME and PDE are easily resolved with P-31 MRS. Although the PME and PDE peaks show similar changes in implanted osteosarcoma in mice (158), with decoupling techniques the various components of the PME peak (PE and PC) can be resolved and appear to have individual significance (172). The elevated PME in most malignant tumors is related to increase in PC; however, elevated PE and decreased PC have been reported in human colon cancer (173). The PE/PC ratio may be a more sensitive indicator of malignancy and of tumor response to therapy than PME alone (172).

(3) The P-31 spectrum has no solvent signal to interfere with resolution of metabolite peaks, unlike the water signal seen with in vivo H-1 MRS.

Treated and Untreated Mice

Our goal is to develop better techniques to monitor the chemotherapy response of tumors. In the present study, we used phosphorus NMR spectroscopy to compare the changes in phosphomonoester(PME) signal and the phosphocreatine/inorganic phosphate (PCr/Pi) ratio from implanted human osteosarcoma in the nude mouse with and without chemotherapy (treated and untreated). We evaluated the accuracy of the change in PME and PCr/Pi in detecting the untreated mouse. This is a logical precursor to

studying resistant and sensitive tumors in mice. In the latter case we would wish to predict which tumors are resistant.

The study protocol, data acquisition and preliminary analysis was performed by Haejin Kang, Ph.D. as part of his graduate work. The study is included in this dissertation because extensive work has been done with the raw data beyond that presented previously. Specifically, the following work was done by or under my direction: a) spectra were refit, b) statistical analysis was performed on the PME changes with treatment, c) the possible explanation of volume changes accounting solely for the PME changes was addressed, and d) changes in PCr/Pi were investigated in terms of predicting treatment response independent of volume change. In addition, experiments were performed by myself to check the reproducibility of metabolite measurements using repeated spectral acquisitions on three mice.

Materials and Methods

Animal preparation

The nude, athymic mouse is a well characterized and accepted model for the study of the properties of human tumor cells (155, 174-176). Human tumors studied in nude mice include small cell carcinoma of the lung (155, 164, 174), mammary carcinoma (164), ovarian carcinoma (164), neuroblastoma (177) and prostate carcinoma (178). Human osteosarcoma in mice has not been studied with MRS to my knowledge; however, the murine Dunn osteosarcoma has been (164). Our experience has shown that human osteosarcomas, unlike some other human tumors, grow relatively well in nude mice. Our spontaneous regression rate of implanted osteosarcomas in nude mice is 1.5% (n=180) with none occurring in study mice. The mice

that showed regression were from earlier preliminary studies. These mice were approximately 14 weeks old at time of implantation and were not irradiated. Nude mice older than 12 weeks have been shown to gradually develop T-cell activity that is apparently the cause for the observed tumor regression (179, 180). This tumor cell line makes bone in the mouse, repeating its human origin. We have also shown that the cell line responds to the same chemotherapeutic agents as do native osteosarcomas in humans. The kinetics of chemotherapeutic agents in nude mice has been studied and compared to the kinetics in humans (177, 181-184).

Twenty-two female Balb-c mice, weighing between 25-30 grams, were quarantined and acclimated to environmental conditions of 27°C±2° and 40-50% humidity for 5-7 days before implantation. The mice were fed and watered ad libitum.

At 10 weeks of age, the mice were irradiated in a Cs^{137} gamma irradiator (Gammacell 40, Atomic Energy of Canada Limited, Ottawa, Canada) at a dose of approximately 500 Rads to suppress any early T cell activity (185, 186). The next day, a suspension of 6×10^7 trypsinized cells from a standard tissue culture (187) of the human osteosarcoma cell line 791T (Zoma Corp., Berkeley, CA) was implanted subcutaneously over the gluteus maximus of the anesthetized mice. The mice were anesthetized for both implantation and spectroscopy. An intraperitoneal (i.p.) injection of 0.04-0.05 ml of Innovar-Vet (fentanyl citrate 0.4 mg/ml and droperidol 20 mg/ml, Pittman Moore, Washington Crossing, NJ), diluted to 10% v/v with normal saline, was used for anesthesia. This dose provides adequate anesthesia for one to two hours. The mice were irradiated and implanted with tumor cell suspension by

Carol Sweeney, laboratory technician. The tissue culture work that she did was under the direction of Byron Croker, M.D., Director of Pathology at the VA Medical Center, Gainesville, FL.

Cisplatin (7 mg/kg, Bristol Laboratories, Evansville, IN), dissolved in 0.9% sodium chloride, was administered in 11 mice via a tail vein on day nine post implantation. This dose of cisplatin is a dose that is pharmacokinetically equivalent to the clinical dose in humans (Rational Dose) (177, 184). The tumors were followed with MRS for at least three weeks post implantation.

Spectroscopy

Spectroscopy was performed on a Spectroscopy Imaging Systems Corporation Model VIS 85/310 imaging spectrometer with a 310 mm diameter horizontal bore Oxford Instruments magnet operating at 2 T (34.61 MHz for P-31). Haejin Kang Ph.D., built the RF coil, and acquired the data. The spectrometer was operated from and the spectra analyzed on a Sun 3/110 work station (Sun Microsystems, Inc., Mountain View, CA). A home-made, 3-turn solenoid coil with an internal diameter of 13 mm and a depth of 6 mm (volume of the coil: 0.80 cc), double-tuned to H-1 and P-31 (54), was positioned over the tumor as shown in Fig. 3-1. A fenestrated Faraday shield was positioned around the base of the tumor for further localization by excluding signal from adjacent muscle (not shown) (55). On histological evaluation, the skin of the nude mouse is quite thin and frequently has no muscle associated with it. It probably contributes little to the NMR signal. This is unlike the rat where significant subcutaneous muscle is present. There is probably a significant contribution to the signal from muscle

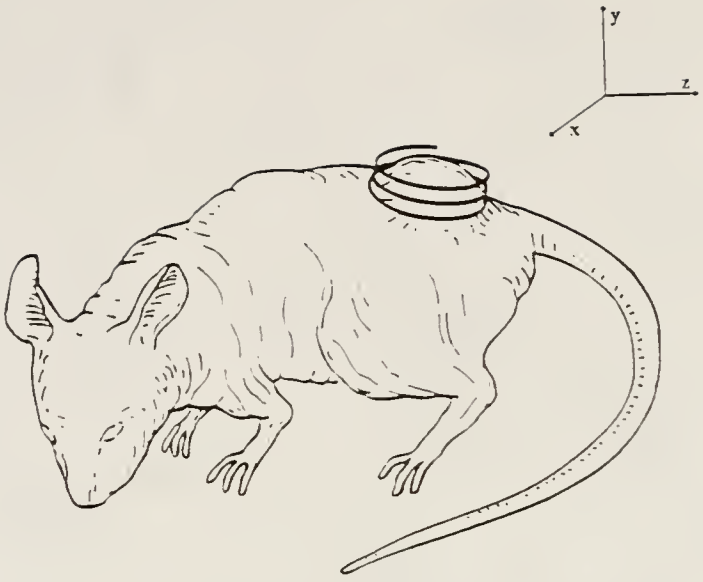

Figure 3-1 RF coil positioned over mouse tumor.

underlying the tumor that is not shielded by the Faraday shield. This is discussed later under the Results and Discussion section.

The magnet was shimmed on the water peak on each mouse to a line width of between 0.2 and 0.4 ppm. P-31 spectroscopy was performed with a non-selective 3-lobed, 12 μsec, 90°, sinc-shaped RF pulse followed 30 μsec later by acquisition of the FID signal. The 90° RF pulse power was set by maximizing the signal from the tumor. The acquisition parameters were: 2000 acquisition points, TR=1.5 sec, spectral width=2000 Hz, 1024 averages, and a 26 min acquisition time. The total exam time was about 50 min. Spectroscopy was performed one day before implantation, then twice a week starting when the tumors were 0.23 cc ±0.07 in volume (nine days post implantation).

The volume of the tumors was initially calculated with the formula for an ellipsoidal volume $(\pi/6)*L*W*D$ from measurements made with calipers where L, W, and D are the length, width, and depth of the tumor respectively (156). Later, the tumor volume was calculated as the average of the formulas for an ellipsoid and a prolate spheroid (formed by rotation of an ellipse about its major axis, L): $(\pi/6)*L*W*D$ and $(\pi/6)*L*W^2$. We have found that this method of volume calculation is the best estimate of tumor volume. The average of these two formulas had a better correlation coefficient with the volume of water displaced by excised tumors of different sizes (compared to the two formulas separately, as shown in the Results and Discussion section). Imaging of the tumor to determine size was tried but failed to give adequate signal-to-noise (S/N) to distinguish the tumor, muscle interface in a 15 min period. The filling factor for the coil during the acquisitions immediately before and after chemotherapy ranged from 0.25 to 0.625. Reproducibility of spectra and metabolite signals was checked by J.R. Ballinger by obtaining 6-7 sequential spectra each in three additional mice with tumors (See Results and Discussion).

After 10 Hz line broadening of the FID and Fourier transformation of the data, the spectra were fit using the Fitspec software provided by SISCO. Zero and first order phase correction were applied to the frequency domain data. Fitting of spectra was performed initially by Carol Sweeney and Haejin Kang and later by Carol Sweeney and J.R. Ballinger.

Analysis of data

Data were statistically analyzed by J.R. Ballinger. The PME area and PCr/Pi ratio were used in statistical analysis. The change in each was compared to the volume changes of the tumors. An unpaired, two-tailed Student's t-test was used to test the difference between the treated and untreated mice in the PME change from the day after chemotherapy to the following session (four days later). The change in the slope of the PCr/Pi curve from pre-chemotherapy to the first study post-chemotherapy was tested for significance in both the treated and untreated mice with a paired, two-tailed Student's t-test. A receiver operating characteristic (ROC) curve was used as an indicator of the predictive value of the change in the slope of PCr/Pi in detecting tumor treatment.

Results and Discussion

Results

Two treated mice died as the result of the anesthesia and a third was sacrificed because of an eye infection. This compares favorably with the rat mortality rate from moderate to high doses of Innovar-Vet (6%-18%) even though the dose per kg in mice is higher (188-190). Smaller amounts of Innovar-Vet were inadequate in sedating the mice.

Using six to seven consecutive spectra, reproducibility of the spectra and metabolite areas was checked in each of three mice by calculating the per cent standard error:

$$\frac{(Standard\ Deviation) * 100\%}{(Mean\ Area)}$$

The range of the per cent standard error for PME was 7.8% to 14.1%, for Pi 9.0% to 11.1%, and for PCr 3.5% to 9.9%. The range of the standard error for the PCr/Pi ratio was 8.6% to 12.1%. Thus, the reproducibility of the spectral acquisition and peak fitting appears quite reasonable.

We had a final number of 10 untreated mice and 9 treated mice. Representative spectra from an untreated tumor at five days and twelve days post implantation are shown in Figure 3-2. Figure 3-3 is a graph of the time course of the average tumor volume of the treated and untreated mice. Comparison of the three techniques of calculating the volume of the tumors was made by using a paired t-test to test the significance of the difference between the three formulas and the volume measured by water displacement of 36 excised tumors. The ellipsoidal volume formula $(\pi/6)*L*W*D$ underestimated the volume by an average of 0.32 cc (31% of the actual volume), which was statistically significant ($p<0.0001$). The prolate spheroid formula $(\pi/6)*L*W^2$ overestimated tumor volume by an average of 0.21 cc (20%), which was statistically significant ($p=0.04$). The mean of these two formulas underestimated the tumor volume by 0.06 cc (5.6%), which was not statistically significant ($p=0.39$).

A graph of the time course of the average amount of PME is shown in Figure 3-4 for the treated and the untreated mice. PME levels of the treated mice decrease from day 10 to day 14 post implantation (day 1 to day 5 post chemotherapy).

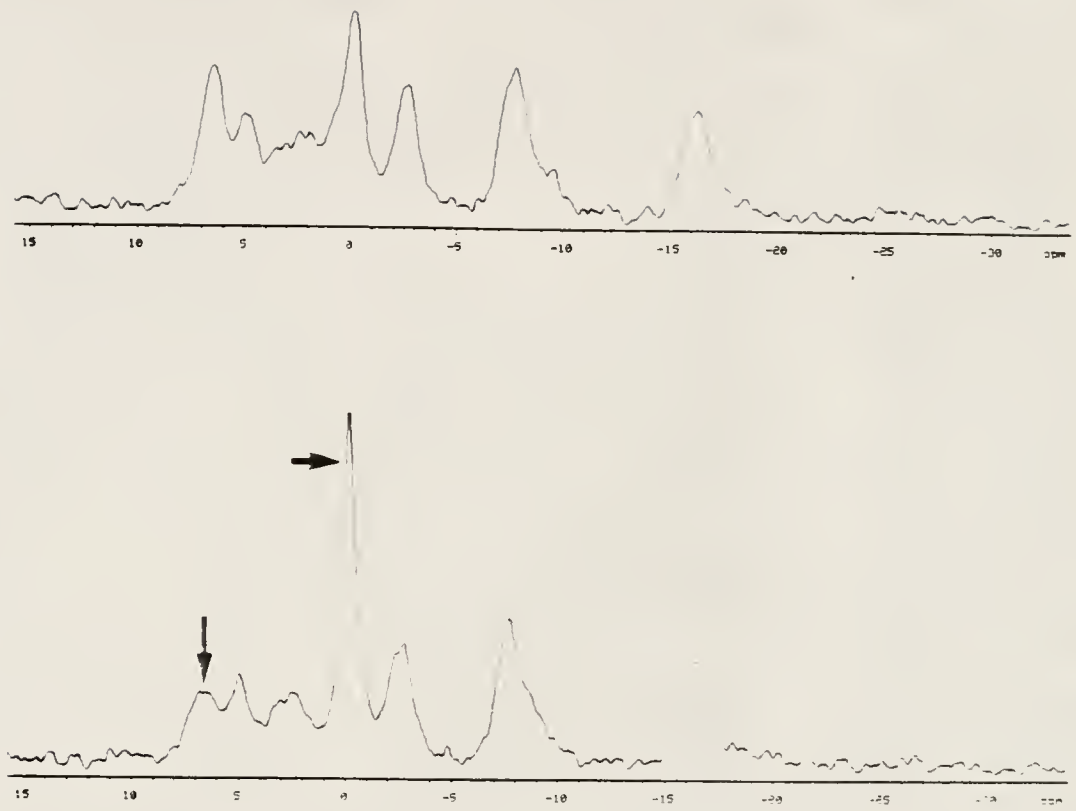

Figure 3-2 Representative spectra from an untreated tumor at five days (Bottom) and twenty-three days (top) post implantation. The PME peak is labeled with a long vertical arrow, the PCr peak with a short horizontal arrow. Note the increase in size of the PME peak and the decrease in size of the PCr peak on day twenty-three.

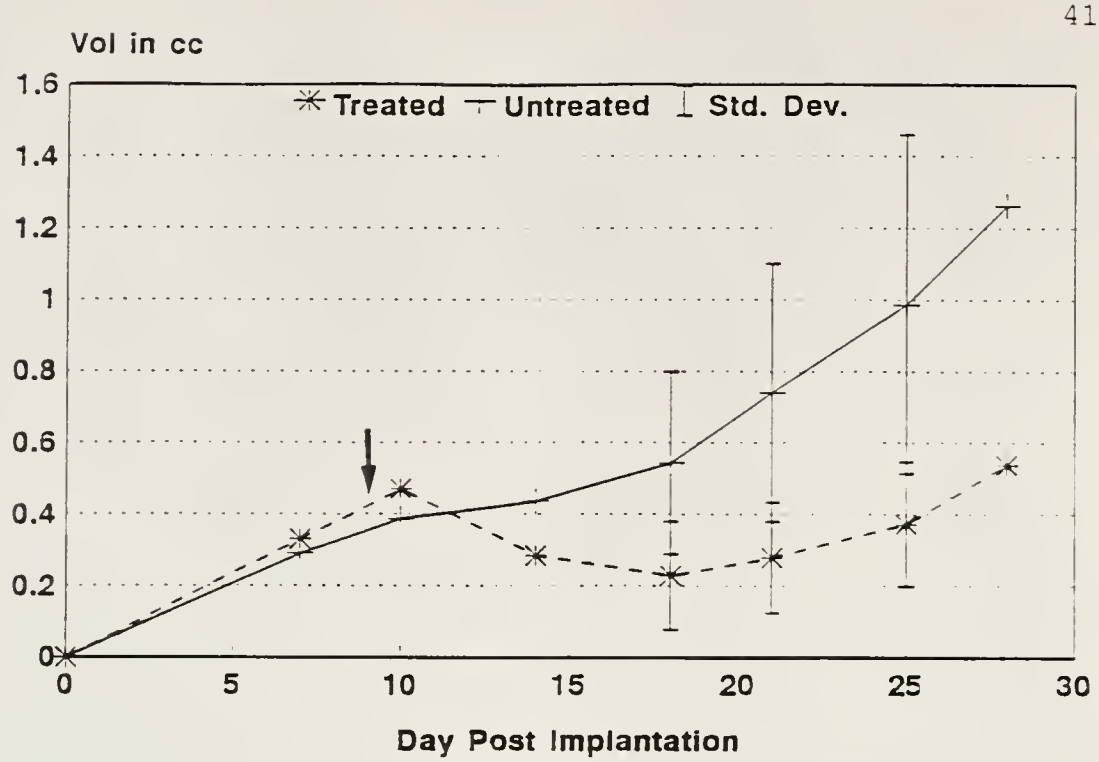

Figure 3-3 Graph of the mean volume of treated and untreated tumors as a function of time. Arrow marks chemo day.

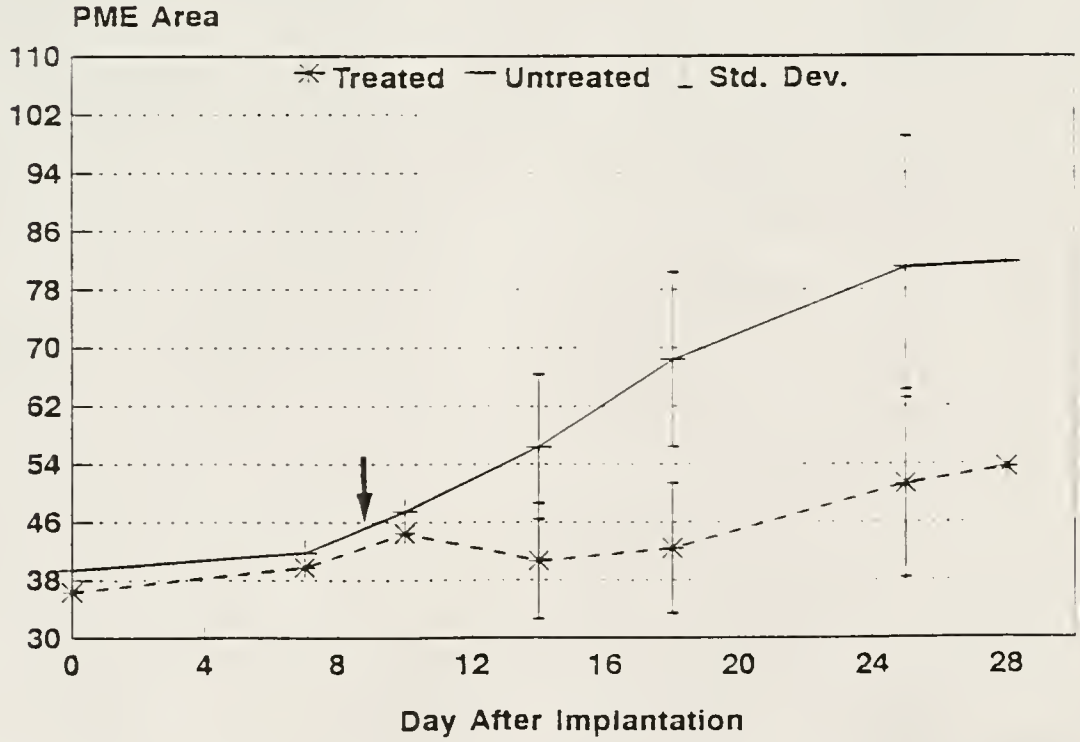

Figure 3-4 Graph of the mean PME of the treated and untreated tumors as a function of time. Arrow marks chemo day.

The changes in Figure 3-4 roughly mirror the changes in volume of the tumors seen in Figure 3-3. PME levels of untreated mice increased or remained unchanged during this period.

Figure 3-5 shows a graph of the PCr/Pi ratio for the treated and untreated mice over time. The posttreatment slope of the PCr/Pi curve for the treated mice shows a significant change (increase) from the pretreatment slope ($p=0.0249$) with a 95% confidence interval of (+0.0669, +0.755). The posttreatment slope of the PCr/Pi curve for the untreated mice does not show a significant change in direction from the pretreatment slope ($p=0.4448$, confidence interval: -0.253, +0.530). During the time that the PCr/Pi slope of the treated tumors changes, the slope of the volume curves does not change (Figure 3-3). Note that the above statistical analysis was not testing directly for differences between the change in PCr/Pi slopes between the treated and untreated tumors. Testing the differences in slope for the same mouse allows use of a paired t-test. The paired t-test, allows use of a smaller number of subjects than an unpaired t-test. The posttreatment slope we have used is from day 7 to day 10 postimplantation, or from two days before treatment to one day post treatment. Ideally, we would want to measure the posttreatment slope from the day of treatment onward. This is not possible for technical reasons and because of the fragility of the mice. An alternative is to project the pretreatment slope to the day of treatment, and use that point as the initial point for the posttreatment slope calculation. This procedure results in little change in the results. The new p value is 0.0303 with an area

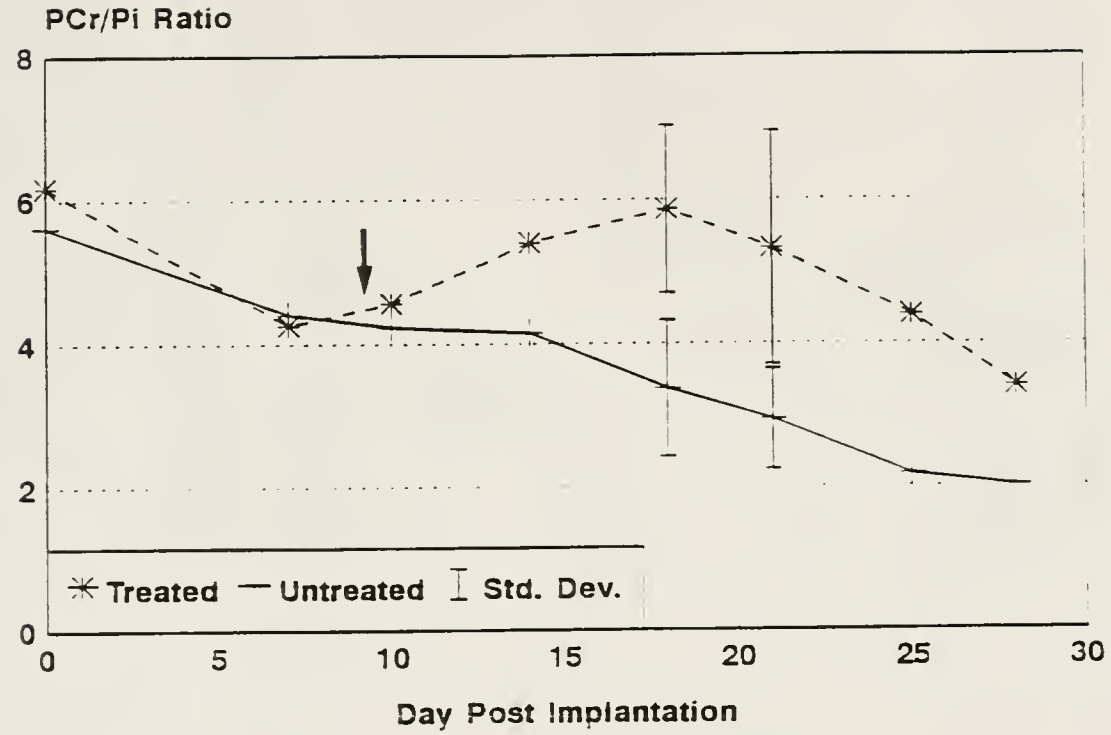

Figure 3-5 Graph of the mean PCr/Pi ratio for the treated and untreated tumors as a function of time.

under the ROC curve equal to 0.723±0.131 (see below for original ROC area).

Sensitivity in this study is the number of detected untreated mice divided by the actual number of untreated mice for a given decision threshold for PCr/Pi slope change. The specificity is the number of treated mice called treated divided by the total number of treated mice. The complementary nature of sensitivity and specificity can be represented with a ROC curve (191-194) as shown in Fig. 3-6.

The sensitivity (true positive fraction) is plotted as a function of 1-specificity (false positive fraction) for detecting an untreated tumor at various levels of PCr/Pi slope change post treatment. The points for our ROC curve were obtained from Charles E. Metz's LABROC1 program that fits binomial curves to the PCr/Pi slope data for the treated mice and from the untreated mice by the maximum-likelihood algorithm (195, 196). A point on the ROC curve is obtained by calculating the area under the binomial curves located to the right of a particular threshold or PCr/Pi value. The calculated areas correspond to the true positive fraction and to the false positive fraction. This process is repeated for several thresholds to obtain the entire curve. A straight diagonal line from the bottom left corner to the top right corner would indicate no predictive value of the test (area=0.5). The larger the area under the curve, up to one, the greater the predictive value or efficacy of the test. In this study we obtained an area of 0.64±0.12. The area under a ROC curve is independent of the position of the decision threshold, unlike accuracy, and may therefore be a better measure of test performance (192).

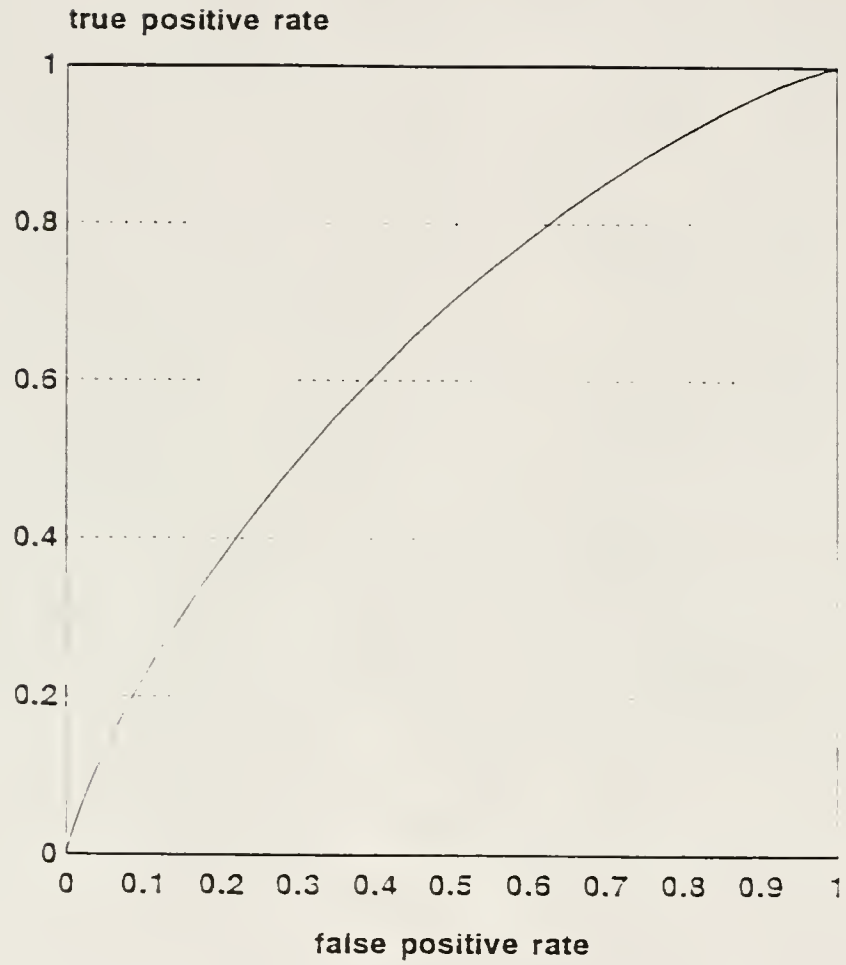

Figure 3-6 ROC Curve for detecting untreated tumors with PCr/Pi ratio. The true positive rate (sensitivity) is plotted as a function of the false positive rate (1-specificity).

Discussion

Our data show a difference in the change of the slope of the PME curves between treated and untreated osteosarcomas implanted into nude mice; however, this PME change occurs simultaneously with the change of the volume of the tumors. The PME changes could be related to differences in the amount of skeletal muscle being volume-averaged from under the tumor rather than actual concentration changes within the tumor. We are currently acquiring data using a slice selective localization technique that will eliminate contamination of our tumor spectrum by underlying muscle.

The PCr/Pi slope changes ($\Delta(PCr/Pi)/\Delta t$) that we see are statistically significant and occur prior to changes in volume of the tumor. There is overlap of the data from these two groups as shown in the figures. We would want to have a high specificity for detecting an untreated tumor (or in humans, a nonresponder to chemotherapy) to avoid discontinuing a treatment that is working. Using a threshold of change in the slope of PCr/Pi equal to -0.63, we obtained an 86% specificity and a 29% sensitivity. Using a decision threshold of 0.40, we can obtain a 60% specificity and a 60% sensitivity. These results will undoubtedly improve with better localization as we will have less of a dilutional effect from skeletal muscle contamination.

Sensitive and Resistant Mice

Materials and Methods

The objective of this experiment was to determine if changes in PCr/Pi and PME can be used to predict lack of tumor response to chemotherapy in a murine model of a chemotherapy-resistant human osteosarcoma.

Introduction

In a previous section, the use of phosphorus NMR spectroscopy (MRS) to compare the changes in phosphocreatine to inorganic phosphate ratio (PCr/Pi) and phosphomonoester (PME) signal from implanted human osteosarcoma in the nude mouse, with and without chemotherapy was described. The accuracy of using post treatment PCr/Pi changes to detect untreated mice was evaluated, and a statistically significant difference between the treated and untreated mice was found. It is hypothesized that a similar difference in the change in PCr/Pi between treated cisplatin-resistant and cisplatin-sensitive human osteosarcomas implanted in the nude mouse will be found.

Tumor cell line characteristics and preparation

The 791T osteosarcoma cell line (Zoma Corp., Berkeley, CA) is a high-grade, non-metastatic tumor cell in humans. The doubling time in vitro is twelve and one half hours. The growth-rate in nude mice depends on the number of cells implanted: 0.4 cc tumors in 40-45 days for 4×10^7 cells and 6-8 days for 8×10^7 cells. In the nude mouse, the tumors can grow to ca. 6 cc, but become very necrotic and ulcerative at this stage. In our study, the mice are sacrificed before the tumors reach 2 cc in size.

Carol Sweeney, Biological Laboratory Technician, cloned the 791T-E10 (E10) cell line from 791T by using limiting dilution cloning, to produce a uniform cell population. Both cell lines grow as monolayers in Dulbecco's modified Eagle medium (DMEM) supplemented with 10% bovine calf serum, 15 mM HEPES buffer, and 2 mM L-glutamine. Drug resistant sublines were derived from E10 cells by intermittent treatment of the cells with increasing concentrations of cisplatin (E10-CIS subline). Cisplatin (cis-diamminedichloroplatinum) was obtained as Platinol (Bristol-Myers U.S. Pharmaceutical and Nutritional Group, Evansville, IN). Cells were seeded in T25 flasks at a concentration of 1×10^4 to 3×10^4 cells/ml; twenty-four hours later they were treated with concentrations of cisplatin in DMEM ranging from 10-22 µg/ml for one hour. The cells were rinsed twice with DMEM and then cultured in fresh DMEM until their numbers reached that of the untreated cells. The concentration of cisplatin chosen for later treatments depended on the length of time it took for cells to recover from the previous treatment.

A modified version of the chromium (Cr-51) release assay, developed by Brunner et al. (197), was used by Carol Sweeney and Jim Scott, Senior Chemist, to measure the short term (<24 hours) cytotoxicity of cisplatin (0 mg/ml - 100 mg/ml) to E10 drug-sensitive and E10-CIS drug-resistant cell lines.

A four-day growth assay was then used to compare the level of resistance of E10 (drug-sensitive) to E10-CIS (drug-resistant) cells beyond 24 hours. 1.8×10^5 cells were seeded on 60 x 15 mm dishes; twenty-four hours later, the cells were treated with varying concentrations of cisplatin in DMEM (0-32 µg/ml). Each

concentration in each cell line and controls was run in triplicate. After one hour, cells were washed once with DMEM, then fresh DMEM was added to all plates. Four days later, cells were trypsinized and counted using a Coulter counter. The concentration of the drug that resulted in 50% cell inhibition after four days (IC_{50}) was determined from a dose response curve.

E10 and E10-CIS were frozen in multiple vials for use in mouse studies so that all mice would receive cells of approximately the same "age" (passage number) and level of resistance. For further information on the cell culture technique see the paper by Blommaert et al. (187).

Animal model

Twenty-one female BALB/c-nu/nu mice, weighing between 20-30 grams, were used for this study. Mice were treated similarly to those used in the treated and untreated study.

When the mice were 7-10 weeks old, and one day after irradiation, a suspension of 6×10^7 E10 or E10-CIS cells in DMEM was injected subcutaneously over the gluteus maximus by Carol Sweeney. The mice were anesthetized with an i.p. injection of Innovar (fentanyl citrate 0.05 mg/ml and droperidol 2.5 mg/ml, Pittman Moore, Washington Crossing, NJ) for implantation (0.05 ml) and for MRS (0.35-0.38 ml) of the tumor site. Innovar is approximately 1/10 the concentration of Innovar-Vet, the later being used for the first mouse study. The change in anesthetic was only because of the lack of availability of Innovar-Vet at the time of the second study. The dose of Innovar was adjusted appropriately to account for differences in concentration.

Each mouse was administered a single injection of 7 mg/kg cisplatin in a tail vein on approximately day 12 post implantation by Carol Sweeney, when the tumor volume reached about 1/2 cc (0.502 cc ± 0.190 cc). The tumors were followed with MRS for at least three weeks post implantation.

Spectroscopy

Spectroscopy data collection and fitting were performed by Haejin Kang, with assistance from Carol Sweeney and J.R. Ballinger, as described in the previous section. In addition, an external standard containing 0.018 cc of 1 M hexachlorocyclotriphosphazene (HCCTP) in benzene was located above the tumor, in the plane of the top of the coil. MRS was performed starting six days before chemotherapy, then twice weekly for three weeks.

Analysis of data

Analysis of the data was performed by J.R. Ballinger. The peak areas were normalized to the external standard to eliminate variability in the data from changes in instrumental sensitivity. The PCr/Pi data were found not to be in a normal distribution by a Shapiro-Wilks test; therefore, a Student's t-test could not be used. Instead, a two-tailed Wilcoxon Rank Sum Test was used to test the difference between the sensitive and resistant mice in the PCr/Pi change from the day before chemotherapy to two days following chemotherapy (three days later). The PME data were tested with both a two-tailed Student's t-test and the Wilcoxon Rank Sum Test. A ROC curve was drawn to show the predictive value of the change in the PCr/Pi slope in detecting the resistant tumors.

Results and Discussion

Tumor cell line

The chromium release assay showed spontaneous release of chromium (2 hours to 24 hours = 5% to 35%, respectively, of total activity) did not differ significantly with drug concentration or cell line. This suggests that the cytotoxic effects of cisplatin at the concentrations tested occurs beyond 24 hours.

Drug sensitivities of the parent and resistant cell lines were compared based on their respective IC_{50}'s determined from the four-day growth assay that was run six times for each cell line (See Table 3-1). The E10-CIS subline was five times more resistant than the E10 parent cell line.

Table 3-1
Results of Four-day Growth Assay

Osteosarcoma Cell Line	E-10	E-10 CIS
Cisplatin Concentration	4.49±0.26 µg/ml	22.56±6.57 µg/ml

Note. Concentration of cisplatin at which the viable cell number is 50% inhibited compared to the cell number of untreated controls (IC_{50}).

Animal study

Two of the cisplatin-sensitive tumors failed to grow well before chemotherapy and were excluded from the analysis. One mouse was sacrificed due to eye infection and weight loss. We had a final number of eight cisplatin-resistant and ten cisplatin-sensitive mice.

Spectra were similar in appearance and quality to those shown in the experiment comparing treated and untreated mice. The mean

volume of the sensitive and resistant tumors as a function of time is shown in Figure 3-7. The graph of the mean PCr/Pi vs time (Figure 3-8) shows a divergence in the slopes after treatment of the tumors. This change in the slope of the PCr/Pi occurs before significant changes in tumor volume. The two-tailed, Wilcoxon Rank Sum Test shows statistical significance at the $\alpha=0.05$ level in the difference between the post treatment slopes for the sensitive and the resistant tumors. The change in the slope of the sensitive tumor from pre- to post-chemotherapy was tested and had a p value between 0.05 and 0.1. The change in the slope of the resistant tumor pre- to post-chemotherapy was not significant with a p value greater than 0.1. Calculating the post treatment slope from the projected value of PCr/Pi at time of treatment resulted in no significant change in these results.

The graph of the mean PME levels vs time (Figure 3-9) showed a transient and statistically insignificant decrease in the slope from day one to day five post chemotherapy in the sensitive tumors, paralleling roughly the change in tumor volume. The resistant tumors showed no change in the slope after chemotherapy.

The ability of the data to detect the resistant tumor may be expressed with a ROC curve as discussed earlier (191-194). The points on the ROC curve (Figure 3-10) were generated using Charles Metz's LABROC1 program that fits a binomial curve to the PCr/Pi data (195, 196). The area under the curve reflects the predictive value of the test with an area of 0.5 indicating no value and an area of one indicating a "perfect" test. Using the post-chemotherapy slopes for the ROC analysis, we obtained an area of 0.6674 ± 0.1249.

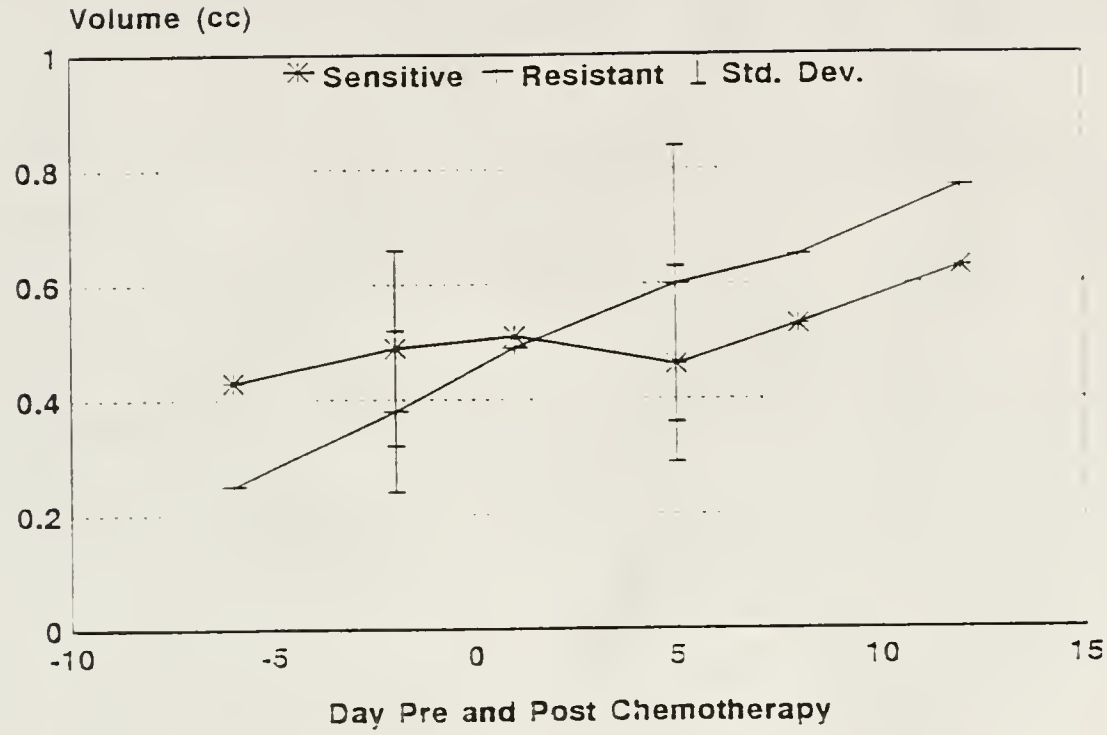

Figure 3-7 Mean change in volume of sensitive and resistant tumors as a function of time. All of the mice received chemotherapy on day zero.

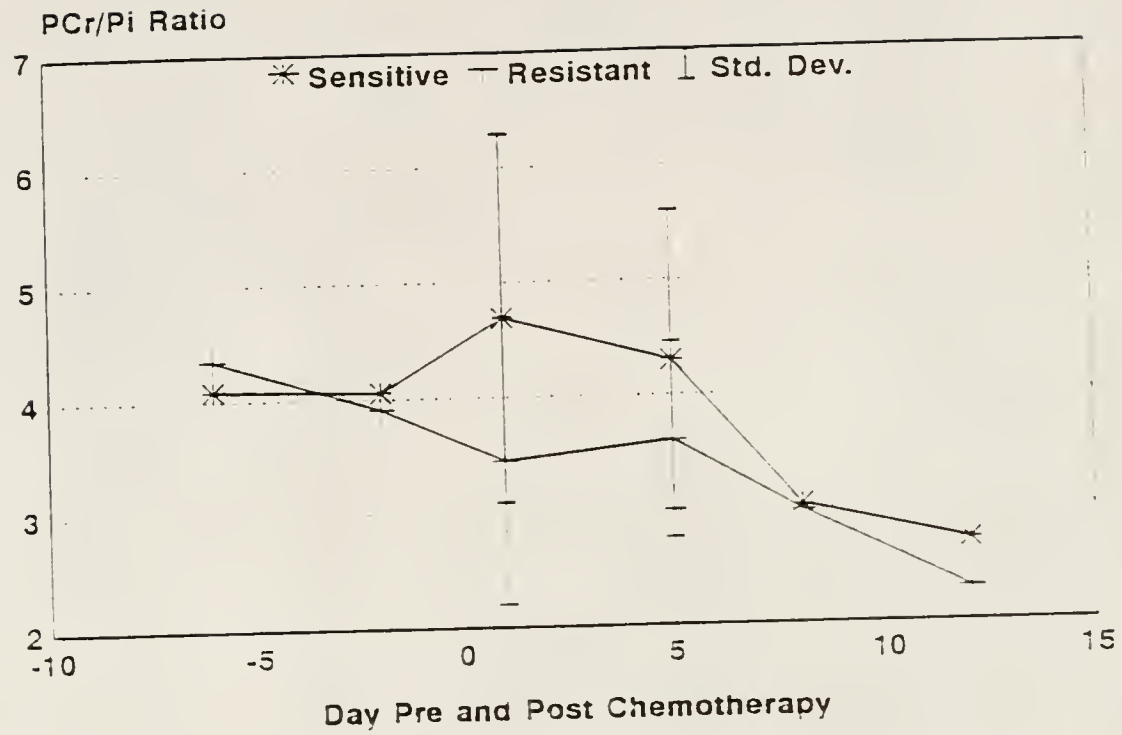

Figure 3-8 Mean change in PCr/Pi for sensitive and resistant mice as a function of time. All of the mice received chemotherapy on day 0. Change in the PCr/Pi ratio is seen as early as day 1 post chemotherapy. This change occurs before any change in the volume of the tumors (compare with Figure 3-9).

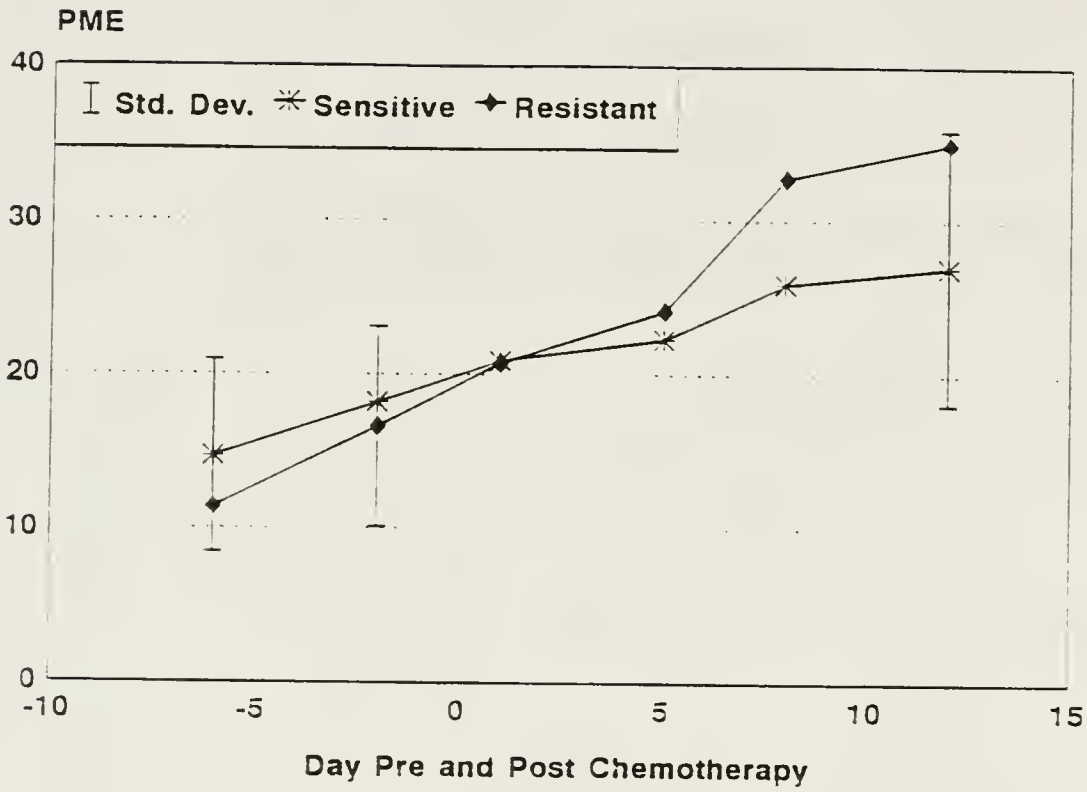

Figure 3-9 Graph of the mean PME ± one standard deviation vs time for sensitive and resistant mice. All of the mice received chemotherapy on day zero.

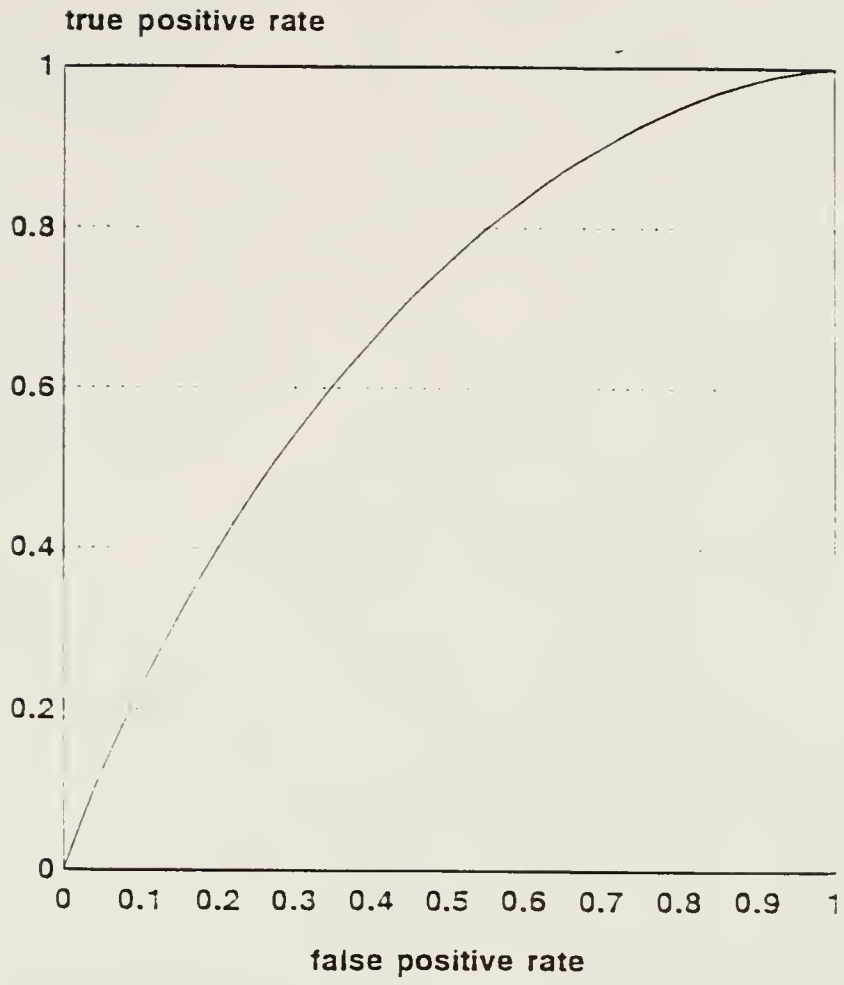

Figure 3-10 ROC Curve for detecting resistant tumors with the change in slope of the PCr/Pi ratio postchemotherapy. The true positive rate (sensitivity) is plotted as a function of the false positive rate (1-specificity).

Discussion

Our data show a slight but statistically significant difference in the change in PCr/Pi after treatment between sensitive and resistant osteosarcomas implanted into nude mice. The PCr/Pi change occurs before change in volume of the tumor. We would want to have a high specificity for detecting a resistant or nonresponder to chemotherapy to avoid discontinuing a treatment that is working. Using the post treatment PCr/Pi slopes to detect the resistant tumor, we can select a threshold that will give us a 70% specificity and a 54% sensitivity. This is similar to our data with treated and untreated sensitive tumors. The minor difference between these two studies is to be expected since there was only a 5-fold difference in drug sensitivity of the two cell lines in vitro. We are currently acquiring data using a slice selective localization technique that may improve our ability to distinguish between sensitive and resistant tumors by diminishing contamination of our tumor spectra by underlying muscle.

P-31 Spectroscopy of Musculoskeletal Tumors in Humans

Materials and Methods

Extensive developmental work has been done with phantoms and volunteers in vivo MRS. Because of the small number of osteosarcoma patients being referred to us and the low signal-to-noise seen in the one tumor patient that had P-31 MRS, we chose to delay acquisition of P-31 spectra from additional patients until after construction of a double-tuned, quadrature H-1/P-31 coil and possibly implementation of proton decoupling of spectra. We were obtaining H-1 spectra from patients that had significantly better

signal-to-noise than the P-31 spectra, and so chose to concentrate on H-1 MRS.

Instrumentation

The 1.5 T GE Signa whole-body magnet was used for phantoms, volunteers, and the patient (Figure 3-11). A half-saddle coil double-tuned to H-1 and P-31 was used for most of the study (54). The coil was constructed by Jim Scott.

Localization development

In the background section, the considerable heterogeneity of tumors was noted. Therefore, we chose to use 2D-CSI for our experiments. This technique gives better spatial resolution than 1D-CSI and is not as time consuming as 3D-CSI. Two problems had to be overcome, the intervoxel bleeding that is inherently present with use of the technique, and registration of the CSI spectra with the image and volume of interest.

The numerical weighting, post processing technique of CSI bleed reduction was used (76) as described in the Techniques chapter. Before FFT, the k-space domain data matrix was multiplied in both directions by the following Hanning equation:

$$W(g) = 0.46[1+\cos(\pi\frac{g}{G})]$$

Where g is the value of the phase-encoding gradient, whose values range from -G to +G. The amount of signal bleeding before and after use of the Hanning function was evaluated qualitatively and quantitatively.

Figure 3-11 Photograph of the 1.5 T General Electric Signa whole-body imager.

CSI and image registration was necessary to know from what part of the tumor or adjacent soft tissues a given spectrum came from. The SA/GE software allows the grid of spectra to be superimposed onto an image for this purpose. Because of differences in the way the images and the CSI data are acquired, flip and translation corrections were needed for an exact match. A left-to-right and top-to-bottom flip were required to match the image and CSI matrix in terms of orientation. A half CSI voxel shift was necessary in both spatial directions because the image localizing and CSI localizing gradients have different symmetry about the x and y axes. The flip and translation corrections were checked with phantoms and volunteers to ensure proper positioning.

Occasionally, a CSI voxel did not fall exactly on the area of interest. The voxel can be shifted by using a first order phase correction on the k-space data in the gradient (not time) dimensions. Susan Kohler, Ph.D., formerly of GE Medical Systems, was kind enough to write a macro for us to do this data manipulation. This macro was also tested on phantoms and volunteers.

Relaxation measurements

T1 relaxation measurements were made on volunteers since we were using a TR on the order of one T1 time of some of our metabolites. Partial saturation experiments were used, varying the TR from 1.6 sec to 11 secs. Data from these experiments were fit with a monoexponential curve using Statistica software (StatSoft, Tulsa, OK).

Shimming

Whole volume shimming on the water peak with H-1 MRS using a hard pulse was initially used in phantoms and in volunteers. The homogeneity obtained was only fair, so a slice selective shimming technique was subsequently used.

Spectral analysis

The CSI experiments use phase encoding gradients turned on after the acquisition 90° RF pulse is applied. In our case, this results in a loss of eight dwell periods (2 ms) of data from the FID. As a result, a large first order phase correction is necessary, resulting in a prominent baseline roll.

This is corrected using the sinc deconvolution technique mentioned in the Techniques chapter. When we first started, this technique had not been automated. I took eight point sine waves with relative frequencies matching those of the major metabolites, Fourier transformed them and added them to the distorted P-31 spectrum. The relative magnitudes of the added functions matched approximately the peak heights of the P-31 metabolites. The absolute magnitudes had to be adjusted empirically. Recently, the sinc deconvolution technique has been automated and included in the SA/GE software.

Reproducibility and linearity

The reproducibility of the signal measurements from phantoms and from volunteers was tested over the short term (~2 hours) and a long term (2-3 months).

The linearity of the signal to the voxel size was checked with phantoms using the CSI technique. We expected to use

different size voxels depending on the size of the tumor and location.

Normalization of data

An external standard containing 2 cc of 0.5 M or 1 M HCCTP was positioned at the base of the coil and used to normalize the data and control for instrumental variation. The CSI volume included the standard in one of the voxels. When the standard overlapped voxels, the shifting technique mentioned above was used to position the signal from the standard in the middle of one voxel. Because we used a half-saddle coil to acquire our data, the sensitivity of the coil to different voxels varied. This positional dependence was corrected for by a factor arrived from measurements of the signal from a large phantom containing a solution of PO_4 in water.

Tumor patient experiment

The single patient that we did was a 75-year old woman with a pleomorphic sarcoma, most consistent with a dedifferentiated liposarcoma, in her leg. We used the double-tuned half-saddle coil described above with the external standard. A localizing T1 weighted SE pulse sequence was used to obtain images through the tumor. At the widest part of the tumor, shimming was performed on an axial slice, 3.0 cm in thickness. Two-dimension CSI was then performed at this slice with a 16 x 16 matrix, 30 cm FOV, 2 sec TR, and two signal averages resulting in an acquisition time of about 17 min. The voxel volume is equal to thickness$[(FOV/matrix)1.6]^2$ where 1.6 is a correction factor for use of the Hanning filter. In this patient's case, this gives us a volume of 27 cc. There were six voxels containing mostly tumor.

Spectra from these voxels were analyzed in the fashion described above. PME was normalized to the external standard with a correction for coil sensitivity differences. The PCr/Pi ratio was calculated.

Results and Conclusions

Localization development

The amount of intervoxel bleed was reduced significantly with the use of a Hanning window. The signal from voxels not containing the phantom represented 31% of the total signal from the standard without the Hanning window and 4.9% with the Hanning window. This was best demonstrated with a small, ~20 cc bottle of 500 mM HCCTP solution.

Good registration of the image and CSI data was obtained. The CSI shifting macro worked well. Figure 3-12 shows a photograph of the CSI data superimposed on an image of a human tumor that we examined with P-31 MRS.

Relaxation measurements

Table 3-2 shows the mean and standard deviation of measurements of T1 time for the P-31 metabolites obtained from calf skeletal muscle of three volunteers:

Table 3-2
P-31 T1 Relaxation Times in Normal Skeletal Muscle

PME	Pi	PDE	PCr	β ATP
3.79±1.31 sec	3.96±0.38 sec	3.34±1.06 sec	3.71±0.26 sec	4.22±0.32 sec

This compares to values from the literature for human skeletal muscle of 4.017±0.90 sec for Pi, 5.52±0.20 sec for PCr

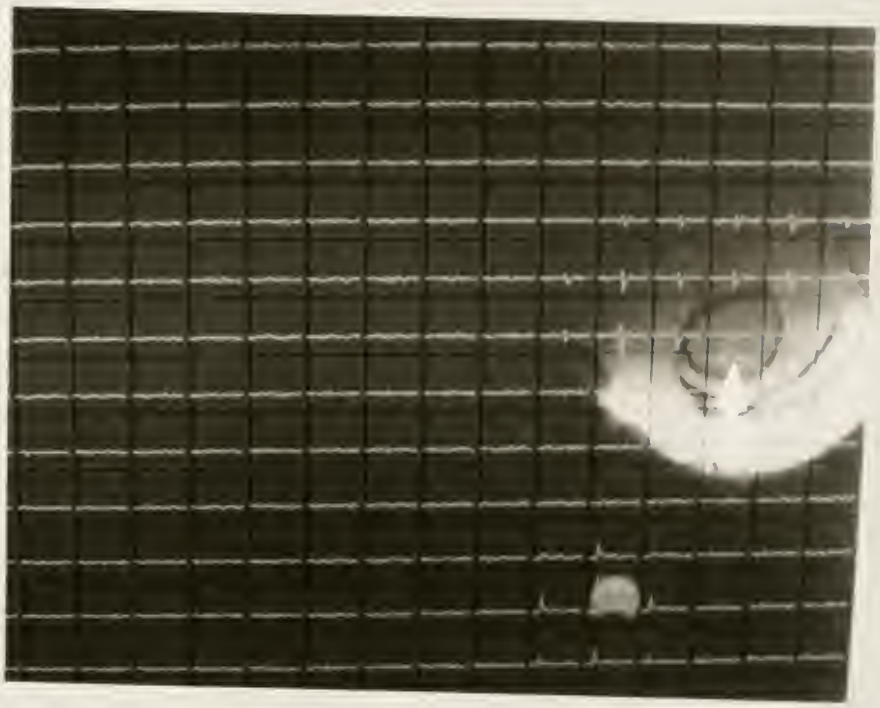

Figure 3-12 Photograph of CSI data superimposed on an axial MR image of tumor. The arrow points to the femur. Surrounding the black cortex of the femur on the left, right and top, is the malignant tumor appearing grey. The white areas below the femur are mostly fat. The small light grey object at the bottom of the photograph is the external standard.

and 4.31±0.60 sec for beta ATP. The values are in good agreement except for the PCr where we get a smaller T1 time. This may be related in part to the fact we went up to a TR of only eleven seconds for the measurements. Eleven seconds was the maximum TR that we could obtain on the whole-body scanner at the time. We expect the tumor T1 times to be different from that of normal muscle. In human brain, tumors have T1's that are about 50% larger than that of normal brain (5). The difference between T1 times in human musculoskeletal tumors has not yet been studied systematically because of the duration of the data acquisition required.

Shimming

With whole volume shimming on the water peak, we obtained line widths of up to 35 Hz from volunteers using the half-saddle coil. With slice shimming the line width ranged from 10-20 Hz in volunteers.

Spectral analysis

The sinc deconvolution of the P-31 spectra was successful in obtaining a flat baseline. Manually, this process took about half an hour per spectrum. The automated method was very quick, though manual adjustments were occasionally necessary, especially with noisy spectra. Figure 3-13 shows a pre and post baseline-corrected spectrum from skeletal muscle of a volunteer performed with 2D-CSI.

Reproducibility and linearity

Short term reproducibility was tested by obtaining six spectra over a two-hour period from a phantom containing 500 mM

Figure 3-13 Pre (bottom) and post (top) baseline-corrected P-31 spectra from the skeletal muscle of a normal volunteer.

phosphate solution. The standard error was 5.0%, probably reflecting instrumental instability.

Long term reproducibility was tested on three human volunteers by obtaining three 2D-CSI acquisitions of calf skeletal muscle spaced over a three-month period. This data will reflect both instrumental variations and physiological variations. The variation was similar for each volunteer and the mean standard error is given in the Table 3-3 for normalized and unnormalized data. The normalized data was obtained by dividing the metabolite signal by the external reference signal, and multiplying by a correction factor for the B_1 differences between the two.

Table 3-3
Variation in Normalized and Unnormalized P-31 Metabolites over Three Months in Skeletal Muscle of Volunteers

	PME	Pi	PDE	PCr	γ ATP	α ATP	β ATP	Mean
Unnormal.	54%	40%	59%	59%	45%	45%	45%	50%
Normalized	33%	13%	36%	9.3%	16%	18%	20%	21%

The normalized spectral data had less variation over time than did the unnormalized data. The smaller Pi peak and the broad PME, PDE, and ATP peaks had greater variation than the tall narrow peak of PCr. The noise contributes to a proportionately larger fraction of the metabolite signal of small, broad peaks, than to larger, narrow peaks. Also, fitting of small or overlapping peaks is more variable.

Linearity was checked by measuring the signal from a phosphate phantom using the CSI technique. Figure 3-14 shows a graph of the PO_4 signal plotted as a function of voxel volume. The

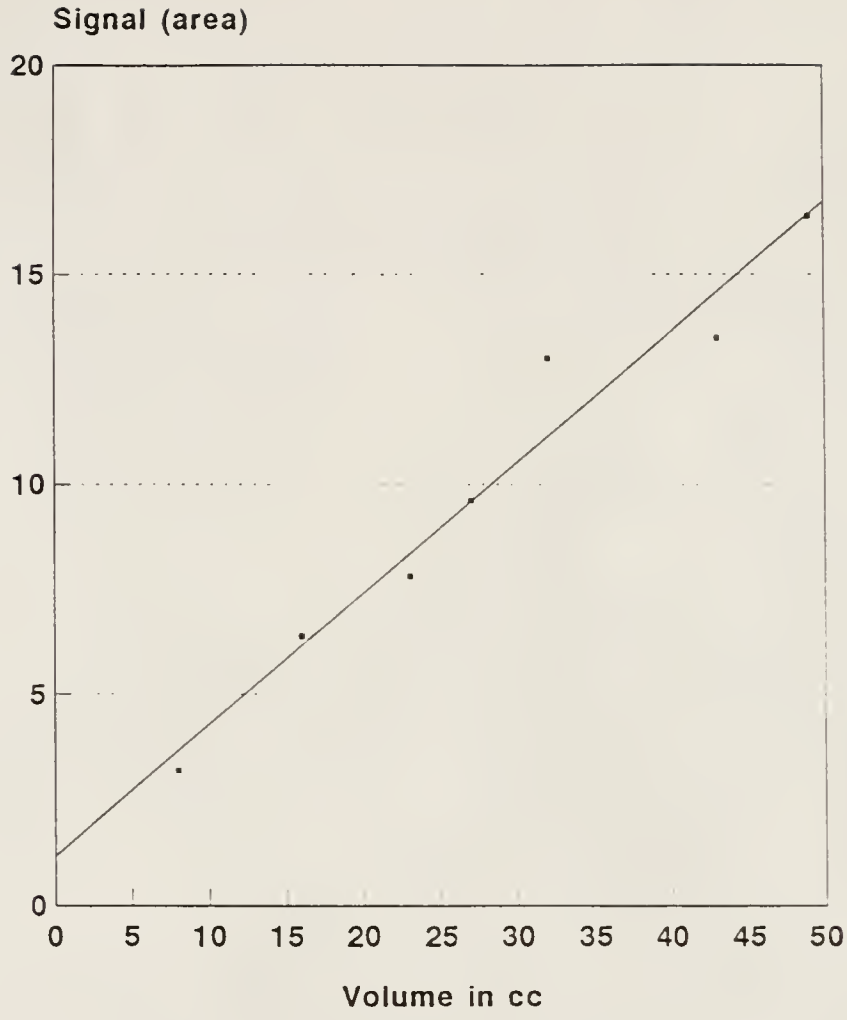

Figure 3-14 Graph demonstrating linearity of the PO_4 signal plotted as a function of the CSI voxel volume.

rity is reasonable considering that we are using a phase
ing technique. The volumes that we use on our patients is
ally on the order of 16 to 30 cc. The regression line fitted
e data intersects the positive y-axis just above the origin
r than through it. This finding may be a result of the
nce of noise in the spectra (estimated to be about 7% of the
signal), as well as the 4.9% bleed from other voxels causing
f the points to be shifted in a positive direction.

patient experiment

The spectra from the single malignant tumor examined (Figure
had worst signal-to-noise than the spectra from our normal
teers (Compare with figure 3-13). Other in vivo
roscopists have reported a similar marked decrease in P-31
olite signal from an osteosarcoma in a human (Personal
nication from William T. Evanochko, Ph.D. from the University
abama at Birmingham). The etiology of this signal abnormality
known. The tumor spectra varied in relative metabolite signal
different locations to a greater extent than spectra from
l muscle. This finding was expected due to tumor
ogeneity. An example of a fitted tumor spectrum is seen in
e 3-16.

A significant difference was seen between the volunteers and
tumor in the following: PME, PCr/Pi, pH, and beta ATP. The
ge and standard deviation of these values over six voxels
ining tumor in this patient and the values from four
nteers are given in Table 3-4.

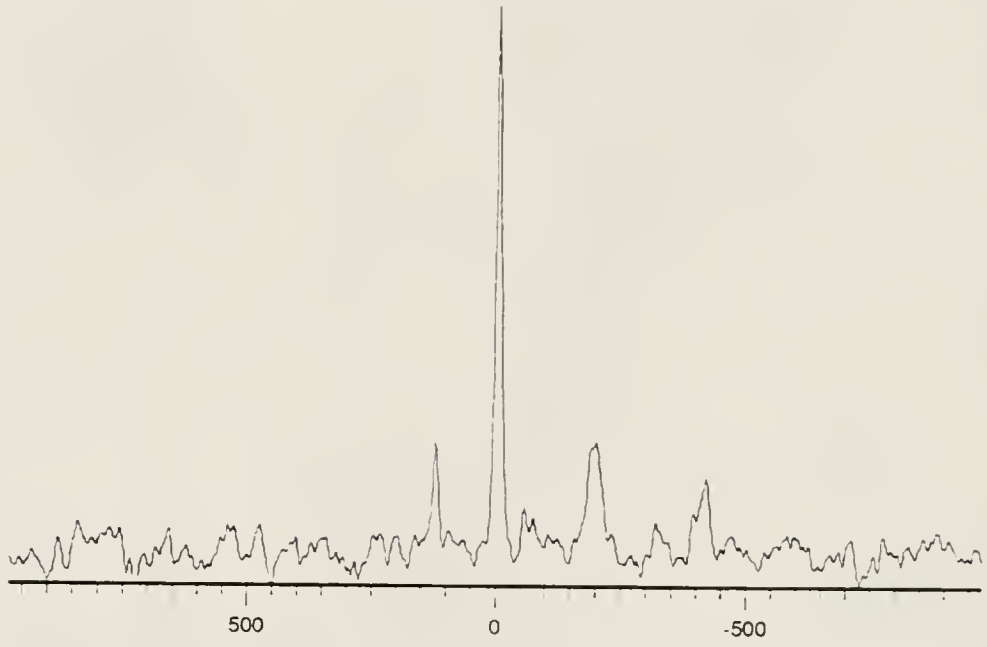

Figure 3-15 P-31 spectrum from malignant tumor in a patient. Note lower signal to noise when compared to a normal volunteer (Figure 3-13).

Figure 3-16 An example of a fitted tumor spectrum from the same patient as Figure 3-15. The spectrum is from a different part of the tumor than that in the Figure 3-15.

Table 3-4
Normalized Metabolite Signal for Tumor and Skeletal Muscle

	PME	PCr/Pi	pH	β ATP
Tumor	23.19±8.53	3.22±1.20	6.99±0.10	31.41±6.18
Volunteer muscle	10.69±4.80	6.27±0.58	7.07±0.04	41.91±9.74

A significant difference in the PME levels($p=0.0107$), PCr/Pi ($p=0.0002$), pH ($p=0.0442$), and β ATP ($p=0.0498$) is seen between the tumor and normal muscle. Statistically significant differences were not seen in the PCr, Pi, and ADP levels because of large variances. It is premature to draw any conclusions from this one patient, except that the elevated PME and depressed PCr/Pi are consistent with the mouse tumor work we have done.

Anesthetic and Temperature Dependence of pH and P-31 Metabolites in Implanted Human Osteosarcoma in Nude Mice

Introduction and Review of the Literature

Innovar-Vet (fentanyl 0.4 mg/ml and droperidol 20 mg/ml, Pittman Moore, Washington Crossing, NJ) is used successfully in this laboratory to sedate the mice for both tumor implantation and for NMR studies. Other anesthetic agents used in mice include pentobarbital, gaseous anesthetics, and ketamine in combination with various sedatives (198, 199). Authors have reported the presence of time dependent temperature and anesthetic effects of pentobarbital and ketamine on P-31 MRS of various tumors including KHT and RIF-1 fibrosarcomas. The anesthetic effects included initial suppression of high energy phosphate levels (PCr and ATP) and are more marked with the use of pentobarbital compared to

ketamine. Reductions of PCr and ATP and elevation of Pi in early spectra of RIF-1 tumors in mice following ketamine anesthesia were observed (166, 200). Similar effects in mice have been seen in RIF-1 tumors (198) and in C3H murine fibrosarcoma and spontaneous mammary carcinoma (201) with sodium pentobarbital anesthesia. A significant upward trend was seen in the pH during recovery from pentobarbital anesthesia in RIF-1 tumors in mice (202). This effect was inconsistently seen in spontaneous fibrosarcomas and mammary carcinomas in mice by other authors (201). Innovar has been shown to cause a 9% increase in proton T2 values in the brain and in proton T1 and T2 of rat kidney (203). No significant change was seen in the relaxation times of muscle, liver, fat, and other organs. A mixture of fentanyl and fluanisome has been used to anesthetize mice with KHT and RIF-1 tumors without change in P-31 metabolite concentrations or pH (204).

The physiological changes associated with Innovar-Vet have been studied extensively in rats and compared with other anesthetics and analgesics (pentobarbital, ketamine-xylazine, and ketamine-diazepam) (188, 189, 205). Innovar-Vet is not a true anesthetic but a combination of a potent analgesic and a major tranquilizer. At low doses Innovar has a low mortality rate, long duration of effect (108 min.), a moderate decrease in mean arterial blood pressure (18%), and the least effect on blood pH, pO_2 and thermoregulation. At high doses of Innovar there is an 18% mortality rate, longer duration of effect (170 min), a 37% drop in blood pressure, and a marked drop in both blood pH and pO_2 (189).

We wanted to determine whether anesthesia with Innovar-Vet would have any effects on temperature regulation or on tumor

metabolite levels in nude mice during NMR studies. Our hypotheses are as follows:

1) That anesthesia with Innovar-Vet causes loss of thermoregulation in nude mice at doses required for immobilization for NMR studies.

2) That a significant difference between the rectal temperature and the skin temperature of mice will be found.

3) That pH in implanted osteosarcoma in the nude mouse exhibits similar temperature dependency as that reported in skeletal muscle of the rat and frog and in heart and brain of humans.

4) That anesthesia effects may be seen in the pH and P-31 metabolites of osteosarcoma.

Methods and Materials

Animal preparation

Twelve female Balb/c nude mice, weighing between 25-30 grams, were quarantined and acclimated to environmental conditions of 27±1 °C and 40-50% humidity for 5-7 days before tumor cell implantation. Laminar flow ventilation and individual air-filter covers over the cages help to maintain an aseptic environment. The mice were provided food and water ad libitum.

A suspension of 6×10^7 cells of the human osteosarcoma cell line 791T (Zoma Corp., Berkeley, CA) was implanted subcutaneously over the gluteus maximus of anesthetized, seven week old mice by Carol Sweeney. The tumors were studied after approximately two weeks. The size of the tumors at the time of spectroscopy, measured with calipers and calculated as the volume of an ellipsoid (pi/6)*L*H*W, was 0.516±0.155 cc.

Anesthesia

The mice were anesthetized with an intraperitoneal injection of 0.04-0.05 ml of Innovar-Vet that was diluted to 10% with normal saline (7 mg/kg). This dose provides adequate anesthesia for one to two hours.

NMR experiments

In the first set of experiments, six mice were injected with anesthetic and positioned in the magnet with no external heating. The temperature in the bore of the magnet was 20.4± 3.0 °C. In the second set of experiments, another six mice were anesthetized, positioned in the magnet, and warmed with 39 °C air circulated through the bore. The mice had a preanesthetic rectal temperature of 36.6±0.5°C. For both groups, spectra were obtained at 15 min intervals starting approximately 30 minutes after injection of the mouse. The 30 minutes were used for sedation, positioning the mouse and shimming. Spectra were obtained for two to three hours after injection with Innovar-Vet.

A third set of experiments was performed with four mice to determine if single mice, placed in the bore of the relatively cold magnet, dropped their temperature without the use of anesthetic. The temperature of the mice was measured at time zero, at 30 min, and at 60 min. The mice were removed from the magnet for about two minutes to measure their rectal temperature at the 30 min and 60 min time points.

The rectal temperature of the mouse was monitored with a fiberoptic probe connected to a Fluoroptic Thermometry System (Luxtron 750), covered with a modified 5 french teflon angiography dilator (Cook, Bloomington, IN). The probe was inserted between

1.5 and 2.0 cm into the rectum. The temperature was measured just before sedation, at the beginning and end of each acquisition, and every 5-10 minutes throughout the spectroscopy session. Besides rectal temperature, skin temperature overlying the tumor was measured with a second probe on three heated and three unheated mice. To measure skin temperature, the tip of the probe was placed so that it slightly indented the skin of the mouse overlying the tumor. The probe was then taped to the coil support. The preanesthetic tumor temperature was 35.2±0.36 °C.

Spectroscopy was performed on a Spectroscopy Imaging Systems Corporation Model VIS 85/310 imaging spectrometer with a 310-mm diameter horizontal bore Oxford Instruments magnet operating at 2T (34.61 MHz for P-31). The spectrometer was operated from and the spectra analyzed on a Sun 3/110 work station (Sun Microsystems, Inc., Mountain View, CA). A home-made, balanced-matched, 2-turn solenoid coil double-tuned to H-1 and P-31 (54), with an internal diameter of 12 mm (constructed by Haejin Kang, Ph.D.) was positioned over the tumor with a fenestrated Faraday shield positioned around the base of the tumor to exclude signal from adjacent muscle (55). The magnet was shimmed on the water peak on each mouse to a line width of 0.2-0.4 ppm. P-31 spectroscopy was performed with a non-selective 12 µsec, 90° three-lobed sinc-shaped RF pulse followed 30 µsecs later by acquisition of the signal. The 90° RF pulse power was set by maximizing the signal from the tumor. The acquisition parameters were: number of points=2000, TR≈2.5 sec, 256 averages, 11 min acquisition time.

Each FID was apodized with 3 Hz line broadening, zero-filled to 4000 points and Fourier transformed. Spectra were fit using the

Fitspec software provided by SISCO following zero-order phase correction. pH was calculated from the shift of the Pi peak from the PCr peak using the method of Kost. This method accounts for the temperature at time of measurement (206). For purposes of pH calculation, an average of the temperature at start and end of the spectrum was used. For measurement of peak areas, each FID was apodized to obtain 10 Hz line broadening to improve the signal-to-noise prior to fitting.

Statistical analysis

In the unheated mice, the pH was plotted as a function of the temperature and fitted with a least-squares linear regression line. In the heated mice, the pH was plotted as a function of the acquisition number and therefore as a function of time. The slope for each group of mice was tested with a t-test to determine if it was significantly different from zero (i.e., that there was a significant dependence on either temperature or time). The Pi, PCr, and ATP peak areas were tested as a function of time in a similar fashion as the pH in the heated mice. In addition, a paired t-test was performed on the first and last peak area for each metabolite for both the heated and unheated mice. A paired t-test was performed on the temperature data from the unanesthetized mice comparing the values at time zero with those at 30 mins and 60 mins.

Results

A marked loss of thermoregulatory ability of all anesthetized mice was seen. Unheated mice experienced a marked drop in temperature (Figure 3-17). One mouse showed a spontaneous reversal of the hypothermia. The unanesthetized, unheated mice showed no

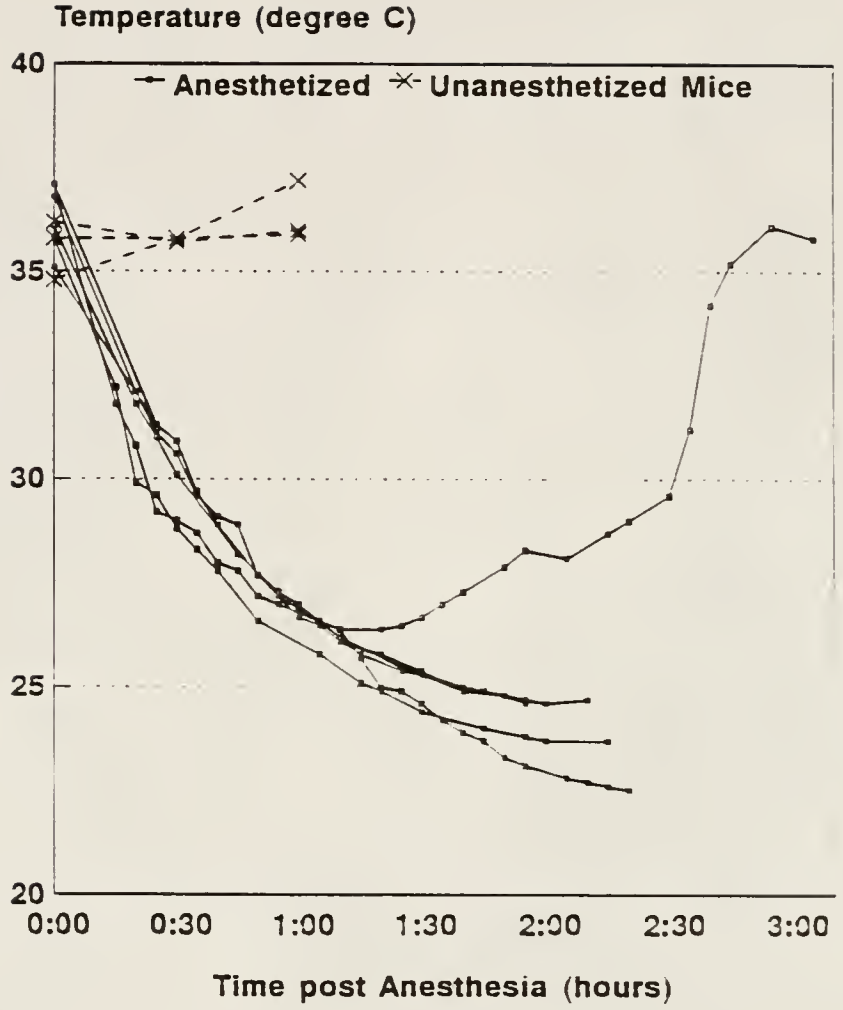

Figure 3-17 Rectal temperature of unheated anesthetized and unheated, unanesthetized mice vs time post anesthesia. One anesthetized mouse showed a spontaneous increase in temperature after about 1.25 hours.

significant decrease temperature at 30 mins (p=0.742, Confidence Interval (CI): (-2.06, 1.73) and at 60 mins (p=0.449, CI: (-4.30, 2.77))(Figure 3-17). The heated mice showed a fairly constant temperature after about 30 mins postinjection of anesthesia. The slight drop in temperature seen before this time (Figure 3-18) occurred while the mice and the coil were being positioned. A heat lamp was used during a part of the initial 30 mins to minimize the heat loss by the mice. The rectal and skin temperatures paralleled each other in both the heated and unheated mice. The mean, standard deviation, and range in temperature difference between the rectal and skin temperatures for the unheated and the heated mice are shown in Table 3-5. The difference between the skin and rectal temperatures was significantly different from zero (p=0.0053) though this difference was small (1.32°C, range 0.4-3.2). The purpose of measuring both the rectal and the skin temperature was to estimate the accuracy of the rectal temperature in predicting the temperature of the tumor itself, where the spectra are obtained. We expected that the temperature of the tumor to be between that of the rectum and skin, since the rectal temperature is close to the core, or highest temperature in the mouse and the skin temperature is the coolest part of the mouse. Since the rectal and skin temperatures were so similar, it is concluded that the rectal temperature is a reasonable estimate of the tumor temperature for purposes of pH measurement.

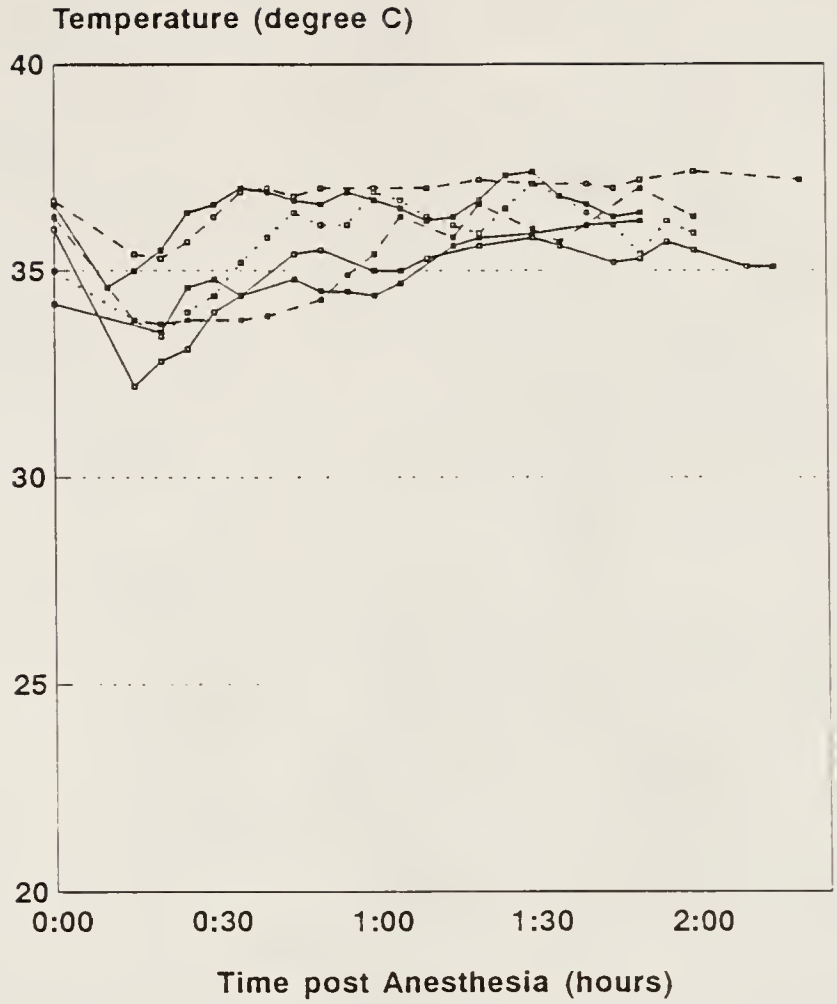

Figure 3-18 Rectal temperature of the heated, anesthetized mice vs time postanesthesia. The slight dip in temperature before 30 mins occurred while the mice and the coil were being positioned.

Table 3-5
Difference Between Rectal and Skin Temperature in Mice

Mouse	Mean Difference in °C	Standard Deviation of Difference	Range of Differences
Unheated 1	2.56	0.44	1.5-3.0
Unheated 2	1.72	0.24	0.4-1.3
Unheated 3	0.81	0.18	0.5-1.0
Heated 1	0.91	0.30	0.4-1.3
Heated 2	1.47	0.95	0.4-3.2
Heated 3	1.43	0.77	0.6-2.9

An insignificant increase in the pH during recovery from anesthesia was seen in the heated mice (Figure 3-19). A significant correlation ($p=0.0021$) between the pH and temperature was seen in the unheated mice (Figure 3-20). The regression lines fitted to the data project to a pH between 6.9 and 7.2 at 36°, like the heated mice, except for one mouse. The reason for this exception is unknown; however, the rectal temperature measurement is highly dependent on the position of the fiberoptic temperature probe in the rectum. Movement of the probe during the experiment might explain this finding. Alternatively, the pH of that particular mouse's tumor might really be 6.5 as regression of the points would suggest. The mice showed an average change in pH of -0.025±0.011 Units/°C (95% CI: (-0.03598, -0.01391)).

Analysis of the peak areas showed no significant change over time in the PCr, Pi, and ATP peak areas (Figure 3-21).

Discussion

Over three years, we have used 86 mice for three to twelve spectroscopy acquisitions each with eight anesthetic fatalities

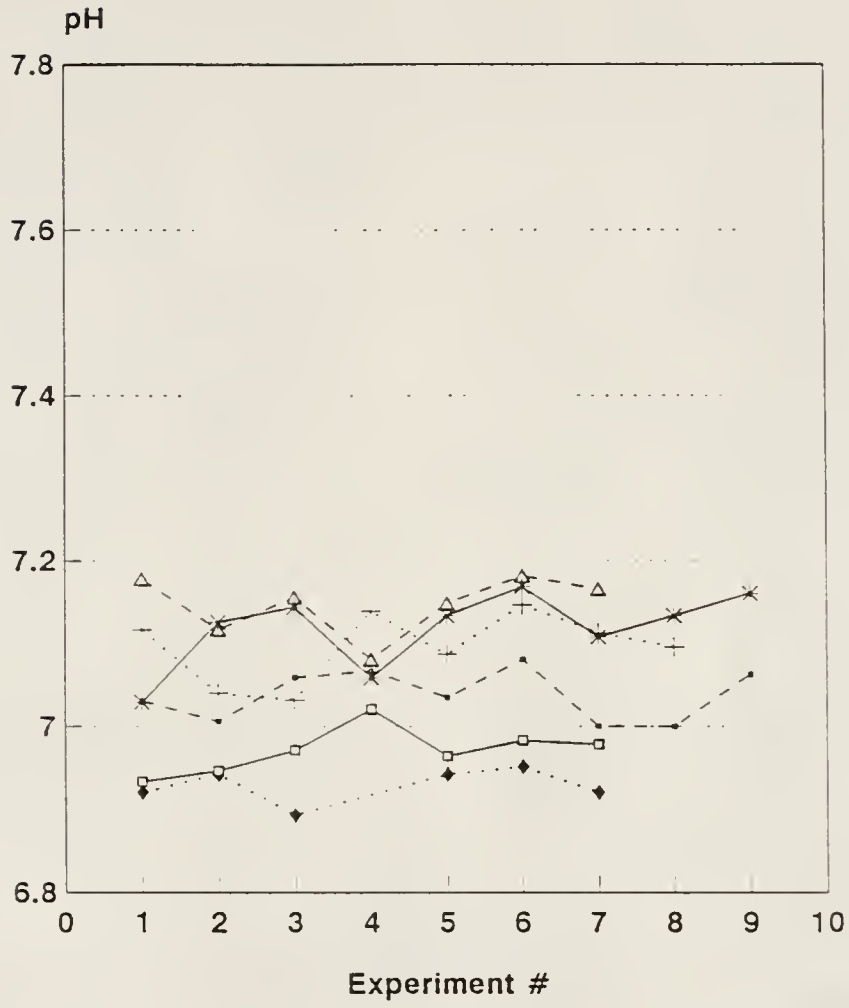

Figure 3-19 Graph of the pH of the six heated mice vs experiment number. Note lack of significant change over time (experiment number).

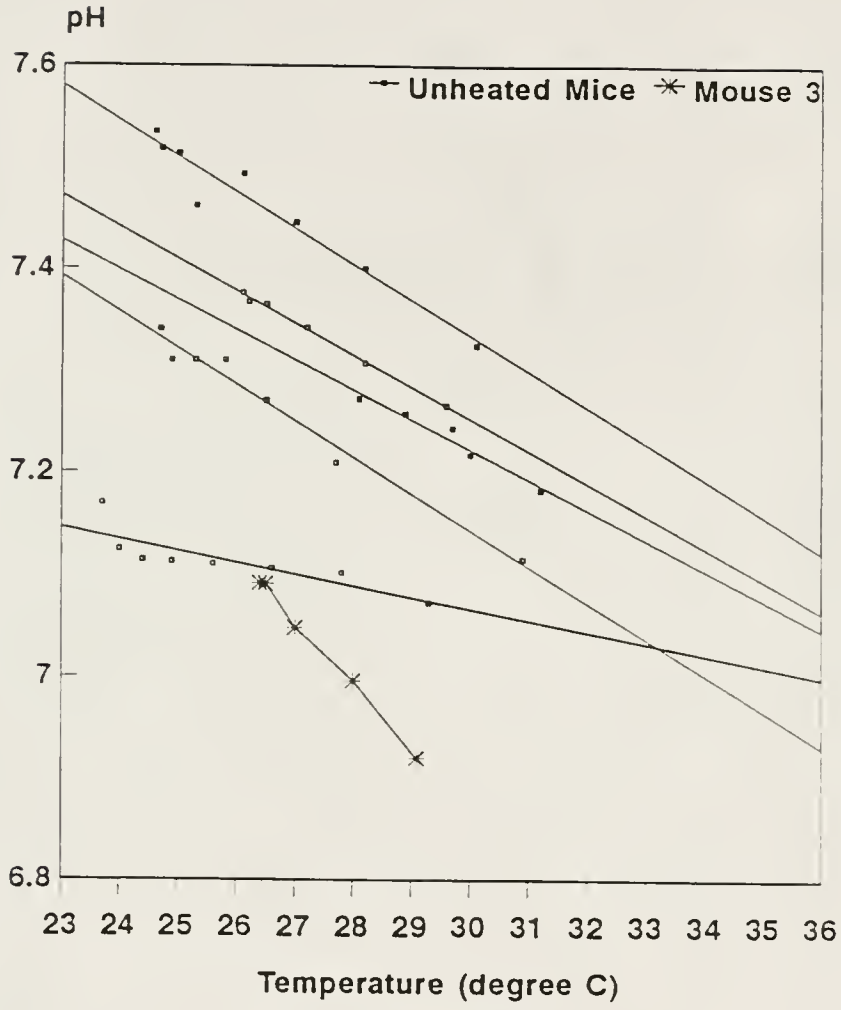

Figure 3-20 Graph of the pH of the six unheated, anesthetized mice vs rectal temperature. Regression lines have been fitted to the data of all but one of the mice. See the text for an explanation.

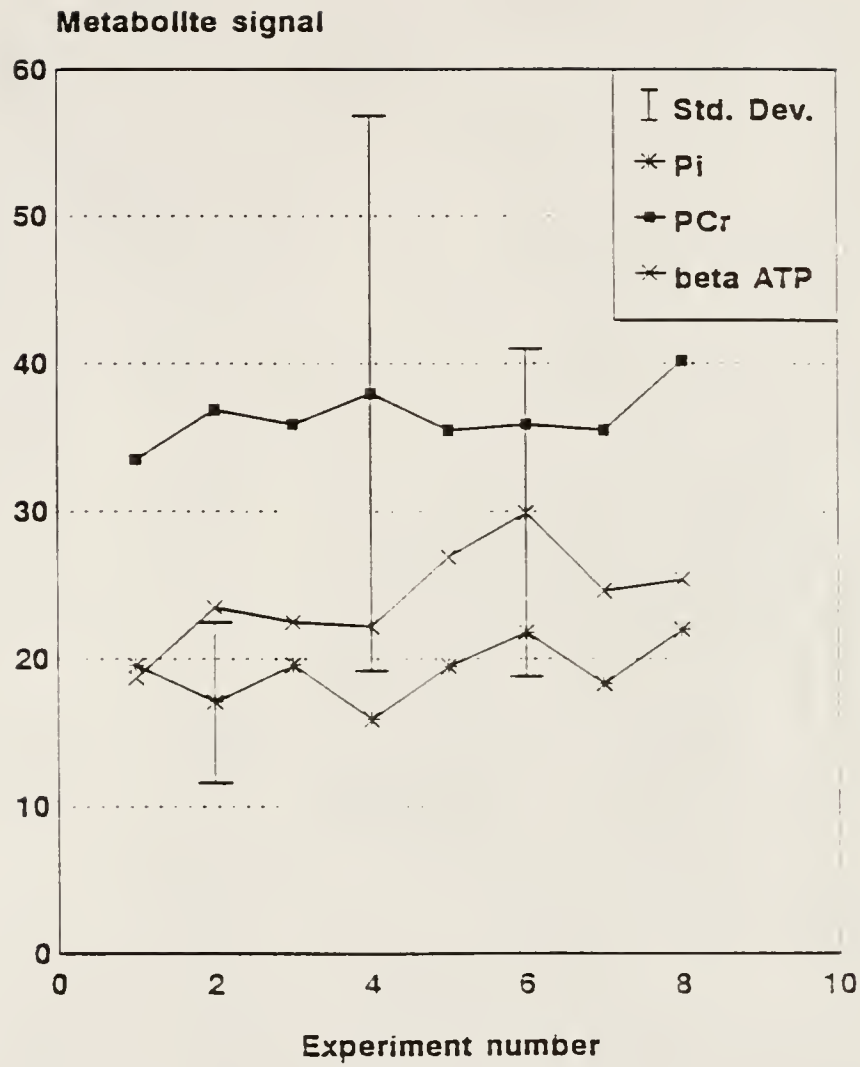

Figure 3-21 Graph of peak areas of the PCr, Pi, and ATP as a function of time. Experiment numbers are at approximately 15 min intervals.

(9%). This compares favorably with the rat mortality rate and duration of effect at low to moderate doses though the dose per kg is higher for the mice.

We have found that, unlike in rats, there is a marked loss of thermoregulation when Innovar-vet is used for sedating the nude mouse. Nude mice lack the thick fur of rats and have minimal subcutaneous muscle, unlike the rat. These differences and also the size discrepancy between the nude mouse and the rat may explain the thermoregulation differences.

A small but statistically significant difference between the temperature measured from the skin overlying the tumor and from the rectum was found. For purposes of calculating the pH this difference has a minimal effect. The mean difference in pH calculated using the two temperatures was 0.0058±.0045 units for the unheated mice and 0.0032±.0019 units for the heated mice.

The temperature dependency of pH has been explained and modeled using a buffer system involving carbonic acid and histidine-imidazole groups (207-209). The pH is directly related to the pK_a of the buffer system. The temperature dependence of the pK_a can be expressed by the van't Hoff equation

$$pk_1 - pK_2 = \frac{\Delta H}{4.576} * \left(\frac{1}{T_1} - \frac{1}{T_2}\right)$$

where delta H is the heat of ionization (cal), T_1 and T_2 are absolute temperatures, and 4.576 is ln 10 times the gas constant, R ($cal*deg^{-1}*mol^{-1}$) (210). This temperature dependency is nonlinear; however, over a small range of temperatures, it can be approximated by a linear function.

A temperature dependency of the pH was demonstrated in this study. The mice showed a mean change in pH of -0.025±0.011 U/°C with a 95% CI: (-0.03598, -0.01391). The confidence interval covers the range noted for sheep brain (-0.015 U/°C) and heart (-0.018 U/°C) during hypothermia (211). Blood and skeletal muscle pH temperature-dependence in cold-blooded vertebrates has been reported in a range of -0.010 U/°C to -0.031 U/°C (207, 210, 212).

Conclusions

We found that anesthesia with Innovar-Vet causes marked loss of the thermoregulatory ability of the nude mouse at doses required for immobilization for one to two hours. With this drop in temperature of the mouse there is an increase in the pH of the tumor as measured with P-31 NMR. This increase in pH is 0.025±0.011 units per °C drop in temperature and compares favorably to measurements of other tissues in other animals. We also found a statistically significant but small difference between the rectal temperature and the skin temperature of the mice (1.32 °C). No significant anesthetic effect was seen on the pH or on the metabolite levels. Innovar-Vet appears to be a useful sedative for nude mice during P-31 NMR experiments.

CHAPTER 4
PROTON SPECTROSCOPY OF MUSCULOSKELETAL TUMORS

Review of the Literature

The literature on abnormal H-1 spectra in tumors is limited primarily to brain tumors and a few soft tissue tumors (see below). In vivo H-1 spectroscopy noninvasively measures the levels of many important metabolic substances. These include free amino acids (glutamate and glutamine (Glu), taurine, alanine, and aspartate) N-Acetyl aspartate (NAA), lactate, γ-aminobutyric acid (GABA), inositols, choline, and creatine/phosphocreatine (91). Elevated levels of glucose have been measured in spectra from the brain of diabetic patients with hyperglycemia (213).

Important peaks in tumor spectra include creatine/phosphocreatine (Cr), choline/phosphocholine (Cho), taurine (Tau), and lactate (Lac). Creatine is phosphorylated to PCr and used as an energy source to replenish ATP. Cho is released from the breakdown of phosphatidylcholine found in membranes. Cho is salvaged and reused by the action of choline kinase, converting it to phosphoryl choline. It is then converted to phosphatidylcholine and incorporated into new membranes (151). Inositol is also converted into a membrane phosphoglyceride, phosphatidylinositol. Tau is found in abundance as a free amino acid in proliferating cells that are rich in membranes and that generate oxidants, such as fetal and neonatal brain, retina,

lymphocytes and lymphoblastoid cells. Tau stabilizes membranes by controlling water and ion permeability of membranes and by acting as an antioxidant (214). The concentration of Tau is elevated in malignant tumors such as RIF-1 tumors in mice (215, 216) and colon tumors in humans (217). Treatment of HeN4 fibrosarcomas in mice with tumor necrosis factor has been shown to cause a 1.6 fold decrease in Tau as demonstrated with extract studies using H-1 MRS (218). Lactate is formed during anaerobic glycolysis (utilization of glucose or glycogen for energy without oxygen) and is found near and within areas of necrosis. Rapidly growing, high grade malignant tumors outgrow their blood supply resulting in anaerobic conditions. H-1 MRS reflects physiological and metabolic processes, and may show very early spectral changes, possibly providing information on biological responses of tumors to therapy.

Current status, H-1 MRS

The use of H-1 MRS in bone tumors has been reported only recently. A few soft tissue tumors, a leiomyosarcoma, a liposarcoma and several malignant fibrous histiocytomas (MFH), have been examined in humans with H-1 MRS (23, 219, 220). In all cases, absence of the Cr signal is seen. Cr is seen in spectra of normal skeletal muscle. No muscle spectra are shown in these reports, so it is uncertain if absence of the Cr peak is a characteristic of the MFH tumor, related to necrosis, or secondary to technical problems such as poor B_0 homogeneity resulting in confluence into the adjacent Cho and Tau peaks. In one MFH, absence of the Cho peak is also noted. This may be related to necrosis of the tumor. There is no mention of the Cho or other

peaks in the three other cases. H-1 spectra of implanted RIF-1 tumors in mice show increases in the Lac, Tau, and Cho peaks and decrease in the Cr peak (58, 166).

Shifts in the 7.2 ppm H-1 peak of endogenous anserine (methylcarnosine or beta-alanyl-N-3-methyl histidine) in frog gastrocnemius muscle (221, 222), and the 8.2 ppm peak in rat gastrocnemius muscle (223), rat thigh muscle (224), and human quadriceps muscle (225) have been correlated successfully with pH. Comparison of pH measurements in rat muscle using Pi position with P-31 and anserine position with H-1 MRS found no significant differences (226). The chemical shift of a resonance is sensitive to changes in pH when the nucleus involved is intimately associated with an acidic or basic group with a pK_a near the local pH (227).

There are H-1 spectroscopic findings reported from more than 250 human brain tumors (8, 28-30, 228-233). These studies consistently show increased Cho/Cr ratios and decreased in N-acetyl aspartate (NAA). NAA is considered a marker for normal, mature brain cells (neurons). Lac is usually present in high grade tumors and in any grade of tumor with necrosis. One study (29) compares P-31 and H-1 spectroscopy of three astrocytomas and finds an association between elevated Lac and elevated pH. Lac is also seen in low grade astrocytomas that are not necrotic. In skeletal muscle elevated Lac is associated with acidosis, rather than alkalosis as here. It has been suggested that the disassociation between Lac and pH may be related to the contribution of Lac to intracellular pH regulation in the brain (29); however, the pK_a of lactate is 3.08 (234) making it an unlikely contributor to pH

regulation. An alternative explanation of the coexistence of high pH and high Lac could be the presence of microscopic heterogeneity of the tissue within the spectroscopic voxel. Similar abnormalities in the Cho, Cr, NAA, and Lac are seen in animal models of brain tumors (235). Parallel H-1 and P-31 spectral findings in brain tumors are: 1) decreased Cr and PCr; 2) increased Cho and PME; and 3) increased Lac and pH.

We hypothesize that the parallel findings seen in H-1 and P-31 spectra from brain tumors can be extrapolated to musculoskeletal tumors. Before therapy, we expect to see high levels of Cho, low levels of Cr and high levels of Lac in H-1 spectra when compared to muscle. Following therapy, decreased Cho and possibly an increase in Cr is expected as a response. Lactate is expected to increase or remain unchanged. Long term decrease in Cho is expected to be associated with >90% necrosis.

Advantages of H-1 over P-31 spectroscopy

1) A wide range of compounds is seen with H-1 MRS that are not accessible to P-31, e.g., amino acids, ketone bodies, fats, and lactate. The elevation of the Cho in malignant neoplasms has been discussed. The presence of Lac in tumors reflects oxygen lack, ischemia, or increased energy demand (236). The amino acid glutamine is used as fuel for metabolism in cancer cells. Glutaminolysis is considered a marker of rapidly dividing cells (161).

2) The greater signal from H-1 spectroscopy allows the use of smaller voxels, and a shorter acquisition time. The smaller voxels allow more homogenous sampling, especially with the use of chemical shift imaging. Significant heterogeneity of P-31 spectra

within individual assorted sarcomas has been reported (237), suggesting the necessity for small voxels. A shorter acquisition time decreases the chance of patient motion, improves patient comfort, and potentially decreases the cost for machine time.

Disadvantages of H-1 MRS

1) ATP has not been detected with in vivo H-1 MRS at 1.5 T. ATP is important as the immediate source of energy for most metabolic processes. Decreased levels are found in tumors with reversal following effective treatment. ATP has been identified and quantified by H-1 MRS in human skeletal muscle at 4.1 T (171). The higher field strength improves the S/N and increases the chemical dispersion.

2) The Cho peak represents both precursor and breakdown products of cell membranes and organelles. PME and PDE are indistinguishable with H-1 MRS. This is probably not a serious problem, as the PME and PDE peaks show similar changes in implanted osteosarcoma in mice (158).

3) The water signal in vivo is approximately 1000 times that of the metabolite signals. This makes water suppression techniques a requirement for H-1 MRS. Several water suppression techniques have been successful with in vivo H-1 MRS (See Water Suppression in the Techniques chapter.

4) Lipid signals may mask the Glu and Lac signals of interest if subcutaneous or perivascular fat is included in the voxel. Fortunately most tumors will displace the fat rather than engulfing it. An inversion pulse has been used with 1-D CSI and surface coil H-1 MRS to suppress the fat signal, analogous to inversion recovery sequences in MRI (113, 238). This method takes

advantage of the short T1 of fat compared to metabolites but results in ≈30-40% reduction in metabolite signal (238). With accurate localization techniques and small voxels, we may not need to suppress the fat signal.

Mouse Study

Materials and Methods

Coil construction

A 3-turn, balanced-matched solenoid coil tuned for H-1 spectroscopy on the 2 T spectrometer was constructed. The coil itself was made of 1.3 mm Cu wire wound to a diameter of 1.7 cm. The circuit diagram of the coil is shown in Figure 4-1. C1 and C2 are nominally 0-30 pF variable capacitors used for tuning and matching the coil respectively, and C3 is a 2.4 pF capacitor. The C2 capacitance is close to 2.4 pF, optimizing the efficiency of the coil (239).

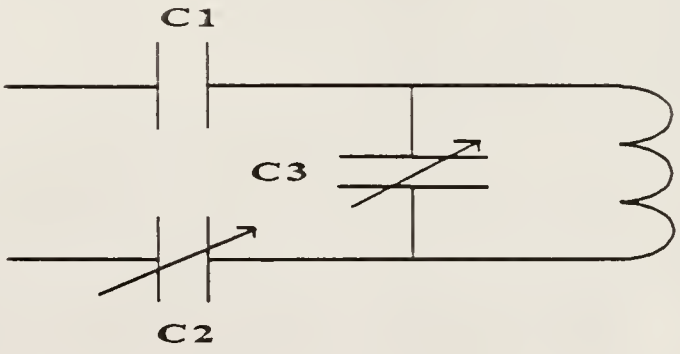

Figure 4-1 Diagram of RF coil used for H-1 MRS and MRI of mouse tumors in the 2 T spectrometer.

Shimming and localization development

Initial phantom studies were performed with a spin echo sequence (TR=2 sec), using the coil to localize only. A Faraday shield was added for the mouse spectroscopy. Later, localization was improved with a slice selective spin echo pulse sequence (Figure 4-2).

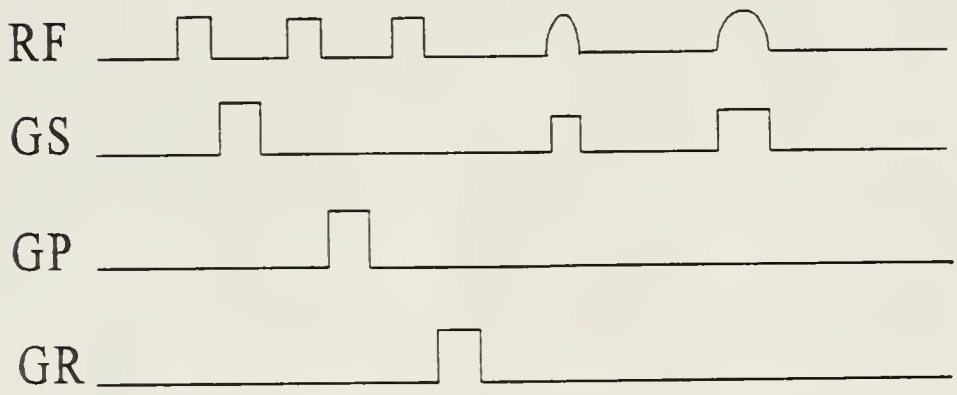

Figure 4-2 Diagram of slice-selective, SE pulse sequence with three CHESS water suppression pulses for H-1 MRS of mouse tumors.

A STEAM localization sequence was not available on the 2 T magnet at the time, so experiments with nine mice were performed on the Signa whole body imager, using a 3-inch proprietary surface coil and a STEAM sequence with three CHESS water suppression pulses. A water bag containing 0.3 normal saline was place over the tumor to eliminate possible susceptibility effects at the tumor-air interface. This was done on the Signa whole body imager. The PRESS sequence was used on two of the mice to improve the signal from the tumors. The spectroscopy volume was positioned graphically after an image of the mouse tumor was obtained. The voxel was $(6\ mm)^3$ and was positioned within the tumor. Signal was averaged for 512 to 768 acquisitions with a TR=2 sec and a TE=30-80 ms. Data processing of the spectra acquired from the whole body scanner were processed with the GE SA/GE software as described previously.

The water bag was tried once in the 2 T spectrometer with the original coil constructed, however the coil geometry and difference in matching were a problem. The fact that susceptibility effects are greater at higher field strength may have contributed to the difficulty.

Water suppression development

The spin echo pulse sequence on the 2 T spectrometer was modified by adding a frequency selective RF (CHESS) pulse and dephasing gradients to perform water suppression. Subsequently, two and then three CHESS pulses were added. One or two dephasing gradients were turned on after each RF pulse and the amplitudes of the gradients varied to prevent undesirable stimulated echos from forming. In addition, the TE was varied between 30 ms and 272 ms

to eliminate lipid and residual water signal, since the metabolites of interest (Cho and Cr) have longer T2 times than water and lipid.

Mouse tumor imaging

At first, some difficulty was encountered in determining the tumor-muscle boundary at the bottom of the tumor with a T1 weighted (TR=0.5 sec, TE=30 ms) spin echo sequence when doing localized P-31 studies previously. A T2 weighted, SE sequence with TR=2.5 sec, TE=70 ms, 128 phase encoding steps, and one average was used. This improved the contrast between the tumor and muscle compared to the T1-weighted sequence but suffered from low signal-to-noise (S/N) and took over 5 min to perform. It was then decided to try a paramagnetic i.v. contrast agent to improve the tumor-muscle boundary delineation. Carol Sweeney injected 0.02 cc of Gadolinium-DTPA (0.2 mM/kg, Magnevist, Berlex Laboratories) into a tail vein of the mice after obtaining unenhanced images. This was done on two mice on separate occasions. The T1 weighted spin echo imaging sequence used the following parameters: TR=0.5 sec, TE=30 ms, 128 phase encoding steps, and one average.

Results and Discussion

Coil construction

The Q factor of the loaded, 3-turn, solenoid coil used for H-1 spectroscopy on the 2 T spectrometer, determined with a Hewlett Packard 8752A network analyzer, was 125-130. This coil was tested with phantoms and with mouse tumors and performed well in terms of S/N and uniformity of the B_1 field as determined qualitatively with H-1 images.

Localization development

Initial phantom studies using localization with the coil gave a line width as small as 5 Hz. When localizing the mouse tumor with the coil and a Faraday shield, the line width of the spectral peaks (30-40 Hz) was too large for proton spectroscopy in spite of shimming. The chemical shift between the Cho and Cr peaks at 2 T is 14 Hz so we need a line width of about 15 Hz or less to resolve them well. Localization with a slice selective pulse sequence, parallel to the surface of the mouse (i.e., perpendicular to the y-axis), resulted in a 30% improvement in the mouse (18-28 Hz). Figure 4-3 shows spectra with and without water suppression from a mouse acquired on the 2 T spectrometer.

Localization of the mouse tumor with the STEAM sequence on the whole body magnet was successful, but suffered from a low SNR. The 20-30 min required to obtain good signal resulted in some degradation of the peak resolution in some of the spectra, perhaps from instability of the transmitter frequency over time or, more likely, due to the mouse waking up from the anesthetic and moving. A water bag was placed around the tumor to avoid broadening of the line width from susceptibility effects that occur at the soft tissue-air interface. This resulted in significant improvement of the line width, dropping from 15-18 Hz down to 8-13 Hz. The PRESS sequence helped the SNR considerably (Figure 4-4).

Water suppression development

Water suppression using the 2 T spectrometer with one CHESS pulse resulted in about a 10 fold decrease in the water peak. Two CHESS pulses gave a 30-70 fold reduction in the water peak. Water suppression with 3 pulses resulted in a 110 fold decrease, which

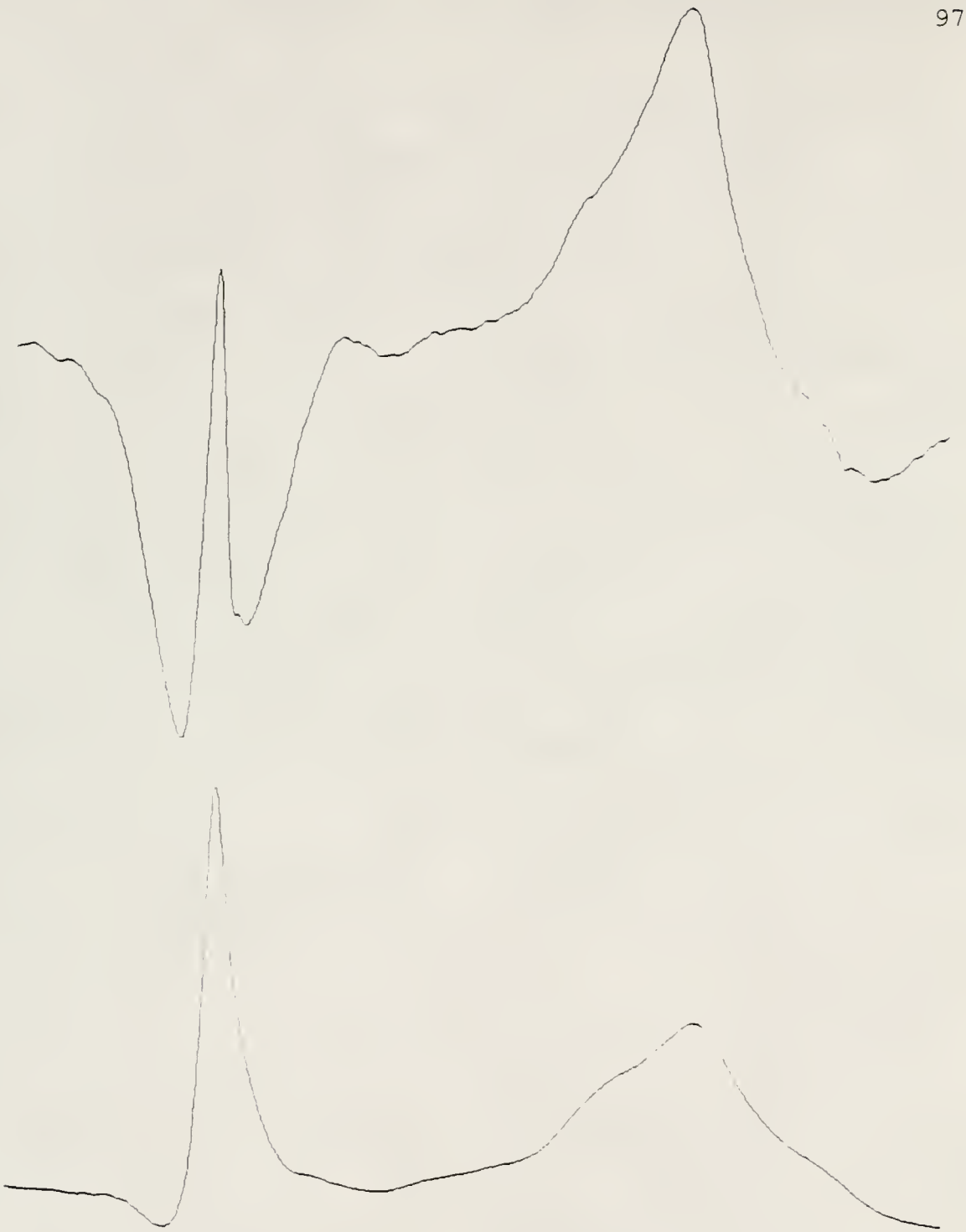

Figure 4-3 H-1 spectra from mouse tumor acquired on 2 T spectrometer. The top spectrum is with water suppression; the bottom spectrum is without water suppression.

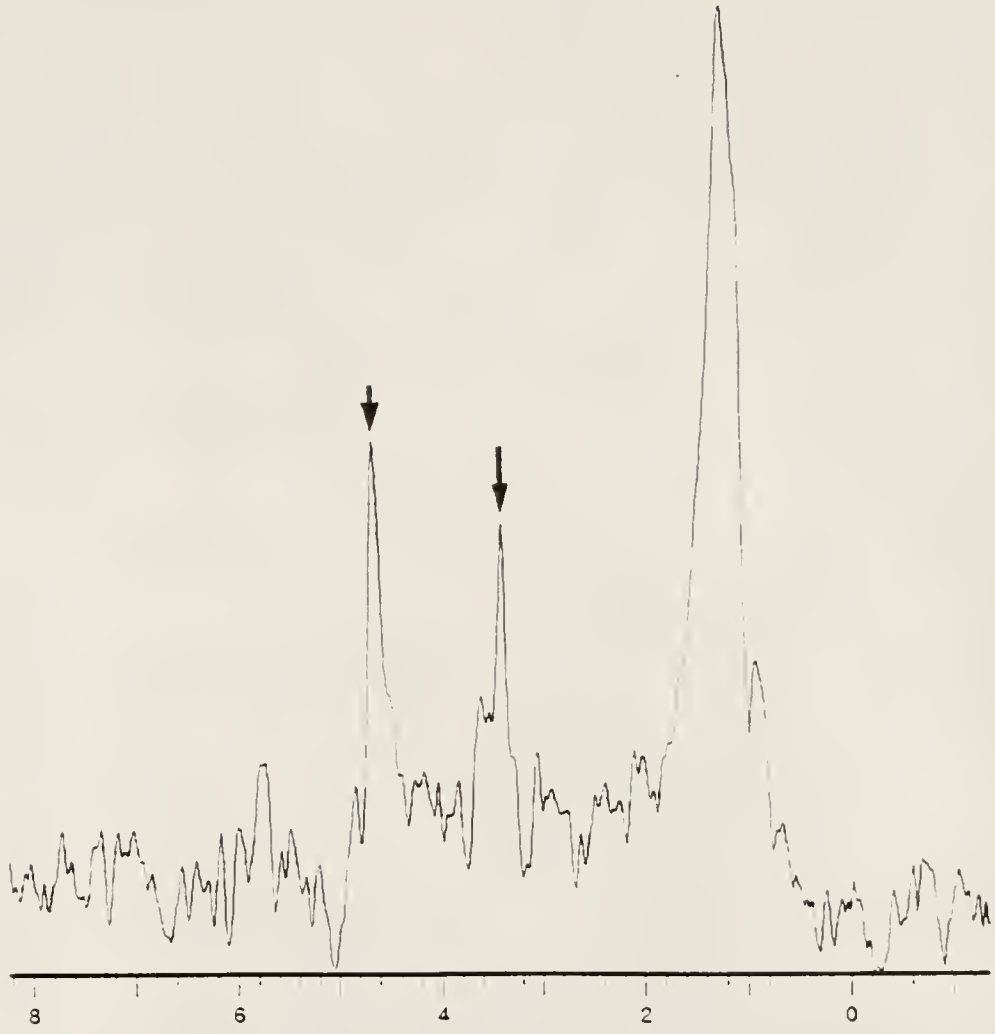

Figure 4-4 Water-suppressed H-1 spectrum from mouse tumor acquired on 1.5 T whole-body MR scanner. The short arrow marks the partially-suppressed water peak and the long arrow marks the Cho/Tau peak. The large unmarked peak is the lipid signal. The number of averages was 768.

was significantly less than that obtained with the whole body magnet where 800+ is possible. Varying the gradient strength and timing of the gradients showed little improvement. Experience with the whole body magnet indicates that a broad water peak is difficult to suppress even with increase in the bandwidth of the suppression pulse. Too wide a band width results in attenuation of the Cho and Cr peaks.

Mouse tumor imaging

Use of the T2-weighted image improved the contrast slightly between the tumor and muscle over the T1 weighted sequence but took over 5 min. to perform (Figures 4-5a,b). Injection of the mice with Gadolinium-DTPA resulted in improved tumor/muscle boundary delineation on T1 weighted images. Figures 4-6a,b show a tumor pre- and post-gadolinium enhancement. Peak enhancement of the tumor occurred about 30-45 min after injection, unlike in humans were 5-10 min is usual. This difference may be related to decrease in blood flow to the tumors during anesthesia of the mice (240). One potential problem using Gd-DTPA is broadening of the spectral peaks from enhanced T2' relaxation (241). In addition, the 30 min delay required for the tumor to enhance maximally is too long to be practical.

Spectroscopy metabolite results

Of the nine mice that were done, five of them resulted in spectra adequate for fitting. In one of these mice, normal muscle was done instead of the tumor. The results are summarized in Table 4-1.

a)

b)

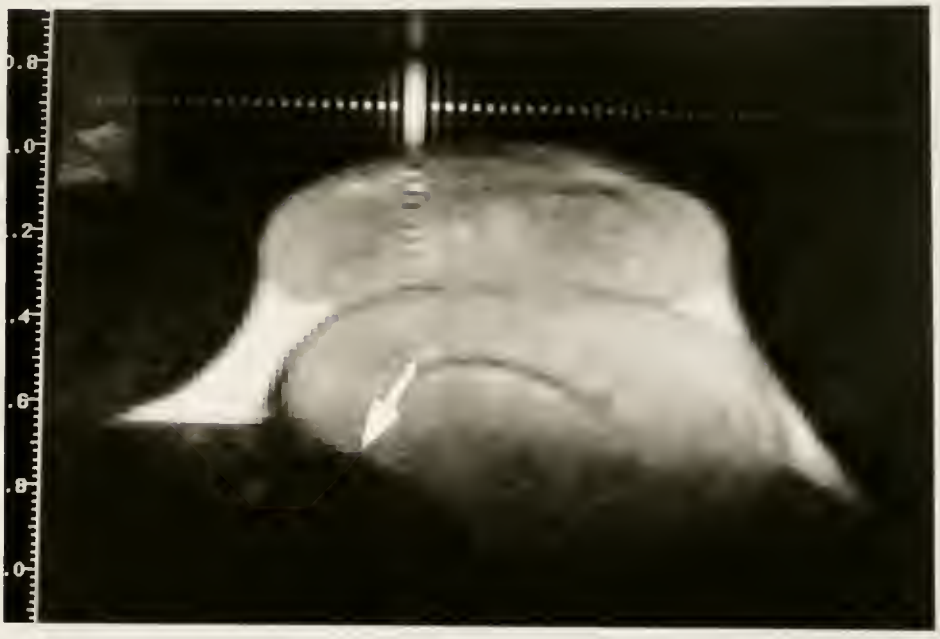

Figure 4-5 T1 and T2 weighted images of tumor in mouse.
a) T1-weighted SE image (TR: 0.5 sec, TE: 30 ms).
b) T2-weighted SE image (TR: 2 sec, TE: 80 ms). The tumor is grey in shade with an arrow pointing to the tumor/muscle interface. The white areas around the tumor are subcutaneous fat.

a)

b)

Figure 4-6 T1-weighted images, pre and post Gd-DTPA enhancement. a) Pre contrast image. b) Post contrast image. Note improved delineation of tumor/muscle boundary (arrows) on post contrast image. The skin is seen as a thin rim of light grey between the bright subcutaneous fat and the black air. Along the far right side of the tumor/muscle interface in the postcontrast image, there is evidence of muscle invasion by the tumor, not appreciated on the precontrast image.

Table 4-1
Mouse Metabolite Results Normalized to Unsuppressed Water Signal

Tissue	Norm Tau	Norm Cho	Norm Cr	Cho/Cr	Sequence
Tumor	79.0	624	171	3.65	PRESS
Tumor	334	444	99.9	4.44	PRESS
Tumor	198	1001	631	1.59	STEAM
Tumor	275	442	133	3.32	STEAM
Muscle	689	729	733	0.99	STEAM

As can be seen, the Cho/Cr ratio is elevated as has been reported in other tumors. Use of the 4.7 T system with improved spectral dispersion, and implementation of STEAM and PRESS localization techniques should prove very useful in doing additional H-1 studies in mice, looking at the effects of chemotherapy.

Human Study

Materials and Methods

Phantom and volunteer experiments

Various phantoms were constructed and used in the GE whole body imager to evaluate and practice shimming, localization, and water suppression techniques. Phantoms included water with and without doping as well as solutions of Cho, Cr, Lac, Glu, and anserine. All water suppression, localization, editing and quantitation techniques were first implemented on phantoms. Seven volunteers were used in development of the H-1 MRS technique.

Water suppression development

Initially a single CHESS pulse, for water suppression prior to the localization sequence (STEAM or PRESS), was used. Later two

CHESS pulses were used. Addition of a saturation pulse between the second and the third localization RF pulses, in addition to the two presaturation pulses, was also tried. Later, three presaturation pulses were made available on the whole-body spectrometer. This is what was used for all tumor patients.

Lactate editing

Using a zero quantum editing technique with STEAM localization (106), and varying the mixing time, spectra can be obtained with the lactate signal inverted and noninverted. These are subtracted resulting in preservation of the lactate signal and elimination of fat and residual water signal. The parameter used were: TR=2 sec, TE=136 ms, and TM=10.8 ms and 13.6 ms. This was demonstrated in a phantom and then in normal human skeletal muscle. It was later tried in several patients.

Localization development

Both STEAM and PRESS localization techniques were used. The voxels could be placed in specific anatomical regions, guided by a preliminary MR image. Localized voxel images were obtained initially with phantoms and then with volunteers to determine the accuracy of spatial localization. The presence of or lack of significant contamination from outside the voxel was shown by comparing the signals from the voxel before and after addition of spatial presaturation pulses around the voxel in volunteers. The use of a two-compartment phantom, one inside the other, would allow quantitation of the contamination from outside the voxel. This degree of precision was thought not to be necessary for our purposes. Linearity of signal with voxel size was checked with phantoms. The uniformity of the signal (i.e., sensitivity of the

coil) over the volume of interest in the extremity coil and in the surface coils was evaluated by examining the signal from both images and proton spectra at different locations. Correction factors from this data were used to adjust for sensitivity differences when comparing spectra from different positions.

Metabolite identification and concentration calibration

Peak identification in spectra from human volunteer calf muscle and in patients was accomplished by comparing to reference phantom spectra and to spectra from the literature (35, 216, 221, 242-244). Peaks corresponding to choline, creatine, taurine, glutamine, anserine, and CH_2 and CH_3 lipid peaks were identified with both the STEAM and PRESS sequence. The peaks were fit with Lorentzian curves using the SA/GE software on a SPARC IPC workstation after zero-filling to 4096 points, FFT, and zero-order phasing. The peaks areas were then normalized to the area of the unsuppressed water peak corresponding to the same voxel.

Absolute quantitation is a desirable goal for in vivo spectroscopy but because of the numerous variables that must be considered (see the chapter on Quantitation), we chose to normalize most of our data to the internal water content of the area of interest. In addition, we use an external bottle of water as a standard to control for instrumental variations with time. This was done initially with phantoms and then with volunteers.

Relaxation measurements

T1 and T2 times of H-1 metabolites of interest (Tau, Cho, Cr, and Lipid) were estimated on the calf muscle of four volunteers using the whole body imager. T1 times were calculated from 4.5 min spectral acquisitions obtained from partial saturation experiments

using the STEAM sequence and varying the TR time from 2 sec to 10 sec. With a 1000 Hz spectral width and use of 5-lobed localization RF pulse, the minimum TR was about 1.8 sec. The T2 time was calculated from spectra obtained by varying the TE time from 20 to 272 ms. Because of the time consumed by these measurements, we made a 2-point measurement of T1 and T2 in a single patient (C.P.) only.

Shimming

Whole volume shimming with a hard pulse was initially used in phantoms, but was inadequate in volunteers and patients. A slice selective technique was used then to shim a 2-D slice containing the voxel of interest. This was successful in most volunteers but not in patients. A voxel selective technique was used then where only the voxel of interest was shimmed. This gave good results in patients. Recently, an autoshimming technique has been implemented on the whole-body spectrometer with mixed results.

Tumor patient experiments

We initially planned to evaluate only osteosarcoma patients, however because of the paucity of osteosarcoma patients, we chose to examine other musculoskeletal tumors as well. We examined eleven patients and twelve tumors. One patient had both a benign and a malignant neurofibroma on a leg and we examined both of them. This was a fortunate case, as it is rare for a patient to have both a benign and malignant tumor of the same basic cell type. Table 4-2 summarizes the patients and tumors that we examined.

Table 4-2
Summary of Tumor Patients

Patient Initials	Age/race/sex[1]	Tumor Type and Location
C.P.	73 y/o W F	Malignant Fibrous Histiocytoma, Grade IV; Left Thigh
I.H.	80 y/o W M	Malignant Myoid fibrous Histiocytoma, Grade II/IV; Right Thigh
G.H.	56 y/o W F	High Grade Pleomorphic Sarcoma; Left Thigh
E.V.	22 y/o H M	High Grade Malignant Hemangiopericytoma; Left Neck
L.D.	10 y/o A M	Ewing's Sarcoma; Left Distal Femur
G.R.	12 y/o H M	Benign Aneurysmal Bone Cyst; Left Proximal Femur
J.K.	27 y/o W F	Osteoblastic Osteosarcoma, Grade IV; Left Distal Femur
M.C.	40 y/o W F	Neurofibrosarcoma and Benign Neurofibroma; Right Proximal Leg and Right Distal Thigh
R.M.	32 y/o B F	Parosteal Osteosarcoma, Grade II/IV; Right Distal Femur
L.W.	73 y/o B F	Mesenchymal Chondrosarcoma; Left Calf
C.M	13 y/o W M	Osteoblastic Osteosarcoma, Grade IV; Right Distal Femur

[1]Abbreviations: W-white; H-Hispanic; A-Asian; B-Black; F-Female, M-Male.

Our patients were referred to us primarily by Drs. Mark Scarborough and Tom Nelson, Orthopedic Surgeons at Shands Hospital. IRB approval for this project was obtained and each patient provided written informed consent after being informed of the purpose of the study, any value to them, the voluntary nature of the study, and the possible risks involved (See Appendix C). In addition, each patient was screened for relative and absolute

contraindications to MRI including claustrophobia, implanted medical devices, metallic foreign bodies, and pregnancy.

The spectroscopy was performed on the Shands Hospital General Electric 1.5 T whole body imager/spectrometer in all cases. The entire exam took approximately 1-1.25 hours. The paired-saddle extremity coil, a five or seven inch surface coil, or the body coil were used to image and obtain spectra from the tumors, depending on the location of the tumor. A small bottle of distilled water was positioned alongside the tumor for use as an external concentration standard. A multislice, dual echo, T2 weighted imaging sequence in the axial plane was performed to localize the tumor for spectroscopy voxel placement and to use as a reference for water content of the tumor, compared to the external standard as described in reference number 125.

After imaging, an appropriate slice location was chosen, maximizing the tumor cross-section. The spectroscopy voxel was then graphically prescribed over the area of interest in the tumor. First order shimming on the water peak was then performed using the gradient coils, either entirely manually, or later in the study, with autoshimming followed by manual fine tuning. An unsuppressed, two average water spectrum was then acquired after four "dummy" RF pulses to equilibrate the T1 effects on the spectrum. The three presaturation RF pulses and dephasing gradients were then turned on and the RF power to the third RF pulse adjusted for maximum water suppression (see parameters in Appendix F). Suppressed spectra were then acquired with either two averages from a 2-D phase-encoded STEAM or PRESS defined voxel of dimensions determined by the size of the tumor (generally 4-6 cm

on a side) or with 128-256 averages for a single voxel. The 2-D phase encoding had 16 steps in each dimension with an effective voxel size of 2 cm on each side. As a result, four to nine spectra would be obtained from the tumor in one acquisition. The voxel volumes for spectra acquired without phase encoding ranged from 3.9 cc to 18 cc depending on the size and shape of the tumor and area of interest.

We used a single voxel (~8 cc) STEAM technique with a TE=30 and 136 ms on our first patient (See Appendix F for additional parameters). We found considerable spectral heterogeneity in the tumor in different locations. We then implemented a two dimensional phase encoding of a larger STEAM voxel (~4-6 cm on a side, 2 cm deep) to obtain spectra from several areas simultaneously. This resulted in worsening of the line width of the spectral peaks.

A large lipid signal was found in some tumors, which tended to obscure other metabolites of interest at short echo times of 20-30 ms. Taking advantage of the short T2 of lipids, we chose to use a long TE of 80-140 ms to decrease the relative contribution of the lipid signal to the spectrum. We did not want to eliminate the lipid signals completely as in vitro studies have shown abnormalities in the lipid signals from tumors (245). The amplitude of the lipid signal was frequently 1/10 to 1/100 of the water signal, even at a TE=136 ms. The lactate concentration in a variety of tumors implanted in mice has been reported to be 6.4±0.9 mM (200). The lipid signal would therefore one hundred times greater than that of the lactate signal, in some cases. A very effective editing technique would be necessary to detect the

lactate unequivocally. To recover most of the signal lost by using a longer TE, we started using a PRESS (Point Resolved Spectroscopy) sequence that collect the entire signal (65, 66). The metabolites of interest such as Cho, Cr, Tau, and Lac have relatively long T2 relaxation times (69-71).

The PRESS sequence gave us adequate signal in a reasonable time and could be used with 2-D phase encoding. Poor line width of the peaks continued to be a problem in some cases; therefore, the use of multiple acquisitions of single voxels using the PRESS sequence was implemented. In at least half of the studies in which multiple single voxels were acquired, shimming had to be performed on each voxel.

Analysis of data

Spectra were transferred to the SPARC workstation and analyzed in an identical fashion to the volunteer spectra described above. Statistical analysis was performed on a personal computer with either Execustat (PWS-KENT Publishing Company) or Statistica (Statsoft, Tulsa, OK) software using two tailed Student's t-test and paired t-test. Spectra were compared qualitatively to the corresponding MRI images and to pathological and histological specimens.

Results and Discussion

Shimming

We routinely obtained a water line width of 2-7 Hz on phantoms and 8-13 Hz with human skeletal muscle with the voxel shimming technique. The malignant tumor spectra had a wider range of line widths, 6-15+ Hz. The two benign tumors had line widths of 7.8 Hz each. It is interesting that the patient with both a benign

and malignant tumor of the same cell type (neurofibroma and neurofibrosarcoma) had a line width of 7.8 Hz for the benign tumor and 15 Hz for the malignant tumor. The lesions were only about 15 cm apart and shimmed separately. The wider range and larger values of line width for the malignant tumors are probably because of the heterogeneity of the tumors.

Water suppression

One, and then two, CHESS pulses for water suppression resulted in 70-fold to 100-fold reduction of the water signal, which was not adequate. Addition of a saturation pulse between the second and third localization RF pulses, resulted in undesirable distortion of the spectra. The use of three saturation pulses prior to localization resulted in an 8-10 fold improvement of suppression to 800+ now. Figure 4-7 shows spectra from phantoms comtaining Glutamine/Glutamate, Creatine/Creatinine, Taurine, and Choline. Figure 4-8 shows a water suppressed spectrum from a normal volunteer. This was quite satisfactory.

Lactate editing

The zero quantum editing technique with STEAM localization worked quite well with phantoms. Subtraction of two spectra obtained from phantoms with different mixing time resulted in preservation of the lactate signal and elimination of the residual water signal (Figure 4-9). In normal human skeletal muscle of volunteers, the metabolite peaks, including most of the lipid and the residual water signal, were removed with lactate editing (Figure 4-10). This is what we would expect since normal resting muscle contained undetectable amounts of lactate. The sequence was then tried in several tumor patients. The large lipid peaks seen

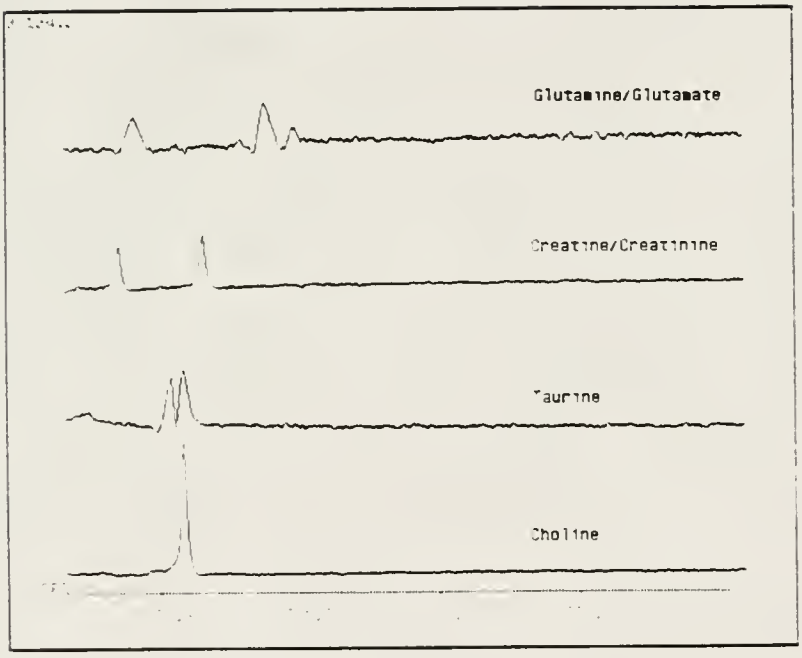

Figure 4-7 Spectra from phantoms containing Glutamine/Glutamate, Creatine/Creatinine, Taurine, and Choline.

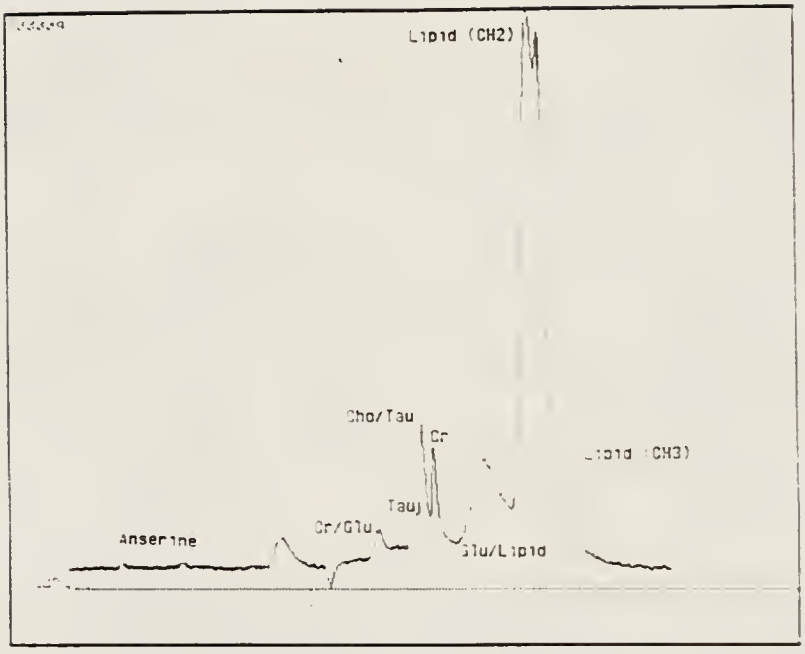

Figure 4-8 H-1 spectrum from skeletal muscle of normal volunteer with metabolite peaks of interest labeled.

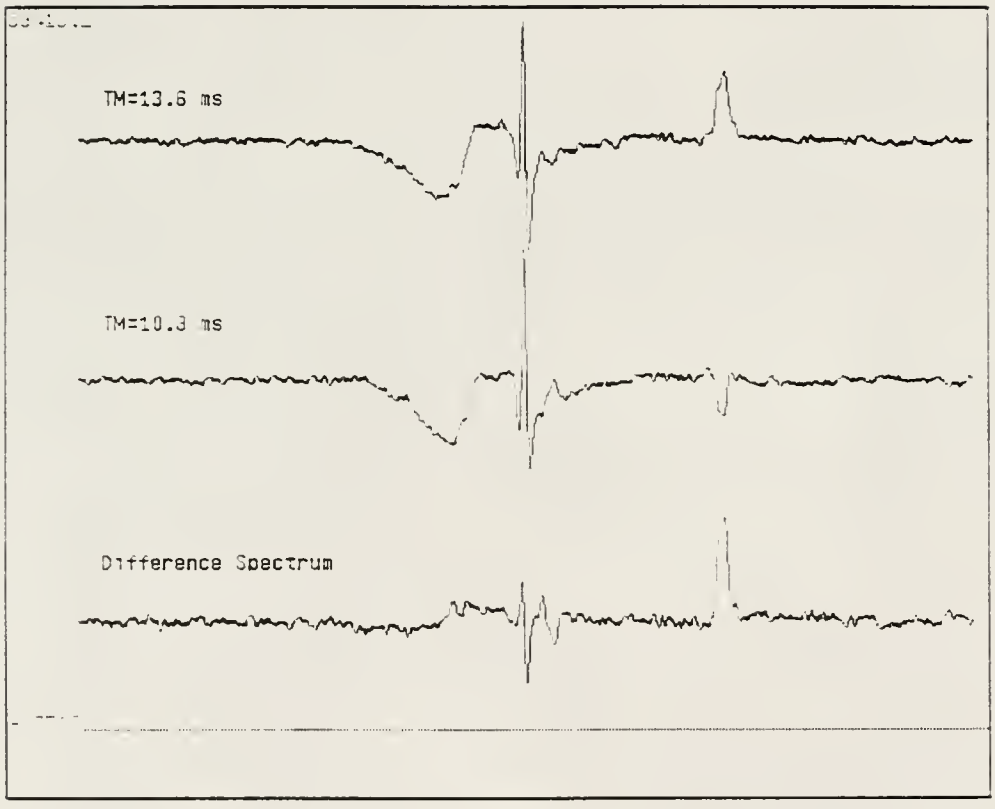

Figure 4-9 Spectra from lactate phantom. The top two spectra were obtained with different mixing times as indicated. Subtraction of two spectra resulted in preservation of the lactate signal and elimination of most of the residual water signal as seen in the bottom spectrum.

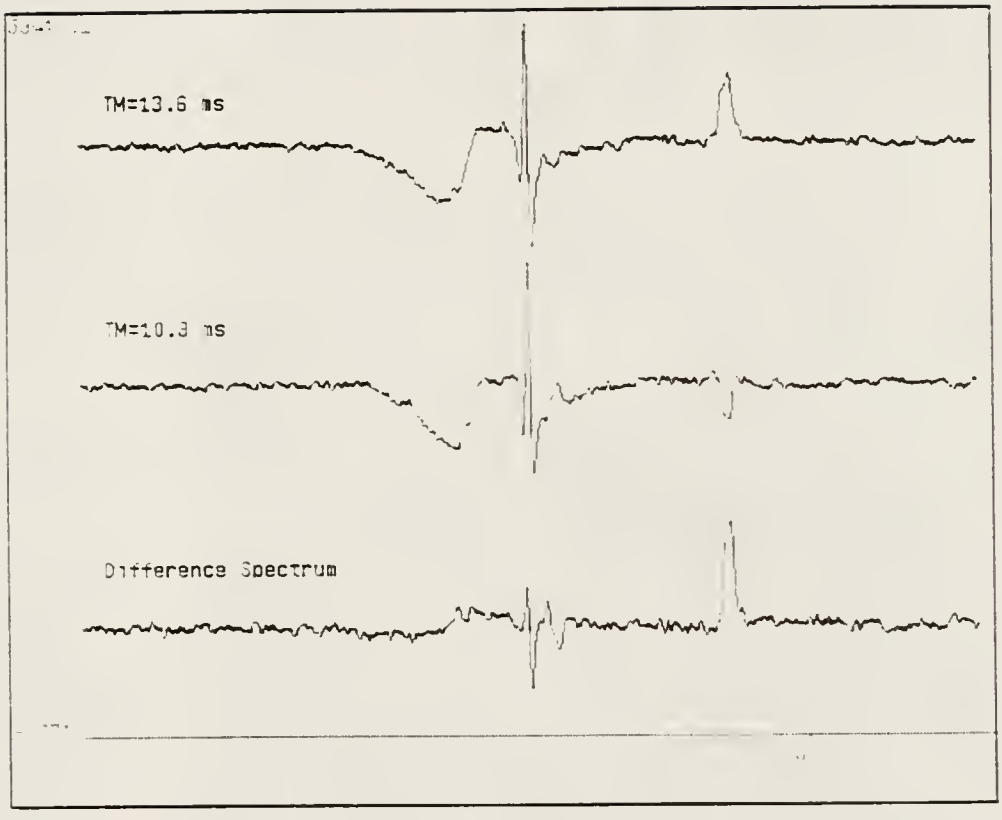

Figure 4-10 Lactate editing of normal skeletal muscle. Note the elimination of most of the lipid and residual water signal. No significant lactate is seen in normal muscle spectra.

in the spectra from most of the patients may have been incompletely eliminated, making it impossible to definitively identify the presence of lactate (figure 4-11). The incomplete elimination of the lipid signal can be explained by the up to 100-fold greater size of the lipid peak when compared to the expected lactate peak. Subtraction of spectra obtained a few minutes apart might be expected to be less than perfect if any variation in transmitter power, receiver sensitivity, or patient position were to occur. In later patients, the sequence was discontinued in order to obtain better signal with a PRESS sequence and to sample more than one area of the tumor.

Localization

Localization with both STEAM and PRESS was accurate in terms of correct location as determined by imaging with these sequences in phantoms and then in volunteers. Figure 4-12a shows a sagittal image of a volunteer's head with a spin echo localizing sequence and Figure 4-12b shows a localized image obtained with STEAM from the area of the box drawn on Figure 4a. Lack of significant contamination from outside the voxel was confirmed by comparing spectra with and without the addition of spatial saturation pulses around the voxel in volunteers. The signal from voxels of varying size was found to be linear from about one cc up to at least 27 cc (Figure 4-13). The intercept of the regression line with the positive y-axis, rather than the origin, can be explained by the approximately 3% noise in the spectrum contributing to the measured peak area. Maps of relative B_1 sensitivity at various locations in the coils are in Appendix H.

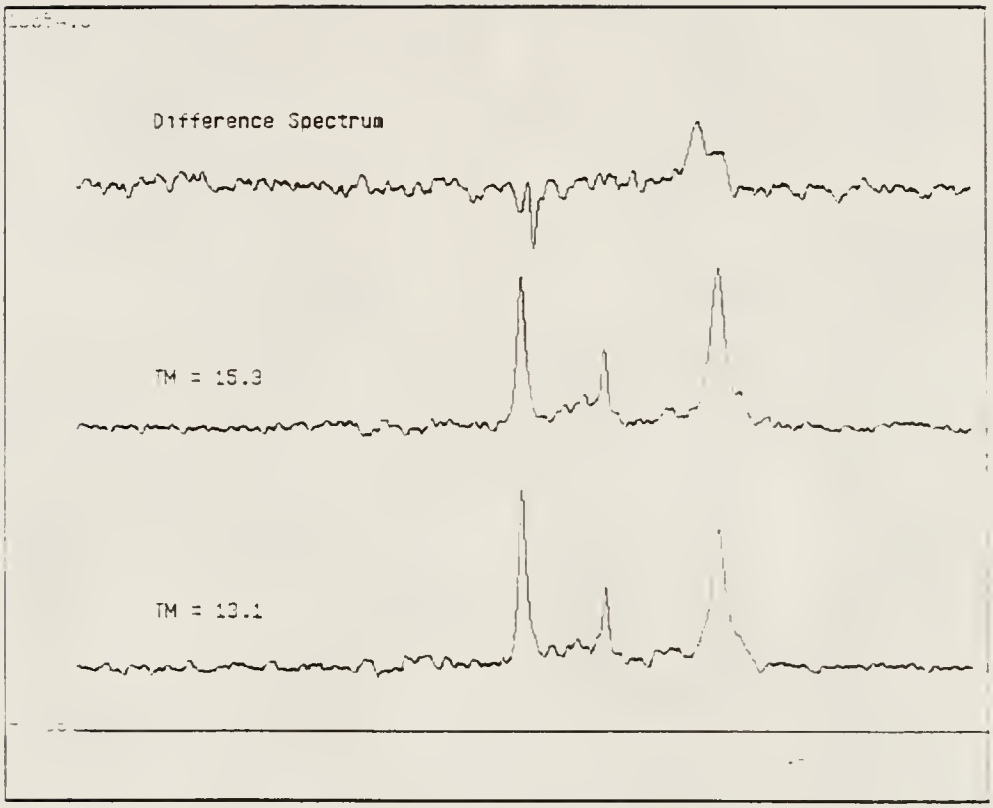

Figure 4-11 Lactate editing of malignant tumor. Residual signal seen on the difference spectrum probably represents both lactate and unsubtracted lipid.

a)

b)

Figure 4-12 MR images showing graphic selection of spectroscopy voxel using the STEAM sequence.
a) Sagittal spin echo image of a volunteer's brain with desired voxel outlined. b) Localized image acquired with the STEAM sequence from area outlined on sagittal image.

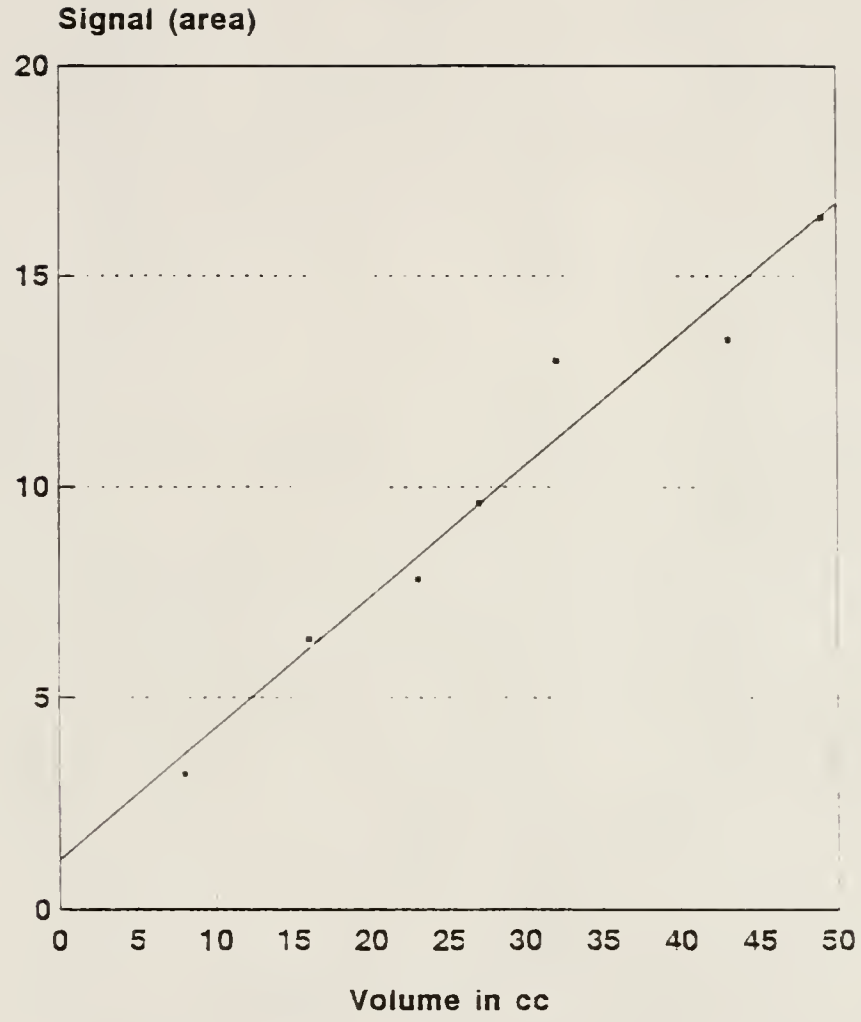

Figure 4-13 Graph demonstrating linearity of the water signal with the voxel volume varying in size from about one cc up to at least 27 cc.

pH measurement

A buffered solution of anserine was examined at near physiologic concentration with good success at matching the pH with that of the buffered solution. A calibration curve was not made because of the lack of visible anserine signal in our tumor spectra. pH's measured from the skeletal muscle of four human volunteers were slightly less than but not significantly different from those measured in our laboratory using P-31 on the same volunteers (H-1 pH: 6.95±0.25, P-31 pH: 7.07±0.036, $p = 0.867$).

Metabolite identification and quantitation

Using the extremity coil, we were successful in obtaining well-localized spectra from phantoms containing choline, creatine, taurine, glutamine, and anserine in physiological concentrations using both the STEAM and PRESS sequences (Figure 4-7). In addition, combinations of these chemicals were used in a phantom to simulate the tumor spectra and to obtain relative peak positions (Figure 4-14). Peaks corresponding to choline, creatine, taurine, glutamine, anserine, and CH_2 and CH_3 lipid peaks were identified in volunteers with both the STEAM and PRESS sequence (Figure 4-8). Table 4-3 lists the peak positions in ppm (parts per million) relative to TSP obtained from our phantom and volunteer data for the various metabolites of interest.

Use of the internal water signal for normalization of peak signals and an external bottle of water as a standard to control for instrumental variations with time showed reproducibility of <5% in phantoms and <10% for Cho and Cr in volunteers. When using the extremity coil and surface coils for collecting data, the

Figure 4-14 Tumor spectrum simulation with combination of spectra from phantoms. The tumor spectrum is on the top, showing a large Cho peak in the middle. The combination of spectra from phantoms is on the bottom (20 mM Cho, 20 mM Cr, 40 mM Tau, 20 mM Glu).

Table 4-3
Peak Positions of Metabolites of Interest

Water	Glu	Cr	Tau	Cho	Lipid	Lactate
4.71	3.75 2.01 2.34 2.60	3.95 3.04	3.33 3.22	3.20	1.48 1.10	1.33

spatial dependence of sensitivity was corrected for by data acquired with large homogeneous phantoms (Appendix H).

T1 and T2 measurements obtained from four volunteers and one patient are listed in Table 4-4. A discrete Tau peak could only be seen in one volunteer.

Table 4-4
Relaxation Measurements from Four Volunteers and One Patient

	Tau	Cho	Cr	Lipid
T1 muscle (sec)	3.5	1.32±0.23	1.10±0.05	0.608±0.215
T2 Muscle (msec)	159±93	112±14	110±43	87±4
T1 MFH (sec)	1.33	1.57	3.27	0.956
T2 MFH (msec)	185	421	100	58.4

The relaxation times for normal muscle for Cho and Cr match those values in the literature well (Cho T1: 1.1-1.6s, T2: 150-210 ms; Cr T1: 1.2-1.7 s, T2: 120-150 ms (246)). I have seen no information on relaxation times for Tau. Lipids (CH_2) have been described as having a T1=280-330 ms, and T2=75-100 ms. Our values are slightly higher than those.

The absolute molar concentration of Cho and Cr was calculated for the skeletal muscle of four volunteers based on the method of Alger et al. (125) as discussed in the techniques chapter. For Cr

a value of 41.8±4.44 mM was calculated. This compares to the literature value of 42.5 mM (247). The calculated Cho (which include Tau) was 14.5±5.4 mM. The author is unable to find the concentration of Cho in the literature for skeletal muscle; however, the sum of the Cho and Tau concentration for brain has been reported as 2.24 mM, determined from H-1 MRS of perchloric acid extracts (35). The value of Cr in the brain, based on this reference, was 9.23 mM. Clearly, there is probably a large difference in these concentrations between brain and muscle.

Spectroscopy findings in musculoskeletal tumors

Using the single voxel STEAM technique on our first patient, we found considerable spectral heterogeneity in the tumor in different locations after therapy started (Figure 4-15). We then implemented 2-D phase encoding of the STEAM voxel to obtain spectra from several areas simultaneously. This resulted in slight worsening of the line width of the spectral peaks.

A significantly lower metabolite signal was seen in the tumors compared to skeletal muscle, which was surprising. The switch to the PRESS voxel localization technique gave additional signal.

The other surprising finding was a large lipid signal in most of the tumor spectra. Some soft tissue tumors such as liposarcomas and malignant fibrous histeocytomas are known to contain fat (Personal communication from Suzanne Spanier, MD, Pathologist). Most tumors do not contain any macroscopic fat deposits. Increase in mobility of membrane lipids has been suggested as a cause of the increased lipid signal from malignant tumors (248). Recently, the MR visible lipid in viable tumors has been compared to that in

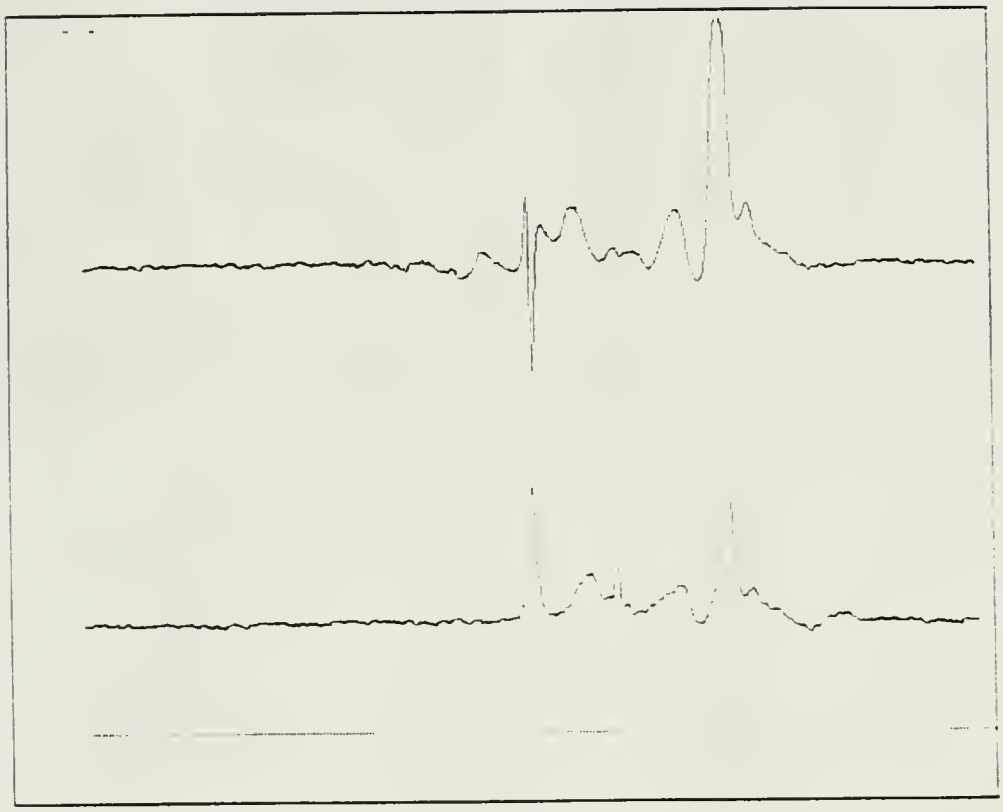

Figure 4-15 Spectra from the same tumor in different locations showing the considerable spectral heterogeneity in the tumor. The bottom spectrum is from viable tumor. The top spectum is from necrosis. Note the large lipid peak in the necrotic spectrum.

necrotic tumors. This was done ex vivo using a high resolution spectrometer and biopsy specimens from human astrocytomas (brain tumors). They found a significant correlation between large visible lipid signals and the presence of necrosis (249). Using a paired t-test to compare the lipid signal in tumor and necrosis in the three subjects (four pairs of spectra) that had necrosis in this study, we found the necrotic areas to have an average of 80% more lipid signal than the areas of viable tumor. This was not statistically significant ($p=0.10$), probably because of the small number of subjects. Determining the minimum sample size to detect a significant difference in lipid content from the published study, we need six subjects. Using our data, the sample size would be 12 subjects. To reduce this signal we increased the echo time of the pulse sequence as described in the Materials and Methods section. This change was successful in allowing visualization of the other metabolites of interest.

We evaluated the resolvable lipid peaks in volunteers and were able to identify CH_2, CH_3, and CH=CH groups. The absolute and relative concentrations of these peaks varied greatly (2-4 fold) between volunteers. It also varied considerably within individual volunteers depending whether the voxel included intramuscular fat or subcutaneous fat. I have not seen an explanation for this intraperson variability in the literature. The interperson variability has been described and explained by differences in age and athletic condition (246). Much of the dietary fat consumed is deposited relatively unchanged in the adipose tissue (250).

The Cho/Cr ratio data are summarized in Table 4-5. This table includes mean and standard deviation, and also confidence interval

(CI) and p value from a t-test comparison of each category with the malignant tumors. There were ten patients with malignant tumors examined, two benign, three necrotic, and one with edema. Two of the three patients have had surgery with histological confirmation of necrosis. The third (C.M.) has yet to have surgery; however, increase in the signal on the T2-weighted MR images and marked decrease in Cho and Cr are highly suggestive of necrosis. The single case thought to represent edema had MR findings of increased signal in muscle adjacent that were suggestive of edema. Pathologic correlation is not available for this case.

Table 4-5
Summary of Cho/Cr Ratio Data

	Malignant Tumors n=10	Benign Tumors n=2	Necrosis n=3	Edema n=1	Muscle n=4
Mean	4.63	1.31	1.13	0.99	0.90
Standard Dev.	3.35	0.57	0.12	N/A	0.28
CI	N/A	(0.694, 10.680)	(0.861, 10.858)	N/A	(1.05, 11.08)
p value	N/A	0.0332	0.0309	N/A	0.0282

The viable tissue in malignant tumors that we examined showed a statistically significant elevation of the Cho/Cr ratio when compared to normal muscle, as we expected. We also see significant differences in the Cho/Cr ratio between viable malignant tissue and necrosis, and benign tumors. With only one subject having edema, we are unable to obtain statistical significance comparing malignant tumor with edema.

Figure 4-16 shows a ROC curve for the accuracy of the Cho/Cr ratio in distinguishing malignant from benign tissue. The area under the curve was estimated to be 0.9727±0.0269. Using a Cho/Cr threshold of 1.56, the sensitivity for detecting a malignancy would be 92.5%, the specificity would be 93.7%. Since we would rather over diagnose malignancy rather than miss a malignancy, we could lower the Cho/Cr threshold to 1.25 and obtain a sensitivity of 99.3% with a specificity of 79.4%. If we were to compare malignant tumors with only benign tumors, the results may not be as good as these. With only two benign tumors, we cannot make any judgements.

Also noted was elevation in the taurine signal in some tumors when compared to skeletal muscle. This type of elevation has been reported in radiation induced fibrosarcomas in mice examined by using extracts and recently in vivo at 11.75 T (58). One taurine peak (3.22 ppm) is indistinguishable from the Cho peak at 3.20 ppm, and in several of our patients we could not separate reliably the second Tau peak (3.33 PPM) from Cho. In areas of necrosis seen on MRI and post surgical histology, we saw marked reduction in the signal from Cr, Cho and Tau when compared to viable tumor. The Cho/Cr ratio was variable in necrotic areas. The peaks are not even resolved in some necrotic areas.

The patient thought to have edematous muscle had a spectrum from this tissue showing the Cho/Cr ratio, and normalized Cho and Cr levels to be similar to those in normal volunteers.

The total per cent change (decrease) in the Cho/Cr ratio and also the per cent change per day from start of treatment to follow up is shown in Table 4-6 from the four malignant tumors that had

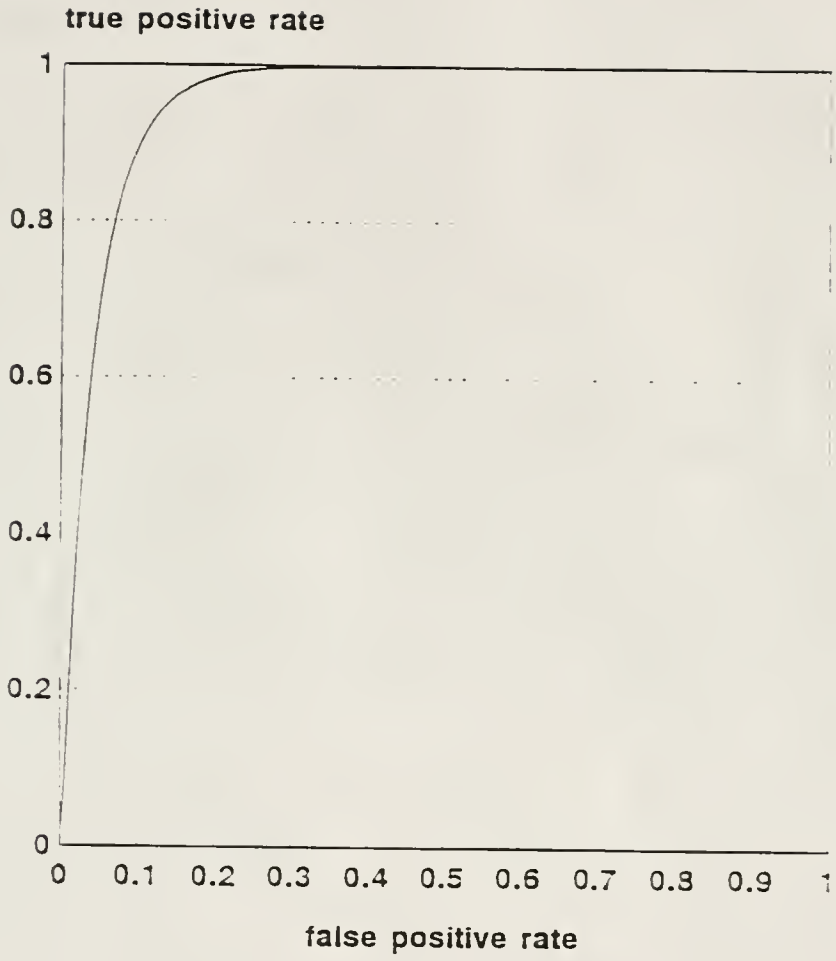

Figure 4-16 ROC curve for the accuracy of the Cho/Cr ratio in distinguishing malignant from benign tissue. The area under the curve was estimated to be 0.8560±0.0519.

repeat measurements. The per cent change per day for the four tumors with followup was statistically different from zero ($p=0.0142$, CI: (0.163,8.38)). The other seven patients did not have followup studies for several reasons. One refused further studies; one patient had his HMO send him to Atlanta for treatment and followup; one patient had only a benign lesion, requiring no followup; two had immediate surgery; and two patients were not referred to us on their followup visits.

Table 4-6
Per Cent Change (decrease) in the Cho/Cr Ratio
in Tumors with Follow up

Patient	C.P.	L.D.	C.M.	L.W.[1]
Total % Change	65	29.7	87.7	66
Daily % Change	2.32	0.83	4.2	2.36
Number of Days	28	36	21	28

[1]These results are from the first month only. After this period, the tumor stopped responding to treatment and started to grow larger (see Figure 4-19c).

Figures 4-17 a-d show actual spectra from these tumor patients. Figures 4-18 a-d show graphs of individual tumor changes in Cho/Cr and volume. The imaging data from one patient (C.P., Figure 4-18a) was incomplete, so accurate volume measurements could not be made. One patient (L.D., Figure 4-18b) was judged clinically to have an incomplete response to chemotherapy and radiation therapy and is undergoing a bone marrow transplantation. Excluding the data from L.D., which was obtained before transplantation, we have greater statistical significance ($p=0.0061$, CI: (1.44,2.90)). Another patient, L.W., had an initial response based on change in tumor size and Cho/Cr ratio. Later,

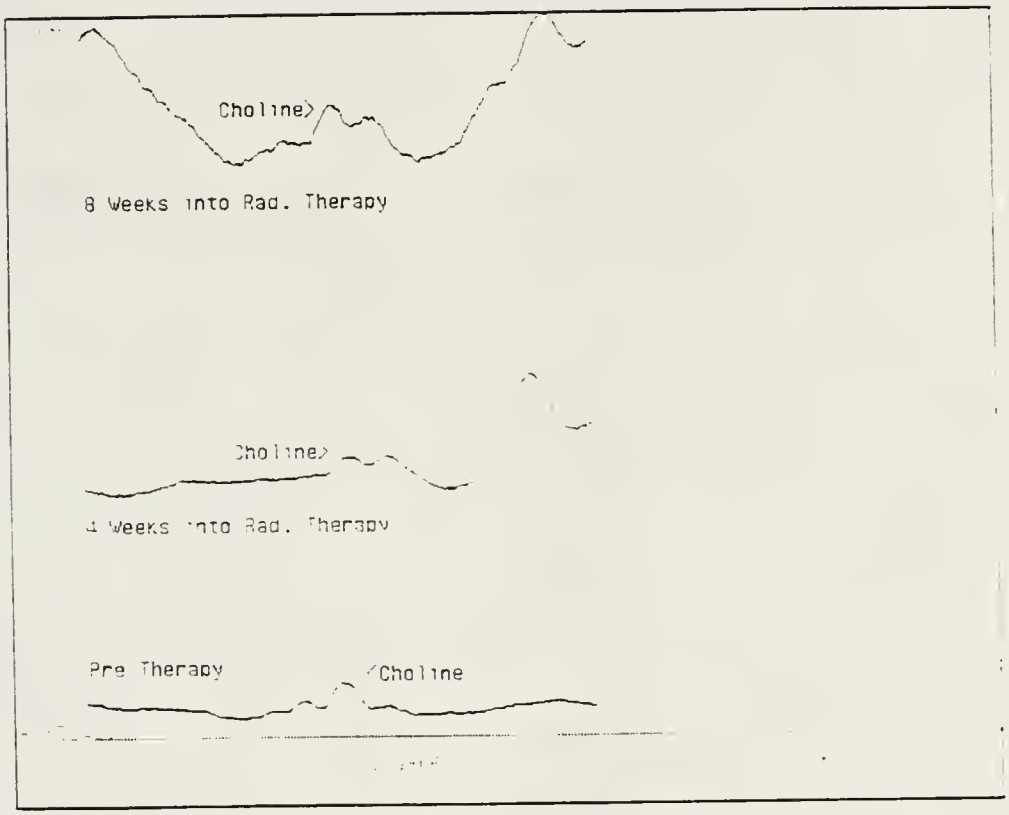

Figure 4-17a-c Spectra from three of the tumors with followup. a) Chondrosarcoma. (L.W.) Note the initial decrease in size of the Cho peak followed by an increase.

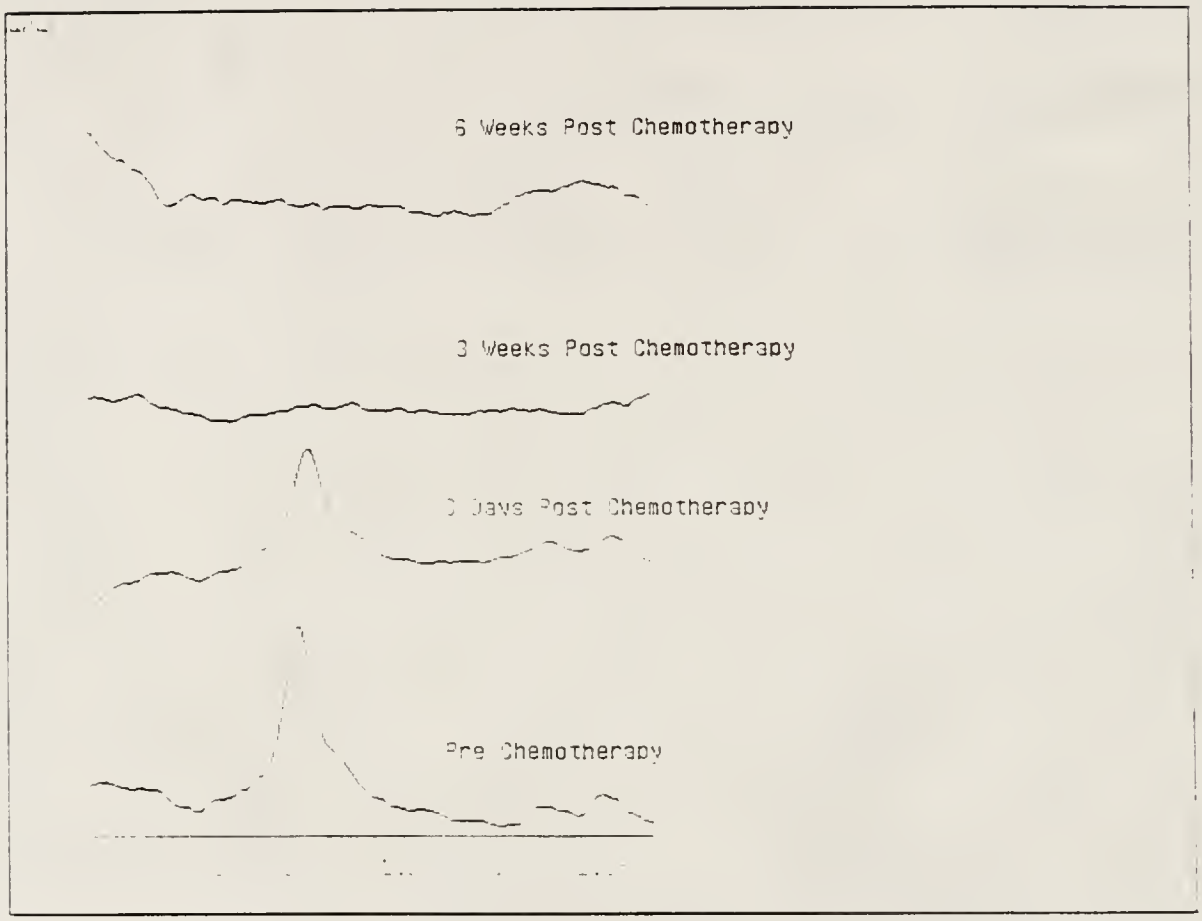

Figure 4-17--continued
b) Osteosarcoma. Note the slight decrease in the Cho peak after three days of chemotherapy. At three weeks and six weeks, the Cho signal has disappeared.

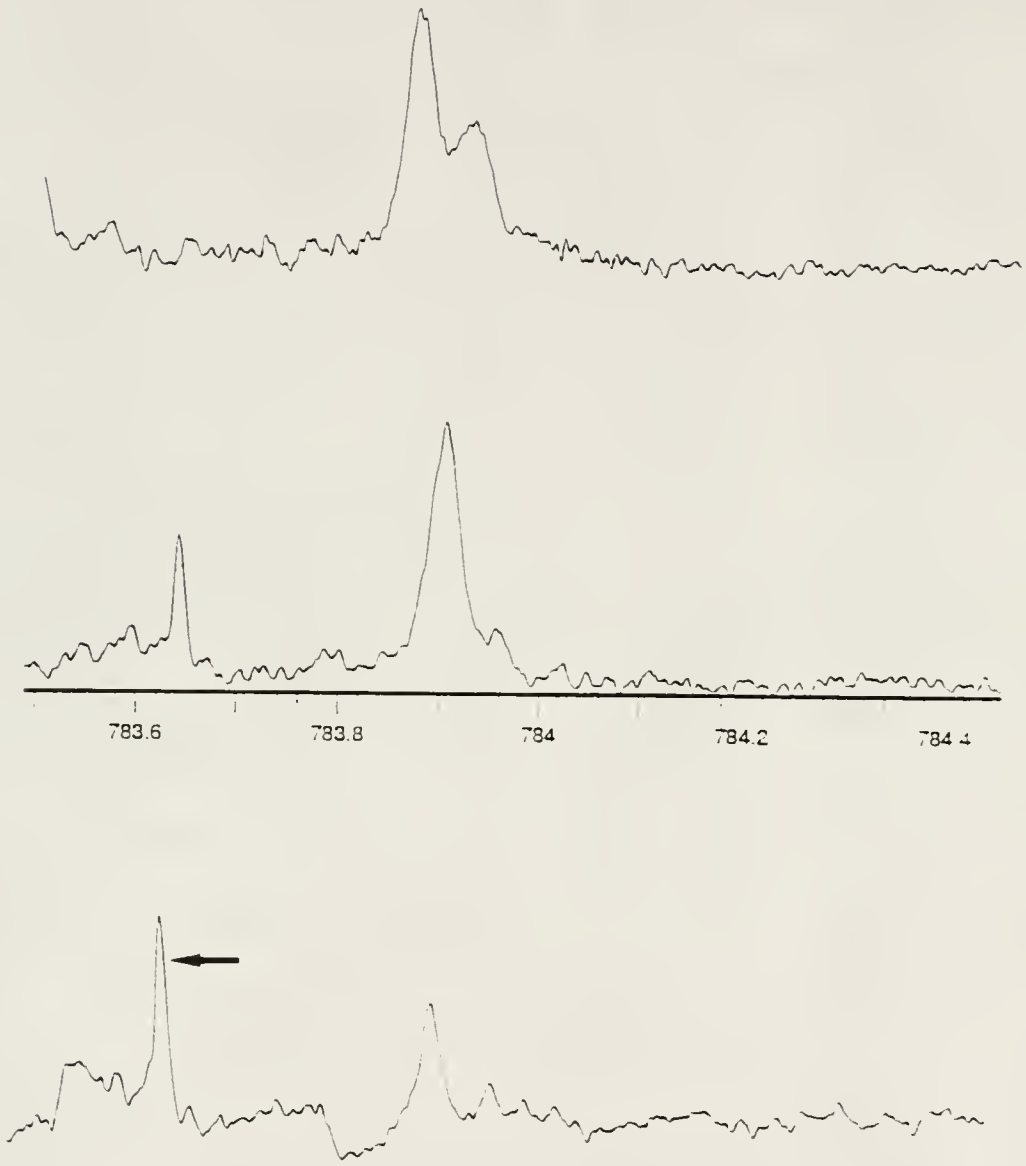

Figure 4-17--continued
c) Spectra from patient with MFH. The bottom spectrum is preradiation therapy; the middle spectrum is after four weeks of radiation therapy; the top spectrum is after eight weeks of radiation therapy. Note that the initially large Cho peak (arrow) dissappears by eight weeks.

a)

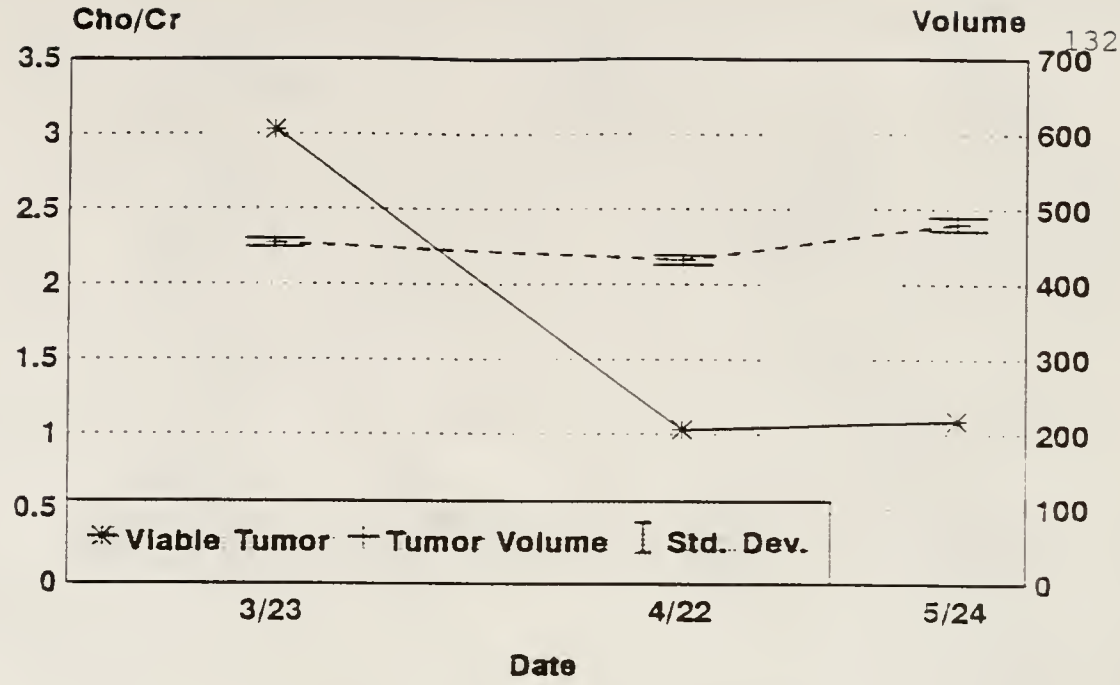

b)

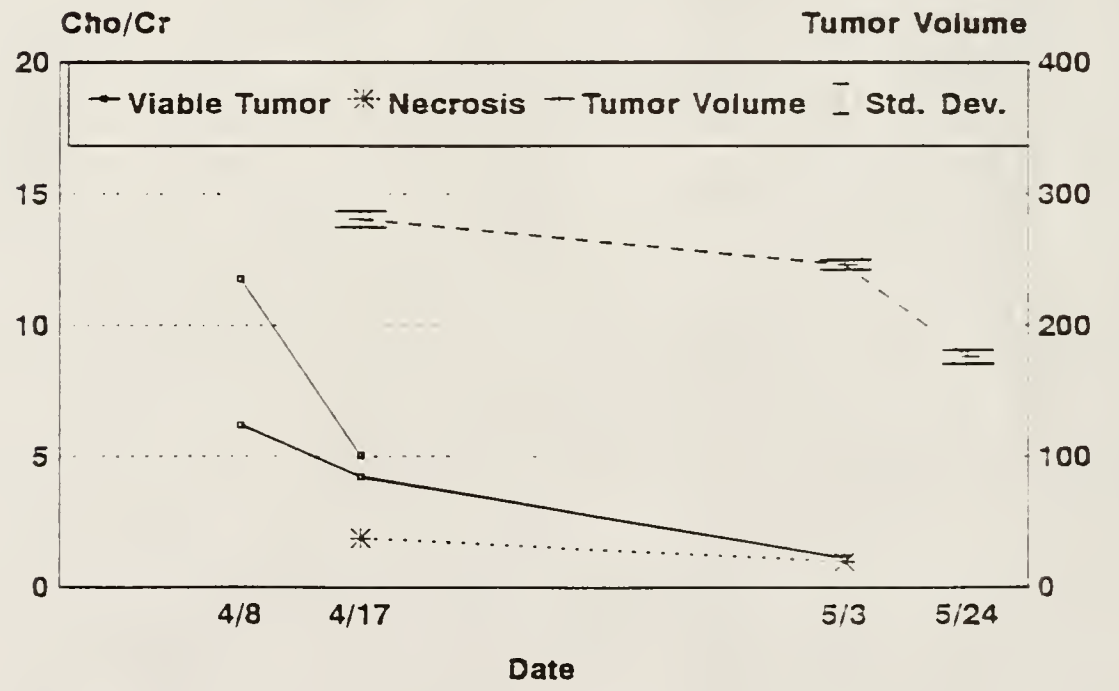

Figure 4-18 Graphs of the change in the Cho/Cr ratio for four patients and volume of tumor for three patients with follow up.
a) Patient L.W., Chondrosarcoma; b) Patient C.M., Osteosarcoma.

c)

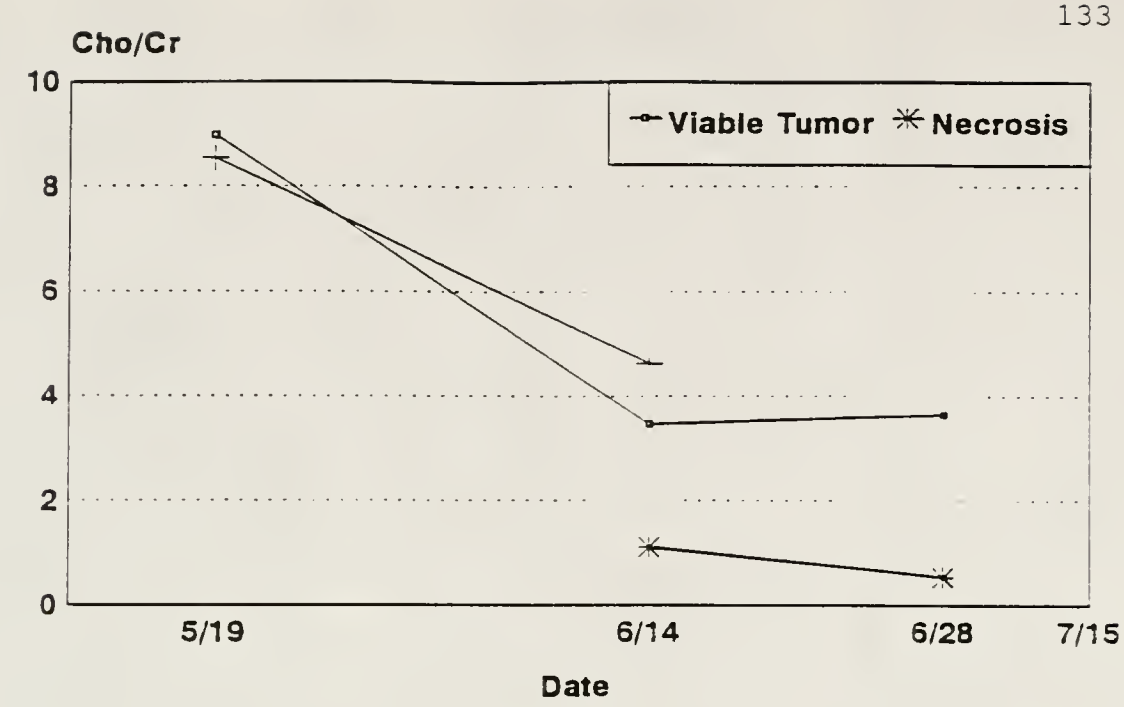

d)

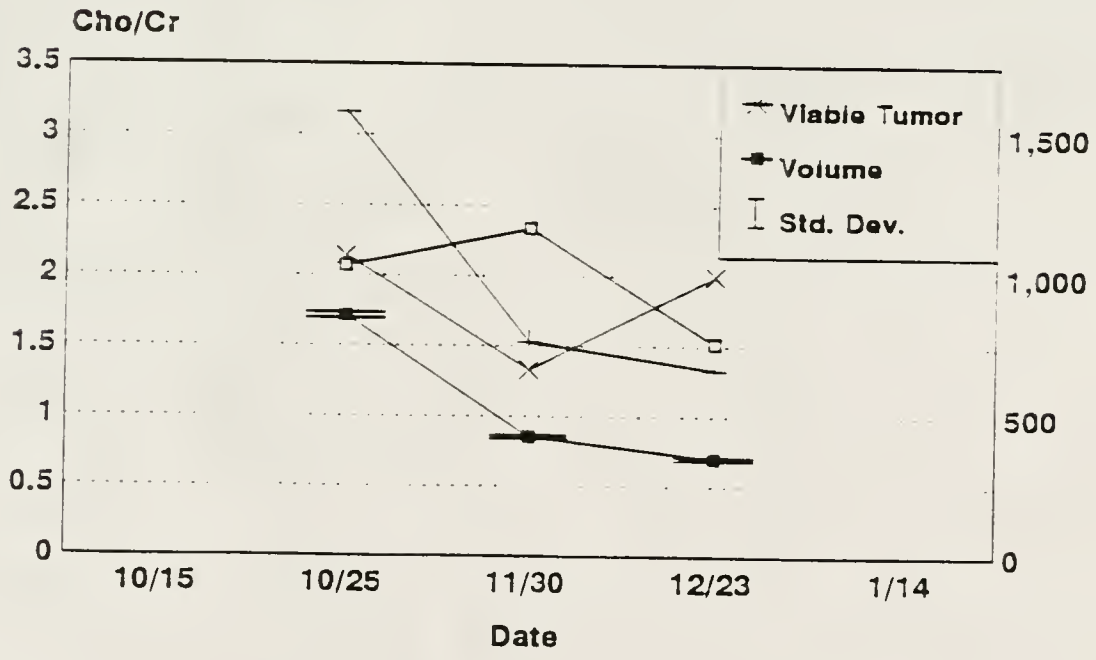

Figure 4-18--continued
c) Patient C.P., Malignant fibrous histiocytoma;
d) Patient L.D., Ewing's Sarcoma.

the tumor stopped responding and started to grow again (Figure 4-18c). The per cent change in the Cho/Cr ratio for L.W., shown in Table 4-6 is only for the period when the tumor was decreasing in size. All patients started their therapy within one week of the initial MRS study. Figure 4-19 shows the average change with treatment of the normalized Tau, Cho, and Cr separately.

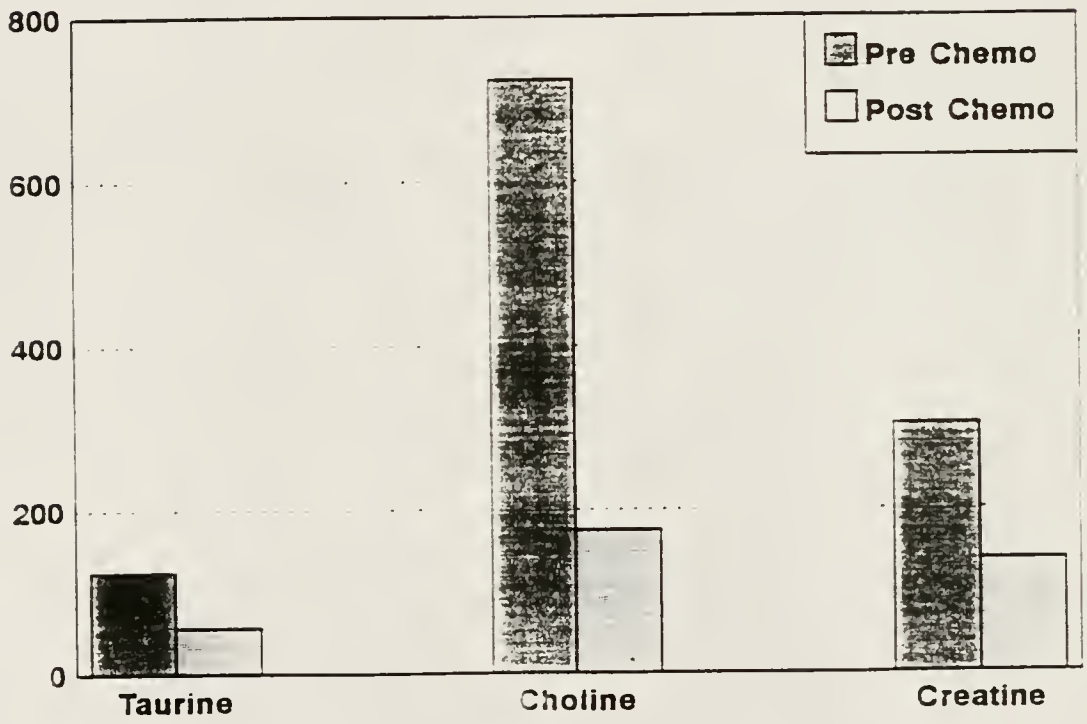

Figure 4-19 Graph showing the change of the normalized H-1 metabolites in the four tumor patients with follow up post therapy. The concentration units are arbitrary.

CHAPTER 5
PHOSPHORUS SPECTROSCOPY OF SKELETAL MUSCLE IN PERIPHERAL VASCULAR DISEASE AND CONGESTIVE HEART FAILURE

P-31 MRS Monitoring of Low Intensity, Pain Free Exercise Therapy for Individuals with Intermittent Claudication due to Peripheral Vascular Disease

Introduction and Review of the Literature

The primary complaint of most peripheral vascular disease (PVD) patients is intermittent claudication (IC), which is defined as severe pain in the leg muscles during walking, which subsides with rest. The pain is a result of decreased blood flow to the exercising muscle, frequently related to atherosclerotic disease. PVD usually occurs in patients with a history of smoking and is more severe in diabetic patients. Arteriosclerotic disease related to smoking usually involves the large vessels while diabetes usually involves smaller vessels that are less amenable to surgical or radiological intervention. Urgent operative intervention is required within 4-7 years in about 25% of IC patients. The rate of amputation for these surgical patients ranges from 4% to 8% (251). The five-year mortality rate for IC patients is about 30%, primarily from cardiovascular disease (251). Therefore, therapies that can prevent or delay these surgical procedures and reduce the mortality rate are very important.

A continuous, pain-free, low intensity (LI) training program, where training was individually prescribed just below the pain threshold, was introduced by Stopka (née Boyd) in 1984 but has received little attention (44). High intensity training has been the suggested treatment for IC patients. The patient is told to exercise beyond the pain threshold until they can no longer tolerate the pain. Improvements in functional walking ability with LI training for 10 weeks were comparable to published results from training at high intensity for 3-8 months (252-254). LI exercise was chosen not only to encourage patient motivation and discourage attrition, but also because endurance training (in normals) produces improvements in aerobic (oxidative) metabolism. LI training has been shown recently in normal elderly patients (without IC) to be as effective as high intensity training in improving exercise tolerance (255). Anaerobic metabolism is used extensively by PVD patients during exercise and may be related to the development of their claudication pain. Therefore improving their aerobic metabolism is expected to result in less reliance on anaerobic metabolism and less pain.

The cause of the improvement seen in IC patients with exercise training is uncertain. Possibilities include altered walking techniques, adaptations in pain tolerance, improvement of blood flow to or within the muscle, improved oxygen extraction from the blood into the cells, decreased viscosity of the blood, and increased or more efficient use of oxygen by the mitochondria (256). The relationship between large vessel blood flow and the severity of IC has not been found to correlate well (257). Improvement in maximum blood flow to the calf with training has

been shown to increase by some authors (258) and remain unchanged by others (259), even with two-fold increases in walking distance (252). One explanation of these discrepancies is that local muscle blood flow does not necessarily correlate with flow in the larger vessels (45). Stopka's study showed about 23% improvement in a subgroup of her patient population that excluded one patient that only participated 61% of the time. She used a xenon washout technique that correlates with muscle blood flow and capillary permeability (260). If all patients are included, the difference in perfusion is still 20% though this is not statistically significant probably due to the small number of patients used. Sample size determination, using the method outlined in Appendix A and Stopka's original data on all of her subjects, suggests that about 30 subjects would be necessary for statistical significance. Studies of endurance-trained rats show an increase in the capillary density after training (261). Increase in regional blood flow to individual muscle involved with exercise training has been shown in rats (261). High intensity training results in an increase in blood flow to muscles containing a large proportion of fast, glycolytic fibers. These same fibers acquire increased potential for oxidative metabolism. When moderate intensity training is used, increase in blood flow and oxidative enzymes is seen in slow-twitch, oxidative fibers. Thus, exercise training of different intensities produce changes in the vascular beds and fibers of the muscles that have the greatest relative increase in activity during the training sessions (261). An increase in oxidative mitochondrial enzyme activity with endurance training has been seen in humans (262-264) and animals (259). Increase in

oxidative enzymes as a result of PVD has been shown in humans (265, 266) without training. Training of rats with surgically reduced blood flow (267, 268) and humans with mechanically reduced blood flow to an extremity (269) has shown increased oxidative mitochondrial enzymes in skeletal muscle. Evidence of increased ability to extract O_2 has been demonstrated in perfused rat muscle that has previously become trained under conditions of reduced blood flow (268) and in human claudicants after training (270). This improved extraction of O_2 in PVD patients is in addition to the approximately 25% increase in O_2 extraction seen in PVD patients prior to exercise training (271).

Metabolic differences in skeletal muscle between normal subjects and IC patients include the following (45, 46, 272): (1) IC patients show a greater depletion in PCr and greater fall in pH during exercise and a slower recovery of PCr and pH after exercise. (2) A slower rate of recovery of ADP is seen after exercise in IC patients. Oxidative mitochondrial activity is tightly controlled by ADP except at very low levels of PCr (273, 274). The maximum ADP recovery rate is therefore an indication of maximum oxidative mitochondrial function (247).

Objective

Our aim was to monitor IC patients' calf muscle with P-31 NMR spectroscopy before and after the course of LI exercise training. By looking at recovery rates of PCr, Pi, pH, and phosphorylated sugars, we hoped to gain a better understanding of the mechanism of improvement of exercise performance in IC patients. It was hypothesized that improvements in recovery rates of PCr, Pi, pH and phosphorylated sugars would be seen.

Materials and Methods

Patient population

Two groups of patients were trained and evaluated, approximately one year apart from each other. Both groups consisted of nine patients each. The age of the patients was 63±9 years (range: 46-75). The nonspectroscopy data and results of the first nine patients have been previously described in the master's thesis by Lori K. Marburger (256). The spectra obtained at that time have been re-fitted and re-analyzed in combination with the spectral data obtained from the second batch of patients. The criteria for patient selection were the presence of IC and an ankle-brachial index (ABI) < 0.8. The normal ABI is 1.0 and severe PVD patients may have an ABI < 0.5 (275). The patients were referred from Gainesville vascular surgeons. Five age-matched, healthy control volunteers were evaluated with P-31 MRS but did not participate in the exercise training program. All patients gave written informed consent for the study.

Exercise program

The patients were exercised three times a week for 10 weeks. Each exercise session began with 10 minutes of stretching and light calisthenics to prepare the body for aerobic exercise and to reduce the risk of injury. The aerobic exercise consisted of walking around the indoor track in the Steven C. O'Connell Center at a rate that allowed continuous pain-free walking for 15-20 minutes. Once the patients could walk at a speed of 1.5 mph or greater, they used Trackmaster TM200E treadmills (whose minimum speed is 1.5 mph) at the Center for Exercise Science/Living Well

Program. The speed of the treadmill was increased gradually at 0.1 mph increments and the duration of exercise was increased to 20-60 min, maintaining a continuous, pain-free intensity. Data collected on the treadmills included total distance walked, duration, speed, and pre- and post-exercise heart rates.

Noninvasive blood flow testing

Segmental doppler systolic blood pressure measurements and photoplethysmography (PPG), in conjunction with toe systolic blood pressure measurements, were obtained before and immediately after a graded exercise test. These measurements were performed both before and after the 10-week training period. The graded exercise test was used for these measurements and for the spectroscopy sessions. The test protocol began with a speed of 1.5 mph at a 0% grade and was increased by 0.5 mph every 3 min. The first batch of patients was instructed to continue until they felt severe claudication pain or reached 10 min, whichever came first. The second batch was instructed to continue until they felt severe pain, at whatever time. During the first test (not with spectroscopy) the patients were monitored before and after with 12-lead ECG and blood pressure measurements.

Segmental doppler blood pressure measurements are obtained by inflating cuffs around the legs at several locations from thigh to ankle and measuring the maximum (systolic) pressures in the cuffs. The maximum systolic pressure is that pressure at which blood flow is stopped, as detected by continuous wave doppler ultrasound. A drop in pressure between two cuff levels of 20 mm Hg or more is indicative of a stenosis or occlusion of the arteries (275). The ABI is calculated as the ratio of the systolic pressure in the

ankle over that in the arm. This is a standard method for detecting and predicting the severity of PVD in a patient. A drop in the ABI post exercise, compared to pre exercise is another indicator of significant PVD.

PPG uses infrared light and a detector to measure changes in blood volume in the great toe during the cardiac cycle and is used to obtain systolic pressures in the toe when used in conjunction with a pressure cuff (275). This method of measuring pressure is more accurate than ankle pressures in patients with stiff, calcified arteries in the ankle (a common occurrence in diabetic patients).

Ventilatory measurements were also obtained during the stress test for noninvasive blood flow measurements. These included oxygen consumption (VO_2), carbon dioxide exhalation (VCO_2), and ventilatory exchange (liters per min). Measurements were made from expired air collected into multiple balloons at five minute increments, throughout the stress test.

Spectroscopy

We obtained a P-31 spectrum, immediately before treadmill exercise, and then 3-4 spectra consecutively immediately after treadmill exercise. This allowed us to assess the P-31 energy status of the resting muscle and the course of recovery from exercise. Spectra were obtained either with a Siemens 1.5 T whole body Magnetom (the first batch of patients), or a General Electric 1.5 T whole body Signa imaging spectrometer (the second batch of patients). A home-built, 12 cm diameter, half-saddle RF coil double-tuned to H-1 and P-31 was used for transmitting and receiving. After shimming on the water signal, unlocalized P-31

spectra were obtained with TR=2 sec, 128 averages, 2000 data points, and a spectral width of 2 kHz. Each spectrum required 4.3 min to accumulate. The total examination time from first spectrum to last was about one hour.

The spectra were analyzed on a Sun 3/110 work station using Fitspec software provided by SISCO or on a Sparc IPC workstation running GE SA/GE software. Spectra were apodized with 3 Hz line broadening and zero filled to 8K. After FFT, phasing, and sinc-deconvolution correction of the baseline, the peaks were fit with Lorentzian curves. The pH was measured from the chemical shift between the Pi and PCr peaks (1) using the following form of the Henderson-Hasselbalch equation (247):

$$pH = 6.75 + \log_{10}\frac{\sigma - 3.27}{5.69 - \sigma}$$

The values of pH and the P-31 metabolite levels during recovery were plotted against time after cessation of exercise in minutes and fitted with a monoexponential curve to obtain a recovery rate. The differences between the values of the first two postexercise acquisitions was also tested. The recovery rates pretraining were compared to those posttraining using a two-tail paired t-test. The duration of exercise, speed, total distance and vascular data from both sets of patients were analyzed using paired t-tests to test for significant differences pre- and posttraining.

Results and Discussion

In the first batch of patients, two subjects dropped out because of unrelated problems, one an accident and one, medical

problems. Two additional patients had spectroscopy data lost by the computer or incomplete, leaving five completed patients. In the second batch, seven of the nine patients completed the study. In one of the seven subjects, some delayed spectra from the first test period were lost by the computer. We therefore were able to obtain pH and metabolite recovery information from a total of eleven patients.

Exercise results

After ten weeks of training, the subjects improved significantly ($p< 0.0001$) in duration, rate, and total distance walked without pain. The mean pain-free training time increased from 23.3 to 49.1 minutes, the mean pain-free training rate increased from 1.2 mph to 2.1 mph, and the mean pain-free training distance increased from 0.46 miles to 1.70 miles.
During stress testing, the time to onset of pain increased from 2.09 min to 6.89 min ($p<0.0001$) and the maximum time walked increased from 9.01 min. to 12.52 min. ($p=0.0001$). There was a trend toward significance in the maximum heart rate during the stress test ($p=0.0589$), increasing from an average of 70 to 95 beats per min.

Ankle-brachial index

The ABI, tested with a paired t-test, showed a modest but statistically significant 5.3% increase post training ($p=0.0222$). The mean and standard deviation of the ABI changed from 0.57±0.22 to 0.60±0.23. The range of the per cent change of the ABI from pre- to posttraining was fairly large, -9.5% to 67%.

Segmental pressures

The segmental pressures showed no significant change in pressure from pre- to posttraining at any of the levels in the leg including the toe pressures performed with PPG.

Ventilatory measurements

The VO_2, VCO_2, and Ventilatory exchange showed no significant change from pre training to post training at the time of onset of pain nor at the time of end of the test. The ratio of VCO_2/VO_2 did increase significantly. The ratio increased from 0.789 to 0.868 ($p=0.0025$) at time of onset of pain, and from 0.984 to 1.057 ($p=0.0097$) at the end of the exercise test. At five minutes, the ratio was not significantly different from pre- to posttraining ($p=0.394$).

The VCO_2/VO_2 ratio reflects the relative proportion of use of glucose and fat as energy sources (276). The breakdown of one mole of glucose to CO_2 and water requires six moles of oxygen and produces six moles of CO_2 resulting in a VCO_2/VO_2 ratio of one. The breakdown of fat produces about seven moles of CO_2 for 10 moles of oxygen consumed resulting in a VCO_2/VO_2 ratio of 0.7. The increase in the ratio from pre to post training, seen at time of onset of pain and at the end of the test, can be explained by the fact that the patients exercised for both a longer period, and at higher intensity. Low intensity, endurance exercise is known to favor the use of fat for energy and therefore a low VCO_2/VO_2 ratio. High intensity exercise, as seen toward the end of the exercise stress test, favors the use of glucose for energy and therefore a higher ratio as we see in our post training testing. At a constant time

(i.e., 5 min) and therefore constant work load, the ratio would be expected to remain the same, as it did in this study.

Spectroscopy

Figure 5-1 shows a set of spectra for one of the patients obtained pre- and postexercise test. A significant decrease in the pH ($p=0.0048$) and increase in the PME peak ($p=0.0003$) was seen immediately after the exercise test in the claudication patients. Slight elevation of the PME peak was seen in the normal volunteers immediately after exercise. After exercise, the elevated PME peak promptly returned to preexercise levels in the normal volunteers, with the first post exercise spectrum showing a mean 6.3% elevation from rest that was not statistically significant($p=0.486$). The IC patients showed a 74.1% increase in PME at the first postexercise spectrum with a prolonged rate of recovery. The aged-matched normal volunteers also showed a significant drop in pH at the first post exercise spectrum ($p=0.0034$) and a trend toward significance in the decrease of PCr ($p=0.0998$). The volunteers had a mean resting pH slightly higher than the patients with a trend toward significance ($p=0.0896$) that disappeared after training ($p=0.4502$). Accumulation of phosphorylated sugars (such as fructose phosphate) has been found in biopsies of ischemic rat muscle (277) and the elevation in the PME peak during exercise has been attributed to accumulation of these phosphorylated sugars as a result of energy demands exceeding that provided by aerobic glycolysis (45). The increased demand for energy results in activation of anaerobic glycolysis with production of lactic acid in the muscle. The lactic acid causes decrease in the pH, which when low enough, inhibits the

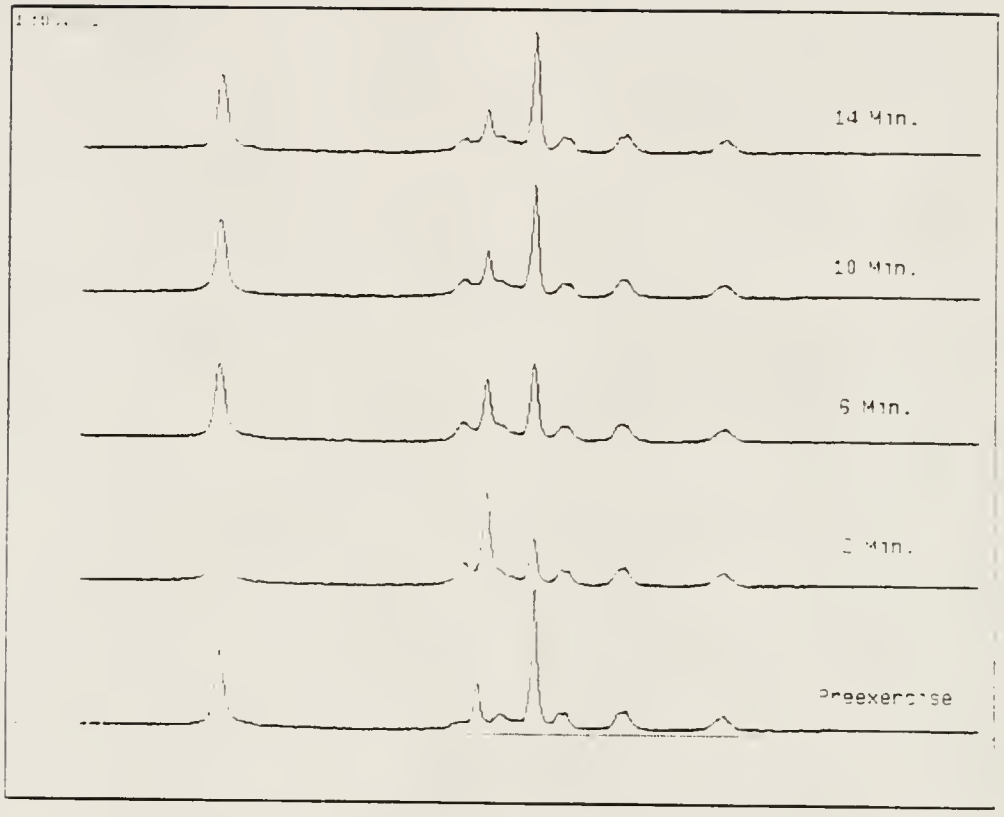

Figure 5-1 Set of spectra from one of the exercise patients, pre- and postexercise test. The bottom spectrum is preexercise, the remainder are postexercise in order of time posttest.

enzyme, phosphofructose kinase. This enzyme converts fructose-6 phosphate to fructose 1,6-diphosphate. As a result, fructose-6 phosphate, and its precursor, glucose-6 phosphate accumulate. The enzyme that converts glucose-6 phosphate to fructose-6 phosphate is also inhibited by a low pH, contributing to the accumulation of phosphorylated sugars at low pH during exercise.

Little lactic acid is metabolized in the muscle. The pyruvate kinase in muscle, which converts pyruvate to lactate during exercise, favors conversion of pyruvate to lactate rather than lactate to pyruvate. Most of the lactic acid diffuses into the blood and is carried to the liver where it is metabolized. The decrease in the lactate and therefore the recovery of pH after exercise, is dependent to the greatest degree on blood flow removing the lactate from the muscle. Therefore, an improvement in the rate of recovery of pH and PME might be expected with improved blood flow to the muscle.

The recovery rates of the PCr and Pi peaks did not change significantly from pre- to posttraining. In half of the patients, the PCr and Pi had recovered to within 10% of their resting values during the 1-1/2 to 3 min. that it took to get the patient from the treadmill to the spectrometer. The resulting fitting of data would not be accurate. Several remaining patients could work considerably longer post training, resulting in a larger decrease in pH than before training. The lower pH will delay the PCr recovery in spite of improved oxidative metabolism. The PME and pH data from three out of eleven of the patients failed to fit well with an exponential curve, either because of rapid recovery or because of statistical variation. Eliminating these three resulted

in some significant changes in the recovery rate of pH and PME; however, this biases the results toward the patients with slower recovery. Testing of the difference between the values from the first and second spectra postexercise on all subjects resulted in no significance difference pre- to posttraining in the recovery of the pH or any of the metabolites. Figures 5-2a-d show graphs of the PCr, Pi, PME, and pH for two of the patients as a function of time after exercise ended. The values at time zero correspond to preexercise data. The top graph in the figures corresponds to a patient with moderate symptoms of IC. The bottom graph corresponds to a patient with severe symptoms of IC. The bottom patient could only walk about 10 meters before stopping to rest. The more severe patient could achieve a higher Pi and a lower pH after exercise training. The patient with moderate symptoms had a lower Pi and higher pH after training but was originally able to change these values to a greater degree before training than the less-fit patient. After the course of exercise training (8-12 weeks), immediately after exercise, the patients' spectra tended to respond more like those of normal subjects. We plan to continue these studies with an in magnet ergometer that will allow us to obtain data during and immediately after exercise.

Blood flow data from this study, a high intensity exercise study (252), and previously published data showing improvement in xenon flow and washout after low intensity training (44) suggest that at least one component to the improved endurance and aerobic capacity of our patients is related to increase in blood flow or capillary permeability. This may be accompanied by an improvement in oxidative metabolism (262) and an increase in skeletal muscle

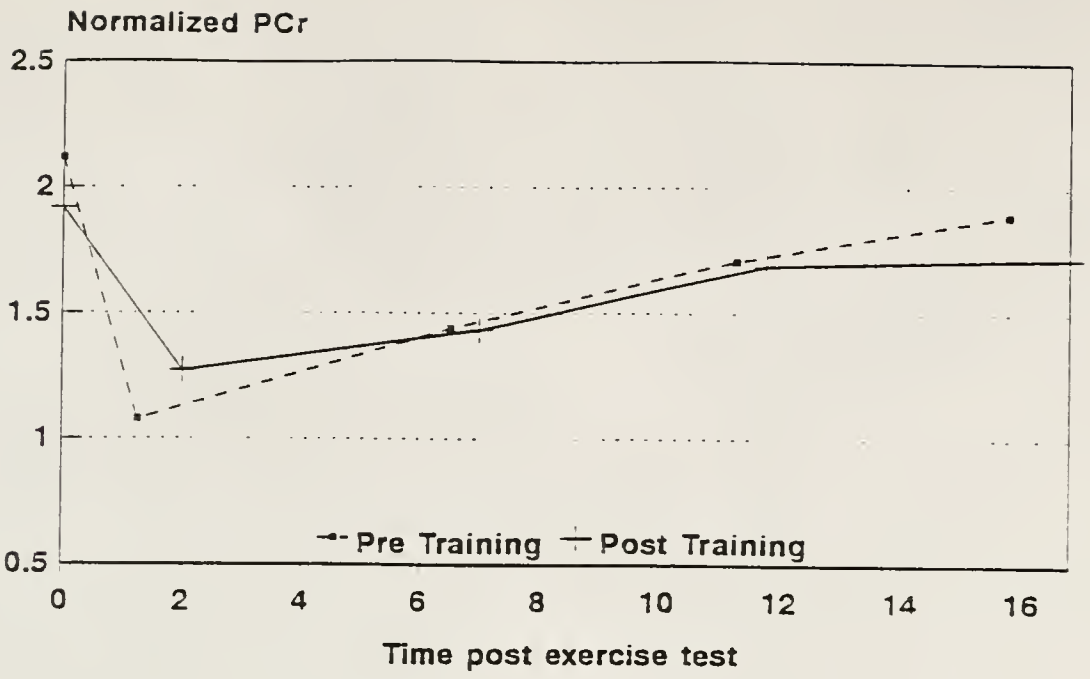

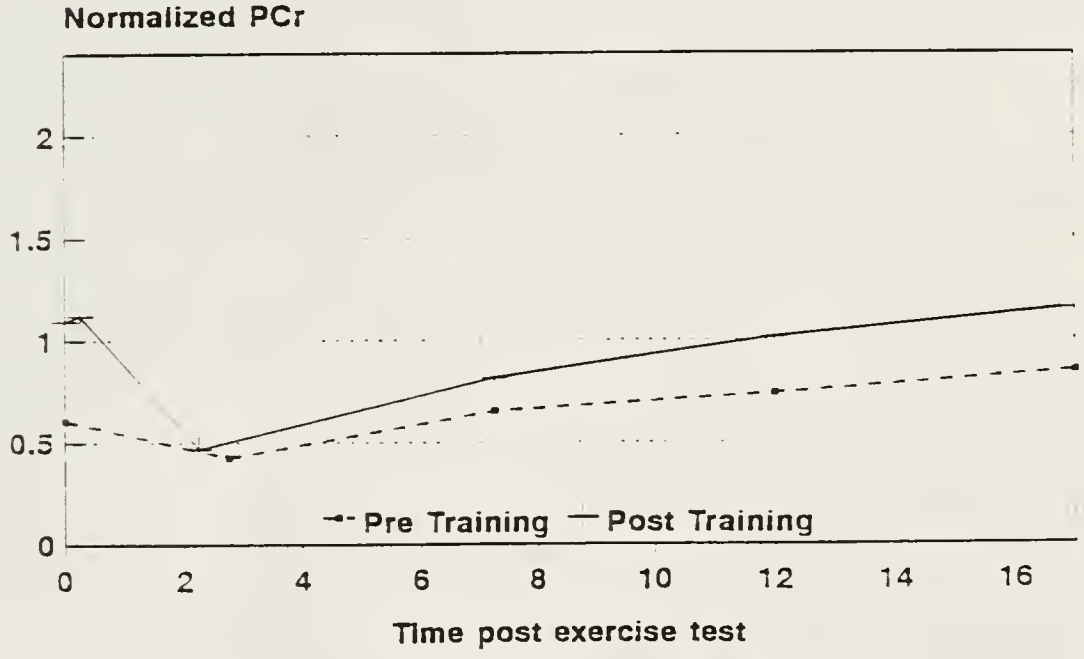

Figure 5-2 Metabolite levels and pH as a function of time for two IC patients, pre- and posttraining. The top is from a patient with moderate disease, the bottom from a patient with severe disease.
a) PCr.

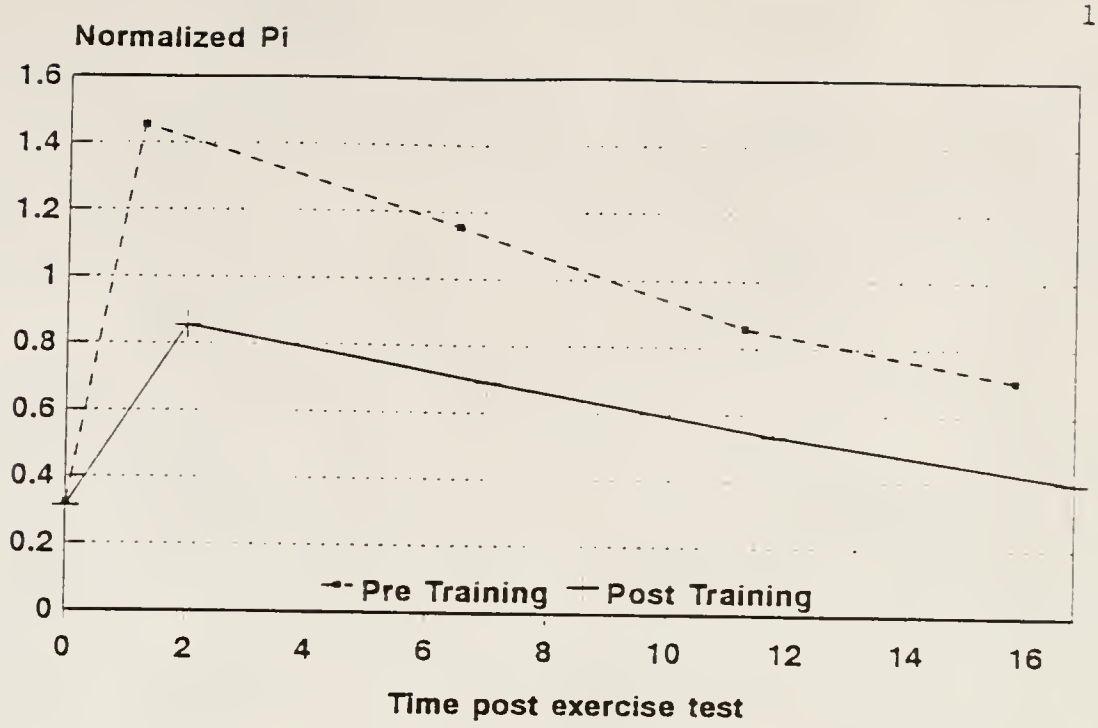
Normalized Pi
1.6
1.4
1.2
1
0.8
0.6
0.4
0.2
0
Pre Training
Post Training
0
2
4
6
8
10
12
14
16
Time post exercise test

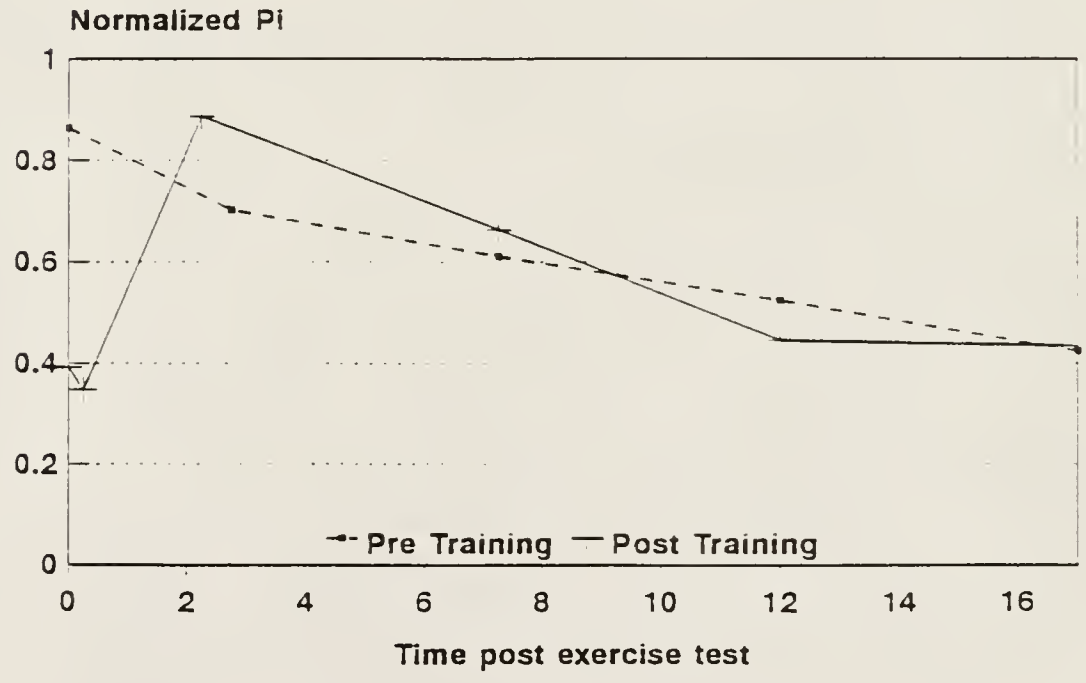
Normalized Pi
1
0.8
0.6
0.4
0.2
0
Pre Training
Post Training
0
2
4
6
8
10
12
14
16
Time post exercise test

b) Pi.

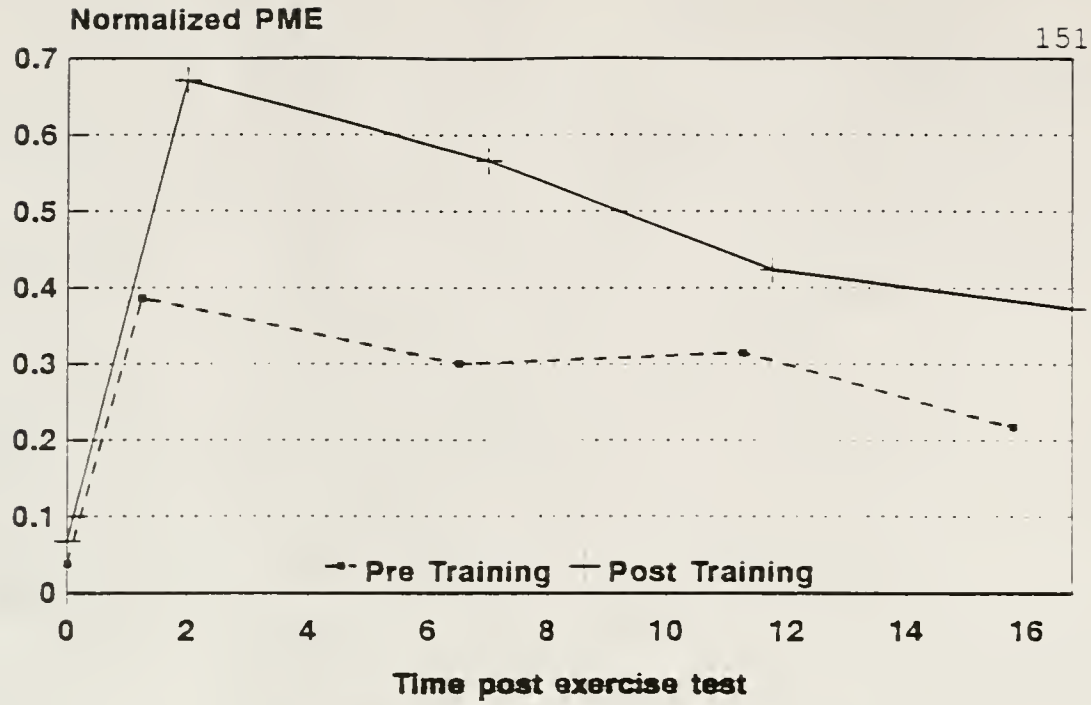
Normalized PME
0.7
0.6
0.5
0.4
0.3
0.2
0.1
0
Pre Training
Post Training
0
2
4
6
8
10
12
14
16
Time post exercise test

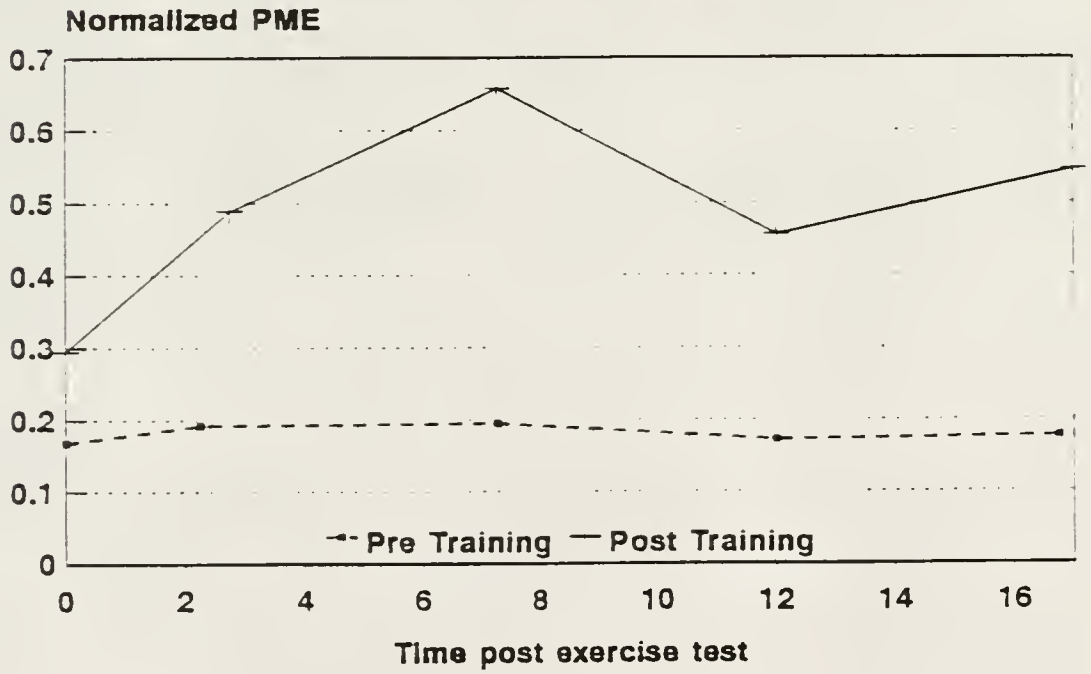
Normalized PME
0.7
0.6
0.5
0.4
0.3
0.2
0.1
0
Pre Training
Post Training
0
2
4
6
8
10
12
14
16
Time post exercise test

c) PME.

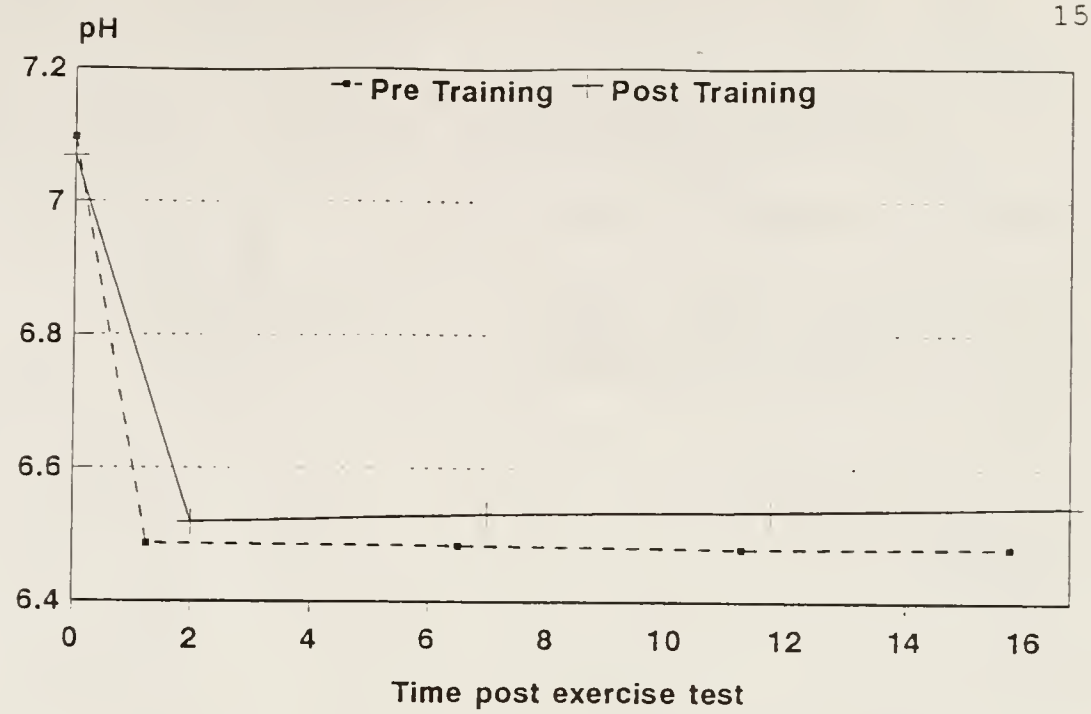
pH
7.2
7
6.8
6.6
6.4
Pre Training
Post Training
0
2
4
6
8
10
12
14
16
Time post exercise test

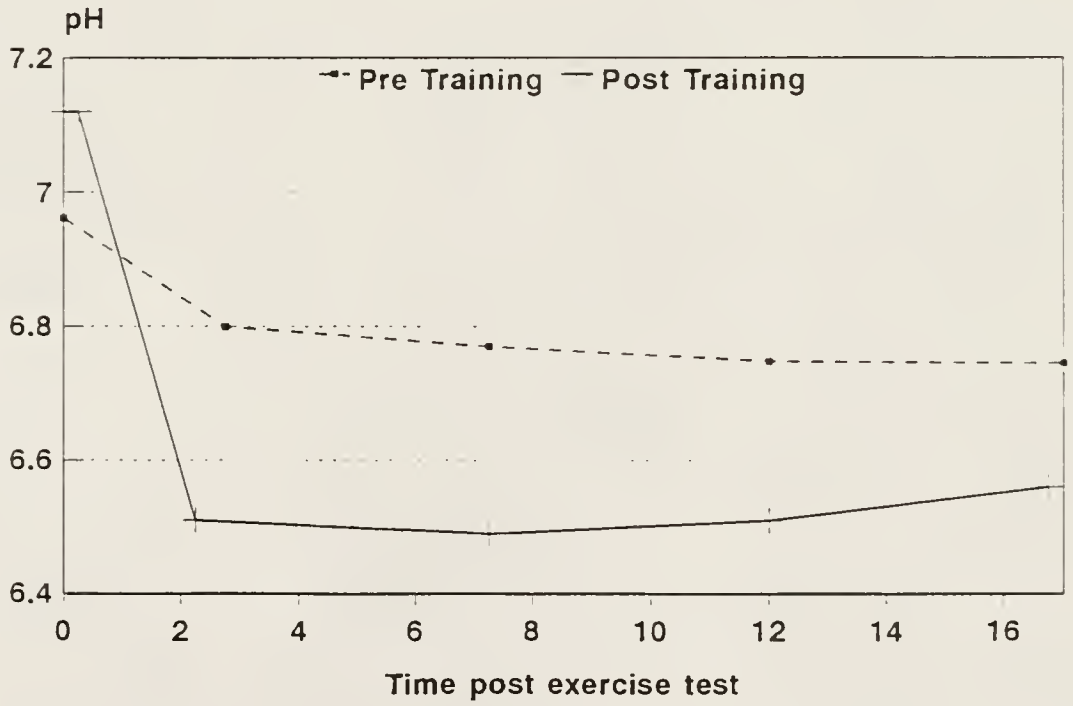
pH
7.2
7
6.8
6.6
6.4
Pre Training
Post Training
0
2
4
6
8
10
12
14
16
Time post exercise test

d) pH.

mitochondria enzymes as described by other authors (267, 268). Increased extraction of O_2 from the blood probably contributes to the improved exercise tolerance. The apparent discrepancy between the modest increase in blood flow and the more marked increase in exercise capacity may be explained as follows. In the claudication patients at rest, a large fraction of the maximum blood flow to the leg (for example, an arbitrary 80%) is used just for maintaining resting metabolism. A 20% increase in the maximum blood flow to the leg as a result of training would result in an increase of the original 20% discretionary blood supply (that could be used for exercise) to 40%. This would result in doubling the aerobic capacity for exercise. This effect is further magnified if the O_2 extraction efficiency increases. Untrained IC patients compensate for compromised blood flow by increasing the efficiency of extraction of O_2 during exercise, as has been indicated by a greater arteriovenous O_2 difference when compared to normals (278). Aerobic glycolysis is nine times more efficient at producing ATP than anaerobic glycolysis (151). This would result in further magnification of the effect of increased blood supply to the leg after training.

Comparison of Cellular Metabolism in PVD Patients, CHF Patients, Heart Transplant Patients and Normal Volunteers using P-31 MRS

Background

A decrease in exercise tolerance occurs in both PVD and CHF patients when compared to age-matched normal volunteers (46, 47, 49, 251, 252, 279). Recent P-31 NMR studies have separately examined PVD patients (45, 46) and CHF patients (47, 48, 279, 280)

and have shown evidence suggesting abnormalities in oxidative metabolism. No single study that I am aware of has examined both PVD and CHF patients with the same exercise protocol. The altered oxidative metabolism may be on a different basis for these two groups of patients. PVD patient with mild to moderate claudication have been reported to have an increase in both glycolytic and oxidative mitochondrial enzyme activity (266). PVD patients with severe claudication or resting pain have been found to have a decrease in glycolytic enzymes and increased oxidative mitochondrial enzyme activity (266). All CHF patients, on the other hand, have been found to have a decrease in mitochondrial enzyme activity (279, 281). P-31 MRS in both PVD and CHF patients has shown no significant change in metabolite levels at rest when compared to normals. During exercise, both types of patients show a faster decline and lower level of PCr and pH and a slower recovery rate of the PCr and pH (45, 48, 49). Calculated ADP levels are also reported to be higher during exercise and to recover more slowly in both sets of patients. The NMR changes could not be explained by alteration in blood flow to the extremity in the CHF patients (47-49). There was only a mild correlation found between the NMR changes and muscle atrophy (280). There is a moderate correlation between the clinical severity of the CHF and the degree of change in the NMR spectra in both humans (47) and in a rat model (282). A statistically significant 46% increase in the percentage of the fast-twitch, glycolytic, type IIb skeletal muscle fibers of CHF patients was reported (279). These findings suggest that there is either shunting of blood flow away from active muscle to inactive

tissues, or intrinsic alterations of skeletal muscle, or both (281). The decrease in mitochondrial enzyme activity mentioned above and the shift in muscle fiber type from oxidative to glycolytic suggests that intrinsic alteration of skeletal muscle exists in CHF patients. Deconditioning could cause the intrinsic alterations and could explain the NMR changes though this has not been proven (281, 282). These alterations have been seen in the dominant arm of the CHF patients, an extremity that would be used regardless of how disabled a patient was (49). These findings in the arm go against the deconditioning hypothesis. Finally, the administration of carnitine, has been found in some studies to increase exercise endurance in coronary artery disease (283-285) and PVD (286) patients. Carnitine carries long chain fatty acids across the mitochondrial membrane to be metabolized and has been found to be deficient in PVD patients in one study (287). These findings hint to metabolic abnormalities in PVD and CHF patients.

Materials and Methods

Population

Initial testing was performed on four 20-40 y/o volunteers. Following refining of the technique, three claudication patients, four CHF patients, four heart transplant, and four age-matched normal volunteers were studied.

Spectroscopy

The patient is placed in the Signa whole body imager with their foot resting against the pedal of an in-magnet ergometer constructed by Jim Scott modeled along a design from the literature (288). The ergometer is constructed of wood and brass fasteners with a brass and plastic piston and cylinder connected

to a nitrogen gas tank. The pressure of the gas is regulated at the tank with a conventional regulator. A T1-weighted multislice image of the calf is obtained with the body coil using the following parameters: TR=800 ms, TE=18 ms, one average, 1 cm slice thickness, 20 contiguous slices. The purpose of the image is to allow quantitation of muscle volume and documentation of muscle anatomy in the area of the P-31 surface coil placed later. An unsaturated STEAM sequence is used to obtain a spectrum from the medial gastrocnemius muscle after shimming on the water peak, to allow quantitation of fat content of the muscle. A home-made 6 cm diameter surface coil, double tuned to H-1 and P-31, is then taped over the body of the medial head of the gastrocnemius muscle. The position of the coil relative to a bony landmark, the head of the fibula, is documented for placement at follow up studies. A small vial of HCCTP (1 M concentration) is taped over the center of the coil to use for normalizing data. The patient's maximum voluntary contraction (MVC) is measured in terms of psi of pressure.

An initial 64 average phosphorus spectrum is obtained at rest with a TR=2 sec, 2 kHz spectral width, and 2000 acquisition points for a 2.1 min spectrum. A series of contiguous, 16-average, 32 sec spectra is started and 3-4 resting spectra are obtained prior to the patient initiating work. Except for the number of averages, the acquisition parameters were the same as the initial 64 average spectrum. The patient is then asked to push the pedal at a rate of one cycle per four seconds against a pressure equal to 85% of their MVC. We have found in our preliminary results that this results in fatigue within 4-6 min in patients, and 5-8 min in volunteers. The rate of pedal pushing is indicated to the patient

by either a person coaching at the scanner or with the use of a metronome. The patient is encouraged to exercise to fatigue. Spectra are accumulated for another 20 mins. We chose 20 min of recovery as some of our claudication patients discussed in a previous section took this long or longer to recover their baseline pH. If complete recovery is in question at the end of the 20 min of rest, additional 64 average spectra are obtained.

Spectral analysis

Spectra were sent by ethernet to a Sparc IPC workstation to be processed with GE SA/GE software. Spectra were apodized with an exponential function to obtain a line broadening of 3 Hz, zero-filled to 4096 points, Fast Fourier Transformed (FFT) and phased with zero order and first order correction. Mild baseline distortion because of loss of the initial points in the first two dwell periods was corrected with a sinc deconvolution method (289). With sinc deconvolution, FIDs are generated for the major metabolite peaks and the Fourier transform of the initial two points of these FIDs is added to the patients' spectra. This was initially done by hand, but was quite tedious. Recently, this feature has been added to the SA/GE software as an automated procedure. After baseline correction, the peak heights are measured as well as the chemical shift of Pi relative to PCr. Changes in peak height were found to correlate well with the changes in area under peaks fitted with a Lorentzian curve on several volunteer and claudication patients. Some broadening of the Pi peak occurs shortly after recovery starts; however, peak fitting of the Pi peak at this time is difficult due to it's small amplitude. For calculation of the absolute values of the

metabolites including ADP and pH, a triangulation method was used for calculating the area of the peaks since the line width of the metabolite peaks varied between the metabolites. The base length of the peak was manually measured and multiplied by half the peak height to obtain the area. Lorentzian curve fitting for 40+ spectra from each study would take hours of time with our current workstation. Automation of fitting is possible with stable spectra but because of the dramatic changes in Pi and PCr during the exercise testing, the current automation techniques do not work well. We are contemplating obtaining a faster workstation so that we can use curve fitting techniques on all of the spectra. The ADP concentrations were estimated via the creatine kinase equilibrium equation (247). ADP is thought to be the primary control of the rate of aerobic metabolism (glycolysis) in muscle. The metabolites including ADP and pH were compared pre and post treatment. In addition, recovery curves for the metabolites that changed and for the pH were generated and fit with mono-exponential curves using Statistica (Statsoft, Tulsa, OK) to obtain rate constants.

Metabolite concentrations

The ADP concentration was calculated from the following equation (247), which assumes equilibrium of the creatine kinase reaction:

$$[ADP] = [ATP][creatine]/K_{eq}[PCr]10^{pH}$$

Where K_{eq}, the equilibrium constant = 1.66×10^{9}.

The ATP concentration [ATP] is constant in exercising muscle until PCr is nearly depleted. The concentration of ATP is reported to be equal to 5.5 mmol/kg wet wt (247). Assuming that muscle is about 67% water, this gives [ATP] = 8.2 mM. The total creatine

concentration (which includes PCr), is relatively constant at 28.5 mmol/kg wet wt. (247). The [PCr] = (PCr signal/ATP signal) * 8.2 mM. The signals are corrected with relaxation factors to account for T1 relaxation differences between Pi, PCr and ATP. The other metabolite concentrations were calculated based on their relative concentration to ATP, correcting for T1 relaxation differences, assuming that T1 relaxation times do not change during exercise. We also use average T1 times of several volunteers for the correction as the time involved in measuring relaxation times on each subject would be prohibitive.

Results and Discussion

Significant differences in the exercise spectra were seen. Figure 5-3 shows selected spectra during exercise testing from a normal volunteer, a PVD patient, and a CHF patient, all done at 85% of the patient MVC. The decrease in PCr and increase in Pi during exercise is mild for the normal subject, moderate for the CHF patient, and severe for the PVD patient. Also the rate of recovery of the PCr peak is delayed in the CHF patient and more severely in the PVD patient.

Figure 5-4 shows a graph of the changes in metabolites and pH as a function of time for a normal volunteer. Figure 5-5 shows the same data for an IC patient. The PCr, Pi, and ADP show more dramatic changes in the IC patient than in the normal patient. Because the normal patient can exercise for a longer period, he shows greater changes in pH and PME than does the IC patient. Table 5-1 shows the mean and standard deviation of the resting PCr, Pi, pH, and ADP for normal volunteers, claudicants, CHF patients, and heart transplant patients.

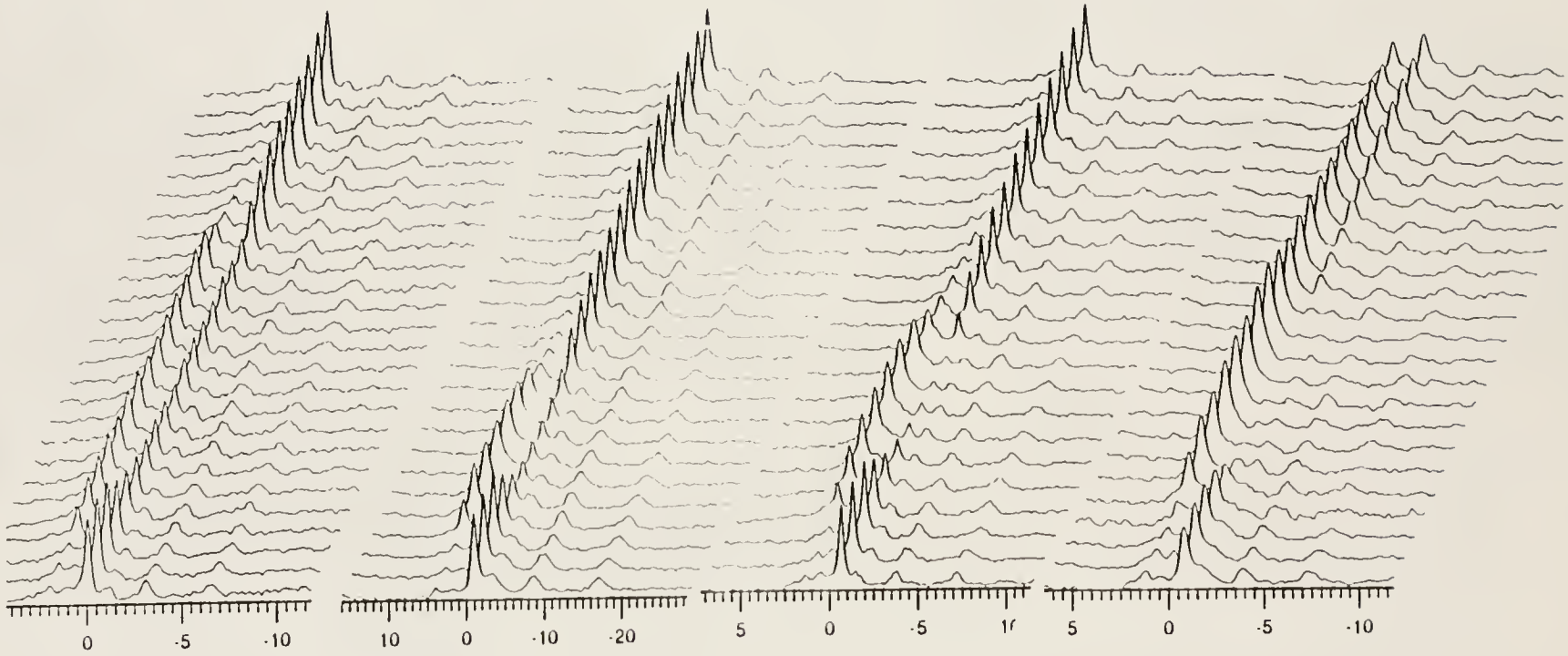

Figure 5-3 Selected spectra from exercise testing of normal subjects and patients at 85% of their MVC. The first three spectra of each are resting. From left to right are the normal subjects, heart transplants, CHF, and PVD patients.

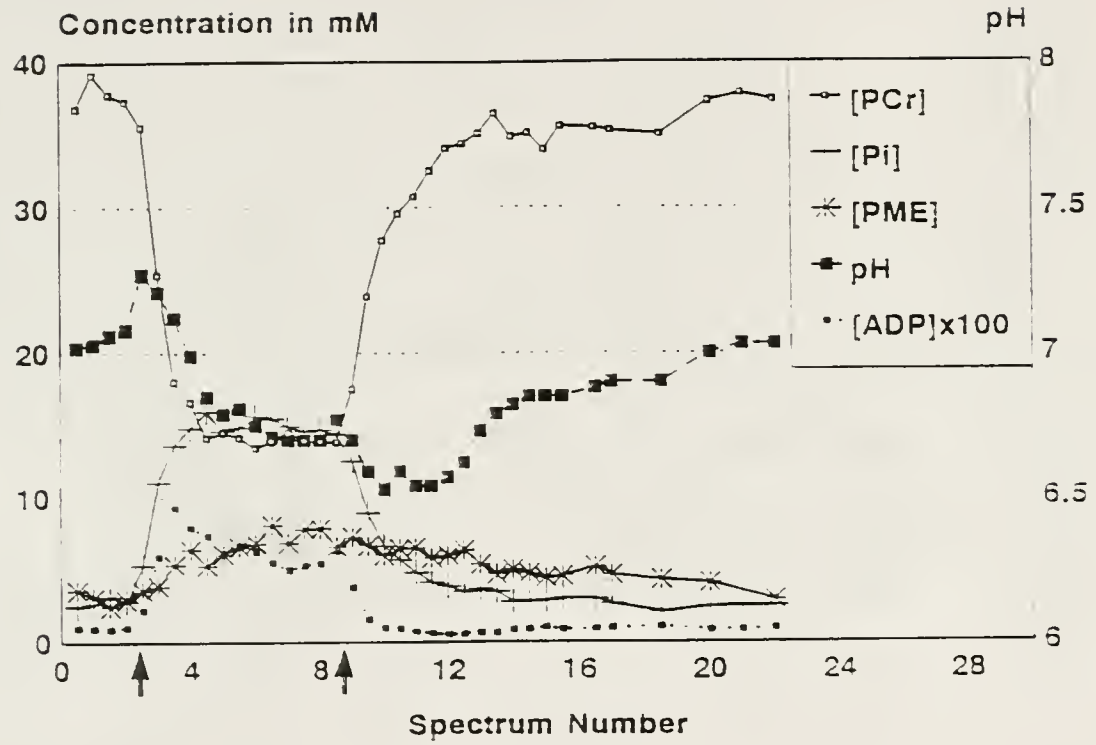

Figure 5-4 Graph of metabolite concentrations and pH as a function of time for a normal volunteer. Each number represents a 32 sec time increment. The arrows indicate the starting and the stopping time for exercise.

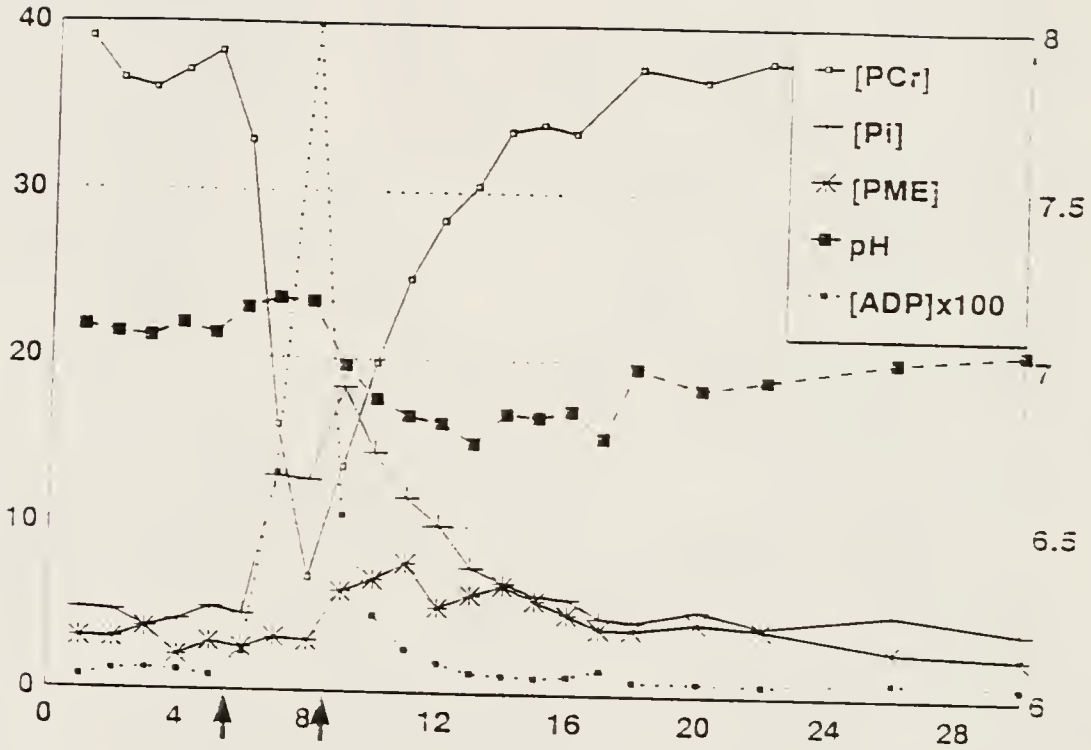

Figure 5-5 Graph of metabolite concentrations and pH as a function of time for a IC patient. Each number represents a 32 sec time increment. The arrows indicate the starting and the stopping time for exercise.

Table 5-1
Mean and Standard Deviation of Resting Metabolites and pH

	PME mM	Pi mM	PCr mM	ADP µM	pH
Normal	1.92±1.14	2.77±0.69	38.1±0.92	8.01±1.91	7.10±0.04
IC	3.86±1.34	5.83±1.34	38.8±2.60	6.92±1.41	7.04±0.06
CHF	2.54±1.89	3.42±0.89	38.7±1.13	7.38±2.55	7.12±0.05
Heart Trans	1.79±0.26	2.81±0.17	37.9±0.70	7.71±0.92	7.08±0.06

Table 5-2 shows the mean and standard deviation of the PCr, Pi, pH, and ADP at their maximum extreme at or near the end of the exercise test.

Table 5-2
Mean and Standard Deviation of the Metabolites and pH at their Extremes

	PME mM	Pi mM	PCr mM	ADP µM	pH
Normal	5.93± 3.54	16.65± 1.32	11.75± 1.27	137±67	6.65± 0.19
IC	10.61± 3.73	24.68± 7.04	5.86± 2.81	283±92	6.54± 0.21
CHF	5.02± 3.16	13.79± 3.06	10.59± 7.58	187±83	6.62± 0.22
Heart Transplant	9.74± 1.97	19.33± 4.75	7.44± 4.17	174±162	6.42± 0.09

Table 5-3 shows the mean and standard deviation for the exponential recovery rates of PCr, Pi, pH, and ADP following high intensity exercise for the same groups of subjects. All measurements, except the PME recovery rates, included the four normal subjects, three claudicants, four CHF patients, and four heart transplant patients. The PME recovery rates for the normal subjects and the CHF patients were calculated from only two people

each. Insufficient change in the PME peaks from the subjects not included was seen, preventing satisfactory curve fitting.

Table 5-3
Mean and Standard Deviation of the Recovery Rates of Metabolites and pH

	PME mM/s	Pi mM/s	PCr mM/s	ADP μM/s	pH u/sec
Normal	0.0087± 0.0131 (n=2)	0.0255± 0.0069	0.0241± 0.0081	59.9± 10.0	0.0087± 0.0048
IC	0.004± 0.0025	0.0076± 0.0045	0.0065± 0.0025	26.7± 11.0	0.0027± 0.0015
CHF	0.0041± 0.0053 (n=2)	0.0085± 0.00058	0.0093± 0.0011	24.9± 7.8	0.0017± 0.0017
Heart Transplant	0.0038± 0.0039	0.0105± 0.0014	0.0105± 0.0014	32.9± 18.6	0.0037± 0.0010

Statistical analyses of the minimum and maximum metabolite and pH values, MVC, length of the exercise test, as well as the recovery rates were performed using one-way ANOVA for the normal volunteers, IC patients, CHF patients, and heart transplant patients. A statistically significant difference at the $\alpha=0.05$ level was seen for the ADP, PCr, Pi, and pH recovery rates between normal volunteers and each of the three sets of patients. The resting Pi in IC patients was significantly higher than that in the other three groups of subjects. The maximum Pi during exercise was significantly higher in the IC patients than in the CHF patients. The MVC of normal volunteers was significantly higher than that of CHF patients. The length of the exercise test was not significantly different between the groups because of a large range of values in each group (See Table 5-4).

Table 5-4
MVC and Time to Fatigue during Exercise Test

	MVC (PSI)	Time to Fatigue (Min)
Normal	95.5±5.26	6.05±2.58
IC	84.7±8.74	3.19±1.32
CHF	72.5±16.58	3.88±2.30
Heart Transplant	76.3±7.01	4.81±1.30

The differences in metabolite and pH levels and recovery rates between normal subjects and the other three sets of subjects were expected and anticipated before the study. The metabolite concentrations and recovery rates for the heart transplant patients were quite different from normal age-matched volunteers and were only slightly better than patients with CHF. This latter finding was unexpected and raises the possibility of permanent peripheral changes in skeletal muscle metabolism that fail to improve with normal cardiac function. We will test patients immediately prior to transplant surgery and at periodic intervals posttransplant to decide if this is actually the case. The IC patients appear to have better strength but worst endurance than the CHF patients as reflected in the MVC and the length of the exercise test, although the lenght of the exercise test was not significantly different between the two groups. The differences in maximum Pi may reflect the higher work load of the IC patients.

CHAPTER 6
SUMMARY AND CONCLUSIONS

P-31 Spectroscopy of Human Osteosarcoma in a Mouse Model

Our data show a significant difference in the change of the PCr/Pi slope after treatment between sensitive and resistant osteosarcomas implanted into nude mice. The PCr/Pi slope change occurs before change in volume of the tumor.

Using the change in the slope of the PCr/Pi ratio after chemotherapy to detect the resistant tumor, we can select a threshold level that will give us a 70% specificity and a 54% sensitivity. This is not quite as good as our data with treated and untreated sensitive tumors but is qualitatively similar. We achieved an 80% specificity and a 63% sensitivity in the treated and untreated sensitive tumors. The difference between these two studies is to be expected since there was only a 5-fold difference in drug sensitivity of the two cell lines in vitro. In the future, we will test in our mouse model drugs that may reverse chemotherapy resistance (290-293). Differences in the PME between treated and untreated mice were seen as we hypothesized; however, these changes occurred while the volume of the tumors was changed. This makes it difficult to differentiate between change in PME as a direct result of the chemotherapy and change in PME as a result in change in volume of the tumor alone. The use of a volume

localization technique may allow differentiation between these two explanations of PME change.

Anesthesia with Innovar-Vet (fentanyl 0.4 mg/ml and droperidol 20 mg/ml) causes marked loss of thermoregulation in the nude mouse at doses required for immobilization for one to two hours. With this drop in temperature of the mouse there is an increase in the pH of the tumor as measured with P-31 NMR. The change in pH is -0.025±0.011 Units/°C and compares favorably to measurements of other tissues in other animals. We also found a statistically significant but small difference between the rectal temperature and the skin temperature of the mice (1.32 °C, range 0.4-3.2 °C). A significant but small increase of 0.037±0.032 units pH was seen as the anesthesia wore off. Anesthesia had no significant effect on metabolite levels. Innovar-Vet appears to be a useful sedative for nude mice during P-31 NMR experiments.

P-31 Spectroscopy of Musculoskeletal Tumors in Humans

A significant difference in the PME levels($p=0.0107$), PCr/Pi ($p=0.0002$), pH ($p=0.0442$), and β ATP ($p=0.0498$) was seen between the musculoskeletal tumor of a single patient and normal muscle from volunteers. Statistically significant differences were not seen in the PCr, Pi, and ADP levels because of large variances. It is premature to draw any conclusions from this one patient, except that the elevated PME and depressed PCr/Pi are consistent with the mouse tumor work we have done.

H-1 Spectroscopy of Human Osteosarcoma in a Mouse Model

H-1 MRS of implanted mouse tumors is technically challenging because of susceptibility effects at the interface between the tumor and air that cause broadening of the peaks of interest. The

Cho/Cr ratio was found to be elevated as has been reported in H-1 MRS of other tumors. Use of the 4.7 T system with improved spectral dispersion, and implementation of STEAM and PRESS localization techniques should prove very useful in doing additional H-1 studies in mice to monitor the effects of chemotherapy.

H-1 Spectroscopy of Musculoskeletal Tumors in Human Patients

Localized H-1 MR spectra were successfully acquired from spontaneous tumors in humans. The H-1 spectroscopy of musculoskeletal tumors showed a statistically significant difference between the mean value of the Cho/Cr ratio for malignant tumors when compared to benign tumors, necrosis, edema, and muscle. Overlap of the range of Cho/Cr values for malignant tumors exist with that of benign conditions. This difference in Cho/Cr between malignant tumors and benign conditions alone is an exciting finding. No significant difference was seen between the benign tissues with the small number of subjects evaluated. Significant changes in the Cho/Cr ratio were demonstrated following therapy, being more marked in the tumors that responded well to therapy. One of the tumors showed a change in the Cho/Cr ratio on the third day after start of chemotherapy, prior to any size or appearance change on MRI! Areas of necrosis in tumors were found to have an 80% larger lipid signal than areas of viable tumor. More subjects need to be done to determine the efficacy of H-1 MRS in differentiating chemotherapy responders from nonresponders. These subjects will need to be followed for several years to determine any correlations between spectra and long-term survival.

Exercise Studies

For IC patients, significant improvements were seen in duration, rate, and total distance walked without pain ($p < 0.0001$). During stress testing, the time to onset of pain increased from 2.09 min to 6.89 min ($p<0.0001$) and the maximum time walked increased from 9.01 min. to 12.52 min. ($p=0.0001$). The ABI showed a modest but statistically significant 5.3% increase post training ($p=0.0222$). These findings suggests that improvement in the blood supply to the exercise muscle in PVD patients occurs after a low intensity exercise training program. Improvement in mitochondrial oxidative enzyme activity may occur as well. Improvement in the patients' exercise endurance with resulting improvement in quality of life was demonstrated. P-31 MRS showed no significant change in the recovery rates of metabolites in the patients from pre- to post-training, probably because of the diversity of the patients in terms of the severity of their disease.

To our knowledge, no other investigators are monitoring LI exercise therapy in PVD patients with P-31 MRS, although this type of exercise has many advantages. Submaximal exercising de-emphasizes the participation of the anaerobic energy systems, which produce energy inefficiently, and are thought to trigger the claudication pain. As a result of de-emphasizing anaerobic glycolysis, the potential length of the exercise bout increases. Submaximal endurance exercising trains the aerobic energy systems which are associated with oxidative, pain-free activity. The motivational advantage of pain-free training is clearly much

greater than that of "no pain, no gain" exercise, in particular for claudicants. Long-term follow up will show if any significant improvement in morbidity or mortality occurs with this type of training.

The exercise testing of normal volunteers, IC patients, CHF patients, and heart transplant patients showed some expected, and also unexpected findings. A statistically significant difference at the $\alpha=0.05$ level was seen for the ADP, PCr, Pi, and pH recovery rates between normal volunteers and each of the three sets of patients. We had expected the normal volunteers to have faster recovery than the CHF and IC patients but had thought that after six months to a year postsurgery, the heart transplant patients would recover at a similar rate to normals. This was not the case. The MVC of normal volunteers was significantly higher than that of CHF patients. The extremes in metabolite concentrations, as well as the recovery rates for the heart transplant patients were quite different from normal age-matched volunteers and were only slightly better than patients with CHF. This raises the possibility of permanent peripheral changes in skeletal muscle metabolism that fail to improve with normal cardiac function. We will test patients immediately prior to transplant surgery and at periodic intervals posttransplant to decide if this is actually the case.

Summary

The most promising results of this dissertation in the long-term are the early changes in H-1 MRS seen in the musculoskeletal tumors of patients that respond to therapy. In one patient,

changes were seen within three days of start of treatment, three weeks prior to any change in size of the tumor. With more experience and long-term followup, we may be able to reduce the long and costly course of chemotherapy for those patients that fail to respond.

In the short-term, the lack of significant difference in the post-exercise spectra and recovery rates between the CHF and heart transplant patients will spur us to do longitudinal studies of the heart transplant patients. We will try to enter patients waiting for a heart transplant into an exercise program before their surgery, in hopes of improving their long term fitness.

APPENDIX A
SAMPLE SIZE DETERMINATION

The proper sample size can be determined given the following information: 1) The expected difference of the mean of the control and experimental group (δ). 2) The standard deviation (σ) of those measurements. 3) The desired confidence limits for making a type I error (α or false positive) and a type II error (β or false negative) (294). The sample size was calculated with a statistical software program (Execustat, version 2.0, Strategy Plus, Inc., Boston, Mass.) using the following equation:

$$n = 2(t_{2(n-1),\alpha} + t_{2(n-1),\beta})^2 * \sigma^2 / (\delta)^2$$

where:

α = .05

β = .05

σ = standard deviation

δ = difference of the means

APPENDIX B
STUDY SUBJECT DEMOGRAPHICS

These are statistics from the last 50 cases of lower extremity osteosarcomas on record in the University of Florida Tumor Pathology Registry:

Gender Distribution:

Male 62% Female 38%

Race Distribution:

White 72% Black 22% Hispanic 4% Asian 2%

Age Distribution (in years):

1-10: 12% 11-20: 54% 21-30: 18% 31-40: 6% 41+: 6%

The age and sex distribution reflect the published statistics of peak occurrence in the second and third decade of life and slight male predominance (128). Osteosarcoma occurring in patients over the age of 40 years is invariably secondary to Paget's disease of the bone or to prior radiation therapy. These patients are excluded from the chemotherapy protocol that is being used. The race distribution reflects that of our community. our subject demographics reflect the above statistics.

APPENDIX C
INFORMED CONSENT FORM FOR MUSCULOSKELETAL TUMOR PATIENTS

Informed Consent to Participate in Research

J. Hillis Miller Health Center
University of Florida
Gainesville, Florida 32610

You are being asked to participate in a research study. This form is designed to provide you with information about this study and to answer any of your questions.

1. TITLE OF RESEARCH STUDY

Therapy Monitoring of Osteosarcoma with Proton Magnetic Resonance Spectroscopy

2. PRINCIPAL INVESTIGATOR(S)

J. Ray Ballinger, M.D.
Consultant, Dept. of Radiology

Telephone Number: (904) 374-6101

Katherine N. Scott, Ph.D.
Professor of Radiology

Telephone Number: (904) 376-1611 ext. 5066

3. THE PURPOSE OF THE RESEARCH

This test is part of a research project to determine the usefulness of nuclear magnetic resonance (NMR) spectroscopy. Our plan is to get pictures of internal parts of the body without the use of X-rays. Another part of our plan is to get information about the chemistry of the muscles and bone without the use of biopsy and laboratory tests.

4. PROCEDURES FOR THIS RESEARCH

You will lie on a bed, which then rolls into the opening of a large magnet. A computer looks at the radio waves passing through your body and constructs pictures and chemical information from them. The total procedure will last about 90 minutes, with "stretch break" half way through. The first half of the test will give the pictures. The second half of the test gives the chemical information.

At a later date, the procedure may be repeated. This is to see what effect therapy has on the pictures and the chemistry of the muscles and bone. The chemical information part of the test is experimental, but has been done on many volunteers and patients at other institutions.

5. POTENTIAL RISKS OR DISCOMFORTS

Although very strong magnets and radio waves can be hazardous, this device operates at lower strengths that have no known risks or danger. There is no discomfort associated with the procedure.

Since the equipment uses a magnet, you must not have any metal objects in your body such as pacemakers, blood vessel clips in the head, or medical pumps. Likewise, metal objects such as coins, glasses, hair pins, jewelry, and mascara should not be present when you go into the magnet.

If you wish to discuss these or any other discomforts you may experience, you may call the Project Director listed in #2 of this form.

6. POTENTIAL BENEFITS TO YOU OR TO OTHERS

There is a chance that the information we get may provide a better understanding of your disease. There is also a chance that you will not receive any direct benefit. If the test is useful, it may provide better pictures than those from X-

rays and CAT scans. In the future, the test may provide information about the chemistry of the body without the use of biopsy and laboratory tests.

7. ALTERNATIVE TREATMENTS OR PROCEDURES, IF APPLICABLE

As an alternative procedure, conventional X-ray and computerized X-rays (CAT scans) are available which might provide helpful information. Biopsy and laboratory tests can provide chemical information. Choosing not to participate in this study, will in no way affect your care.

8. GENERAL CONDITIONS

I understand that will _____/ will not __X__ receive money for my participation in this study.
If I am compensated, I will receive:_____
I understand that I will _____/ will not __X__ be charged additional expenses for my participation in this study. If I am charged additional expenses these will consist of: _____
I understand that I am free to withdraw my/ my child's consent and discontinue participation in this research project at any time without this decision affecting my/ my child's medical care. If you have any question regarding your rights as a subject, you may phone (904) 392-3063.
In the event of my/ my child's sustaining a physical injury which is proximately caused by this experiment, Professional Medical care received at the J. Hillis Miller Health Center exclusive of hospital expenses will be provided to me without charge. This exclusion of hospital expenses does not apply to patients at the Veterans Administration Medical Center (VAMC) who sustain physical injury during participation in VAMC-approved studies. It is understood that no form of compensation exists other than those described above.
I also understand that the University of Florida and the Veterans Administration Medical Center will protect the confidentiality of my records to the extent provided by Law. The Study Sponsor, Food and Drug Administration or either Institutional Review Board may ask to review my records, however the records will remain confidential as only a number and initial will be used.

9. SIGNATURES

I have fully explained to_____
the nature and purpose of the above-described procedure and the benefits and risks that are involved in its performance. I have answered and will answer all questions to the best of my ability. I may be contacted at telephone number: 374-6101 (JRB), or 376-1611, ext. 5066 (KNS)

_____ _____
Signature of Principal or Co-Principal Investigator Obtaining Consent — Date

I have been fully informed of the above-described procedure with its possible benefits and risks and I have received a copy of this description. I have given permission of my/ my child's participation in this study.

Signature of Patient or Subject or Relative or Parent or Guardian (specify)	Date
Signature of Child (7 to 17 yrs. of age)	Date
Signature of Witness	Date

APPENDIX D
SUPERVISORY COMMITTEE MEMBERS

E. Raymond Andrew, PhD, Graduate Research Professor of Physics, Nuclear Engineering Sciences, and Radiology.

Richard W. Briggs, PhD, Associate Professor of Radiology, Affiliate Associate Professor of Biochemistry and Molecular Biology, and Affiliate Associate Professor of Chemistry.

Jeffrey R. Fitzsimmons, PhD, Associate Professor of Radiology and Nuclear Engineering Sciences.

David E. Hintenlang, PhD, Associate Professor of Nuclear Engineering Sciences.

Katherine N. Scott, PhD, Professor of Nuclear Engineering Sciences, Radiology, and Physics, Chairperson of Supervisory Committee.

APPENDIX E
EQUIPMENT LIST

2T Animal Imaging Spectrometer

Spectroscopy Imaging Systems Corporation Model VIS 85/310 imaging spectrometer (a Varian and Siemens joint venture). This included a 2 Tesla, 310 mm diameter horizontal bore Oxford Instruments magnet with a complete shim and gradient system. The system was capable of a maximum gradient strength of 2/gauss/cm with 1 millisecond rise time. The RF capability consisted of frequency synthesizers, two broad-band transmitters, power amplifiers, a heterodyne receiver system, and various RF coils for receiving H-1, F-19, P-31, C-13, and Na-23 signals. The 2T system was used for the osteosarcoma implanted into nude mice portions of this dissertation project.

Sun 3/110 Work Station

Equipped with 4 Mbytes RAM, 15-inch color raster, and Ethernet transceiver that connects all the Shands and VA NMR facilities.

General Electric (GE) Signa Whole Body Scanner

A 1.5 Tesla whole body magnetic resonance scanner at the Shands Hospital Remote Site. The magnet has a one meter bore diameter and resistive shim coils. Used to collect data for the human tumor studies, the second set of claudication patients, and the heart patients.

The scanner currently has the GE 5.4 version of Spectroscopy software. This includes programs to perform 1-D and 2-D CSI, STEAM, SPARS, PRESS, DRESS, ISIS, and single-pulse-acquire sequences.

Sun IPC work station

Equipped with GE SA/GE spectroscopy software to process our data from the whole body imager/spectrometer.

Siemens Whole Body Scanner

A 1.5 Tesla whole body magnetic resonance scanner at the VA Medical Center. Used to acquire data from the first set of claudication patients.

APPENDIX F
EXPERIMENTAL PARAMETERS FOR MRS

STEAM and PRESS

Equipment Parameters

Static Field Strength:	1.5 T
Homogeneity, Localized Volume:	2-7 Hz (Phantom)
	7-9 Hz (Human head)
	8-13 Hz (Human leg)
Frequency of H-1 Nucleus:	63.896 MHz
RF Coil (Leg & Phantoms):	Inductively coupled, paired saddle-shaped coil, 15 cm diameter or 10 cm diameter surface coil.
RF Coil (Human head):	25 cm diameter, quadrature bird cage
Gradient Strength:	1 gauss/cm
RF Amplifier Power:	16 kw

Scan Parameters

Repetition Time:	2 sec
Echo Time STEAM:	30 ms and 136 ms
Echo Time PRESS	80 ms and 140 ms
Mixing Time:	10.8 ms and 13.6 ms
Flip angle:	90°
Volume Selective Pulses:	Optimized 5-lobe sinc pulse
Pulse width:	3.6 ms

Water Suppression Pulse:	Sinc-Shaped
Pulse width:	15.5-24.8 ms
Bandwidth:	50-80 Hz
Spoiler gradient pulse width:	16 ms
Field of View:	16-32 cm (Leg, Phantoms)
	24 cm (Head)
Spectral Width:	1000 Hz
Number of Acquired Points:	2048
Spectra Acquisition Time:	4.3-10.7 min
Total Study Time:	45-75 min
Digital Resolution of Images:	128x256 points

Mouse H-1 MRS Study on 2T System

Equipment Parameters

Static Field Strength:	2 T
Homogeneity, Localized Volume:	4-10 Hz (Phantom)
	20-30 Hz (mouse tumor)
Frequency of H-1 Nucleus:	89 MHz
RF Coil (tumor & Phantoms):	15 mm diameter, 3-turn solenoid coil
Gradient Strength:	2 gauss/cm
RF Amplifier Power:	2 kw

Scan Parameters

Repetition Time:	~2.1 sec
Echo Time:	30 ms
Flip angle:	90°

Water Suppression Pulse:	Optimized 5-lobed sinc pulse
Pulse width:	20 ms
Bandwidth:	250 Hz
Field of View:	8 cm (phantoms and tumors)
Spectral Width:	1200 Hz
Number of Acquired Points:	2048
Spectra Acquisition Time:	17-27 min
Total Study Time:	60-90 min

Surface Coil Phosphorus Exercise Studies

Equipment Parameters

Static Field Strength:	1.5 T
Homogeneity, Localized Volume:	3-7 Hz (Phantom) 7-9 Hz (Human head) 11-17 Hz (Human leg)
Frequency of P-31 Nucleus:	25.87 MHz
RF Coil (Leg & Phantoms):	6 cm diameter surface coil double-tuned to H-1 and P-31. 15 cm half-saddle coil double-tuned to H-1 and P-31.
Gradient Strength:	1 gauss/cm
RF Amplifier Power:	16 kw

Scan Parameters

Repetition Time:	2 sec
Acquisition Delay:	0.98 ms
Flip angle:	90°
RF pulse shape:	gaussian
Pulse width:	1 ms

Spectral Width:	2000 Hz
Number of Acquired Points:	2048
Averages per spectrum:	16 during exercise & recovery, 64 pre- and posttest.
Spectra Acquisition Time:	32 sec each, for 27 min
Total Study Time:	60-90 min

APPENDIX G
CHEMOTHERAPY PROTOCOL

The following table gives an outline of the chemotherapy protocol as well as the imaging/spectroscopy study protocol.

	Prechemo	Week 0	Week 3	Week 6	Week 8	Week 10
CTX	Biopsy	X	X			Surgery
VP16		X	X			
CDDP				X	X	
ADR				X	X	
CT	X			X		X
MRI	X		X	X		X
MRS	X		X	X	X	X

Abbreviations: CTX-Cytoxan; VP16-VePesid; CDDP-Cisplatin; ADR-Adriamycin, MTX-Methotrexate.

After surgery, the following protocol is followed for both the good responders to presurgical chemotherapy (X) and the poor responders to presurgical chemotherapy (Y).

Week:	12	15	18	21	24	27	30	33
CTX	X		X		X		X	
VP16	X		X		X		X	
CDDP		XY		XY		XY		XY
ADR		XY		XY		XY		XY
MTX	Y		Y		Y		Y	

APPENDIX H
B_1 DISTRIBUTION PLOTS FOR RF COILS

B1 distribution on half saddle coil

7.5 cm		0.834	1.6	1.33	1.39	1.95	2.63	
6.25 cm		2.91	2.48	2.64	2.72	2.61	3.06	2.36
5.0 cm	1.83	3.69	3.25	4.42	4.81	3.83	3.67	3.77
3.75 cm	3.9	5.93	4.78	6.37	6.44	5.58	4.48	4.43
2.5 cm	1.96	10.3	8.57	8.62	10.59	7.54	7.12	5.07
1.25 cm		5.69	12.25	14.13	20.19	15.96	7.28	
0		1.14	3.59	7.09	8.75	7.71		
	0	1.25 cm	2.5 cm	3.75 cm	5 cm	6.25 cm	7.5 cm	8.75 cm

B1 Distribution of Large Shoulder Coil
1.1l bottle, NaP04 and NiSO4

11.5 cm		0.67	0.71	0.7	0.63	
9.5 cm	0.88	1.02	1.09	1.05	0.96	0.77
7.5 cm	1.34	1.52	1.59	1.56	1.43	1.15
5.5 cm	2.1	2.22	2.25	2.23	2.1	1.76
3.5 cm	3.23	3.07	3	3	3.04	2.88
1.5 cm		3.65	3.44	3.51	3.87	
	R 4.5 cm	R 2.5 cm	R 0.5 cm	L 1.5 cm	L 3.5 cm	L 5.5 cm

B1 Distribution of Small Shoulder Coil

9.5 cm	0.52	0.65	0.74	0.76	0.71	
7.5 cm	0.76	0.98	1.13	1.19	1.16	0.96
5.5 cm	1.13	1.51	1.71	1.83	1.91	1.82
3.5 cm	1.9	2.33	2.43	2.56	2.9	
1.5 cm		3.56	3.07	2.99		
	R 4.0 cm	R 2.0 cm	R 0.0 cm	L 2.0 cm	L 4.0 cm	L 6.0 cm

REFERENCES

1. R. B. Moon, and J. H. Richards, *J. Biol. Chem.* **248**, 7276 (1973).

2. D. I. Hoult, S. J. W. Busby, D. G. Gadian, G. K. Radda, R. E. Richards, and P. J. Seeley, *Nature* **252**, 285 (1974).

3. R. Kreis, B. D. Ross, N. A. Farrow, and Z. Ackerman, *Radiology* **182**, 19 (1992).

4. H. Bomsdorf, T. Helzel, D. Kunz, P. Röschmann, O. Tschendel, and J. Wieland, *NMR Biomed.* **1**, 151 (1988).

5. B. Hubesch, D. Sappey-Marinier, K. Roth, D. J. Meyerhoff, G. B. Matson, and M. W. Weiner, *Radiology* **174**, 401 (1990).

6. J. W. Hugg, G. B. Matson, D. B. Twieg, A. A. Maudsley, D. Sappey-Marinier, and M. W. Weiner, *Magn. Reson. Imaging* **10**, 227 (1992).

7. C. T. W. Moonen, G. Sobering, P. C. M. van Zijl, J. Gillen, M. von Kienlin, and A. Bizzi, *J. Magn. Reson.* **98**, 556 (1992).

8. M. Bárány, B. G. Langer, R. P. Glick, P. N. Venkatasubramanian, A. C. Wilbur, and D. G. Spigos, *Radiology* **167**, 839 (1988).

9. A. de Roos, J. Doornbos, P. R. Luyten, L. J. M. P. Oosterwaal, E. E. van der Wall, and J. A. den Hollander, *J.M.R.I.* **2**, 711 (1992).

10. R. B. Rehr, J. L. Tatum, J. I. Hirsch, L. Wetstein, and G. Clarke, *Radiology* **168**, 81 (1988).

11. K. Hendrich, Y. Xu, S.-G. Kim, and K. Ugurbil, *Magn. Reson. Med.* **31**, 541 (1994).

12. R. D. Oberhaensli, G. J. Galloway, D. J. Taylor, P. J. Bore, and G. K. Radda, *Br. J. Radiol.* **59**, 695 (1986).

13. D. J. Meyerhoff, M. D. Boska, A. M. Thomas, and M. W. Weiner, *Radiology* **173**, 393 (1989).

14. G. M. Glazer, S. R. Smith, T. L. Chenevert, P. A. Martin, A. N. Stevens, and H. T. Edwards, *NMR Biomed.* **1**, 184 (1989).

15. D. B. Vigneron, A. A. Tzika, H. Hricak, D. C. Price, P. Bretan, S. Aboseif, S. Müller, and T. L. James, *Radiology* **168**, 645 (1988).

16. R. A. Towner, T. Yamaguchi, D. J. Philbrick, B. J. Holub, E. G. Janzen, and H. Takahashi, *Magn. Reson. Imaging* **9**, 429 (1991).

17. R. M. Dixon, and J. Frahm, *Magn. Reson. Med.* **31**, 482 (1994).

18. J. Kurhanewicz, R. Dahiya, J. M. Macdonald, P. Jajodia, L.-H. Chang, T. L. James, and P. Narayan, *NMR Biomed.* **5**, 185 (1992).

19. J. Kurhanewicz, D. B. Vigneron, S. J. Nelson, H. Hricak, A. Kosco, P. Carroll, and P. Narayan, *J.M.R.I.* **3(P)**, 92 (1993).

20. F. Schick, H. Bongers, S. Kurz, W.-I. Jung, M. Pfeffer, and O. Lutz, *Magn. Reson. Med.* **29**, 38 (1993).

21. L. J. Haseler, G. J. Galloway, J. Field, M. G. Irving, and D. M. Doddrell, *Magn. Reson. Med.*, 508 (1987).

22. P. A. Narayana, E. F. Jackson, J. D. Hazle, L. K. Fotedar, M. V. Kulkarni, and D. P. Flamig, *Magn. Reson. Med.* **8**, 151 (1988).

23. P. Bachert-Baumann, M. E. Bellemann, G. Layer, W. Semmler, and W. J. Lorenz, in "Works in Progress: Society of Magnetic Resonance in Medicine Ninth Annual Meeting, New York", p.1220, Society of Magnetic Resonance in Medicine, Berkeley, 1990.

24. T. A. D. Cadoux-Hudson, M. J. Blackledge, B. Rajagopalan, D. J. Taylor, and G. K. Radda, *Br. J. Cancer* **60**, 430 (1989).

25. R. A. Hendrix, R. E. Lenkinski, K. Vogele, P. Bloch, and W. G. McKenna, *Otolaryngol. Head Neck Surg.* **103**, 775 (1990).

26. M. J. Fulham, A. Bizzi, M. J. Dietz, H. H.-L. Shih, R. Raman, G. S. Sobering, J. A. Frank, A. J. Dwyer, J. R. Alger, and G. Di Chiro, *Radiology* **185**, 675 (1992).

27. P. C. M. van Zijl, C. T. W. Moonen, J. Gillen, P. F. Daly, L. S. Miketic, J. A. Frank, T. F. DeLaney, O. Kaplan, and J. S. Cohen, *NMR Biomed.* **3**, 227 (1990).

28. S. S. Gill, D. G. T. Thomas, N. Van Bruggen, D. G. Gadian, C. J. Peden, J. D. Bell, I. J. Cox, D. K. Menon, R. A. Iles, D. J. Bryant, and G. A. Coutts, *J. Comput. Assist. Tomogr.* **14**, 497 (1990).

29. D. L. Arnold, E. A. Shoubridge, J.-G. Villemure, and W. Feindel, *NMR Biomed.* **3**, 184 (1990).

30. J. H. Langkowski, J. Wieland, H. Bomsdorf, D. Leibfritz, M. Westphal, W. Offermann, and R. Mass, *Magn. Reson. Imaging* 7, 547 (1989).

31. P. R. Luyten, A. J. H. Marien, W. Heindel, P. H. J. van Gerwen, K. Herholz, J. A. den Hollander, G. Friedmann, and W.-D. Heiss, *Radiology* **176**, 791 (1990).

32. D. K. Menon, C. J. Baudouin, D. Tomlinson, and C. Hoyle, *J. Comput. Assist. Tomogr.* **14**, 882 (1990).

33. P. A. Bottomley, C. J. Hardy, J. P. Cousins, M. Armstrong, and W. A. Wagle, *Radiology* **176**, 407 (1990).

34. J. S. Wolinski, P. A. Narayana, and M. J. Fenstermacher, *Neurology* **40**, 1764 (1990).

35. O. A. C. Petroff, D. D. Spencer, J. R. Alger, and J. W. Prichard, *Neurology* **39**, 1197 (1989).

36. H. Bruhn, J. Frahm, M. L. Gyngell, K. D. Merboldt, W. Hänicke, and R. Sauter, *Magn. Reson. Med.* **9**, 126 (1989).

37. L. L. Baker, J. Kucharczyk, R. J. Sevick, J. Mintorovitch, and M. E. Moseley, *AJR* **156**, 1133 (1991).

38. E. D. Newman, and R. J. Kurland, *Arthritis Rheum.* **35**, 199 (1992).

39. J. H. Park, J. P. Vansant, N. G. Kumar, S. J. Gibbs, M. S. Curvin, R. R. Price, C. L. Partain, and A. E. James, *Radiology* **177**, 473 (1990).

40. G. K. Radda, *Science* **233**, 640 (1986).

41. P. M. Matthews, C. Allaire, E. A. Shoubridge, G. Karpati, S. Carpenter, and D. L. Arnold, *Neurology* **41**, 114 (1991).

42. P.-Y. Marie, J.-M. Escanye, and F. Brunotte, *Clin. Sci.* **78**, 515 (1990).

43. L. Arnolda, M. Conway, M. Dolecki, H. Sharif, B. Rajagopalan, J. G. G. Ledingham, P. Sleight, and G. K. Radda, *Clin. Sci.* **79**, 583 (1990).

44. C. E. Boyd, P. J. Bird, C. D. Teates, H. A. Wellons, M. A. MacDougall, and L. A. Wolfe, *J. Sports Med.* **24**, 112 (1984).

45. L. J. Hands, P. J. Bore, G. Galloway, P. J. Morris, and G. K. Radda, *Clin. Sci.* **71**, 283 (1986).

46. M. A. Zatina, H. D. Berkowitz, G. M. Gross, J. M. Maris, and B. Chance, *J. Vasc. Surg.* **3**, 411 (1986).

47. B. Massie, M. Conway, R. Yonge, S. Frostick, J. Ledingham, P. Sleight, G. Radda, and B. Rajagopalan, *Circulation* **76**, 1009 (1987).

48. B. M. Massie, M. Conway, B. Rajagopalan, R. Yonge, S. Frostick, J. Ledingham, P. Sleight, and G. Radda, *Circulation* **78**, 320 (1988).

49. B. Rajagopalan, M. A. Conway, B. Massie, and G. K. Radda, *Am. J. Cardiol.* **62**, 53E (1988).

50. E. Achten, M. van Cauteren, R. Willem, R. Luypaert, W. J. Malaisse, G. van Bosch, G. Delanghe, K. de Meirleir, and M. Osteaux, *J. Appl. Physiol.* **68**, 644 (1990).

51. J. J. H. Ackerman, T. H. Grove, G. G. Wong, D. G. Gadian, and G. K. Radda, *Nature* **283**, 167 (1980).

52. R. Tausch-Treml, F. Baumgart, D. Ziessow, and P. Köpf-Maier, *NMR Biomed.* **5**, 127 (1992).

53. H. Kang, *Phosphorus-31 NMR spectroscopy of Human Osteosarcoma cell lines implanted into nude mice: The feasibility of early diagnosis of chemotherapy response and resistance*, Ph.D. Dissertation (University of Florida, Gainesville, 1992)

54. J. R. Fitzsimmons, H. R. Brooker, and B. Beck, *Magn. Reson. Med.* **10**, 302 (1989).

55. T. C. Ng, W. T. Evanochko, and J. D. Glickson, *J. Magn. Reson.* **49**, 526 (1982).

56. C. Y. Rim, J. B. Ra, and Z. H. Cho, *Magn. Reson. Med.* **24**, 100 (1992).

57. S. Singh, and B. K. Rutt, *J. Magn. Reson.* **87**, 567 (1990).

58. D. C. Shungu, Z. M. Bhujwalla, J. P. Wehrle, and J. D. Glickson, *NMR Biomed.* **5**, 296 (1992).

59. W. P. Aue, *Ann. N.Y. Acad. Sci.* **508**, 360 (1987).

60. R. J. Ordidge, A. Connelly, and J. A. B. Lohman, *J. Magn. Reson.* **66**, 283 (1986).

61. H. P. Hetherington, M. D. Boska, G. B. Matson, and M. W. Weiner, in "Book of Abstracts, Society of Magnetic Resonance in Medicine, Eighth Annual Meeting and Exhibition", vol. 2, p.638, Society of Magnetic Resonance in Medicine, Berkeley, 1989.

62. S. Müller, R. Sauter, H. Weber, and J. Seelig, *J. Magn. Reson.* **76**, 155 (1988).

63. J. Frahm, K.-D. Merboldt, and W. Hänicke, *J. Magn. Reson.* **72**, 502 (1987).

64. J. Frahm, T. Michaelis, K.-D. Merboldt, W. Hänicke, M. L. Gyngell, D. Chien, and H. Bruhn, *NMR Biomed.* **2**, 188 (1989).

65. P. A. Bottomley, *Ann. N.Y. Acad. Sci.* **508**, 333 (1987).

66. R. Ballinger, R. L. Magin, and A. G. Webb, *Magn. Reson. Med.* **19**, 199 (1991).

67. P. R. Luyten, AdJ. H. Marien, B. Sijtsma, and J. A. Den Hollander, *J. Magn. Reson.* **67**, 148 (1986).

68. J. A. Den Hollander, and P. R. Luyten, *Ann. N.Y. Acad. Sci.* **508**, 386 (1987).

69. C. T. W. Moonen, M. von Kienlin, P. C. M. van Zijl, J. Cohen, J. Gillen, P. Daly, and G. Wolf, *NMR Biomed.* **2**, 201 (1989).

70. R. Sauter, M. Schneider, K. Wicklow, and H. Kolem, in "Book of Abstracts: Society of Magnetic Resonance in Medicine Ninth Annual Meeting, New York", vol. 2, p.1083, Society of Magnetic Resonance in Medicine, Berkeley, 1990.

71. D. L. Arnold, in "Book of Abstracts: Society of Magnetic Resonance in Medicine Ninth Annual Meeting, New York", vol. 1, p.78, Society of Magnetic Resonance in Medicine, Berkeley, 1990.

72. T. R. Brown, B. M. Kincaid, and K. Ugurbil, *Proc. Natl. Acad. Sci. USA* **79**, 3523 (1982).

73. T. R. Brown, *NMR Biomed.* **5**, 238 (1992).

74. G. G. Steel, V. D. Courtenay, and M. J. Peckham, *Br. J. Cancer* **47**, 1 (2083).

75. L. D. Hall, V. Rajanayagam, and S. Sukumar, *J. Magn. Reson.* **61**, 188 (1985).

76. T. H. Mareci, and H. R. Brooker, *J. Magn. Reson.* **92**, 229 (1991).

77. H. R. Brooker, T. H. Mareci, and J. Mao, *Magn. Reson. Med.* **5**, 417 (1987).

78. A. G. Webb, R. W. Briggs, and T. H. Mareci, *J. Magn. Reson.* **94**, 174 (1991).

79. A. G. Webb, T. H. Mareci, and R. W. Briggs, *Journal of Magnetic Resonance, Series B* **103**, 274 (1994).

80. K. Diem, and C. Lentner, "Scientific Tables", Ciba-Geigy Limited, Basle,Switzerland, 1970.

81. P. J. Hore, *J. Magn. Reson.* **55**, 283 (1983).

82. A. G. Redfield, and R. K. Gupta, *J. Chem. Phys.* **54**, 1418 (1971).

83. A. G. Redfield, S. D. Kunz, and E. K. Ralph, *J. Magn. Reson.* **19**, 114 (1975).

84. P. Plateau, and M. Guéron, *J. Am. Chem. Soc.* **104**, 7310 (1982).

85. H. Bleich, and J. Wilde, *J. Magn. Reson.* **56**, 154 (1984).

86. P. J. Hore, *J. Magn. Reson.* **54**, 539 (1983).

87. Z. Starcuk, and V. Sklenár, *J. Magn. Reson.*, 391 (1986).

88. D. I. Hoult, and R. E. Richards, *Proc. R. Soc. Lond. A.* **344**, 311 (1975).

89. A. Haase, J. Frahm, W. Hanicke, and K. Makkei, *Phys. Med. Biol.* **30**, 341 (1985).

90. J. Frahm, K.-D. Merboldt, M. L. Gyngell, W. Hanicke, and A. Villringer, *Radiology* **165(P)**, 345 (1987).

91. J. Frahm, H. Bruhn, M. L. Gyngell, K. D. Merboldt, W. Hänicke, and R. Sauter, *Magn. Reson. Med.* **9**, 79 (1989).

92. M. Bárány, and P. N. Venkatasubramanian, *NMR Biomed.* **2**, 7 (1989).

93. C. T. W. Moonen, and P. C. M. van Zijl, *J. Magn. Reson.* **88**, 28 (1990).

94. J. Frahm, K. D. Merboldt, W. Hänicke, and A. Villringer, in "Book of Abstracts: Society of Magnetic Resonance in Medicine Sixth Annual Meeting, New York", vol. 1, p.137, Society of Magnetic Resonance in Medicine, Berkeley, 1987.

95. R. E. Lenkinski, D. P. Flamig, and J. Listerud, in "Book of Abstracts: Society of Magnetic Resonance in Medicine Ninth Annual Meeting, New York", vol. 2, p.1073, Society of Magnetic Resonance in Medicine, Berkeley, 1990.

96. J. Frahm, K. D. Merboldt, T. Michaelis, H. Bruhn, M. L. Gyngell, and W. Hänicke, in "Book of Abstracts: Society of Magnetic Resonance in Medicine Ninth Annual Meeting, New York", vol. 1, p.133, Society of Magnetic Resonance in Medicine, Berkeley, 1990.

97. G. A. Morris, and R. Freeman, *J. Magn. Reson.* **29**, 433 (1978).

98. D. B. Glasser, J. M. Lane, A. G. Huvos, R. C. Marcove, and G. Rosen, *Cancer* **69**, 698 (1992).

99. M. L. Lesser, H. I. Braun, and L. Helson, *Expl. Cell Biol.* **48**, 126 (1980).

100. D. L. Rothman, F. Arias-Mendoza, G. I. Shulman, and R. G. Shulman, *J. Magn. Reson.* **60**, 430 (1984).

101. M. Spang-Thomsen, A. Nielsen, and J. Visfeldt, *Expl. Cell Biol.* **48**, 138 (2080).

102. S. Crozier, J. Field, and D. M. Doddrell, *Magn. Reson. Imaging* **8**, 277 (1990).

103. G. C. McKinnon, and P. Boesiger, *Magn. Reson. Med.* **8**, 355 (1988).

104. C. H. Sotak, D. M. Freeman, and R. E. Hurd, *J. Magn. Reson.* **78**, 355 (1988).

105. R. E. Hurd, and D. M. Freeman, *Proc. Natl. Acad. Sci. USA* **86**, 4402 (1989).

106. C. H. Sotak, and D. M. Freeman, *J. Magn. Reson.* **77**, 382 (1988).

107. C. H. Sotak, *Magn. Reson. Med.* **7**, 364 (1988).

108. C. H. Sotak, and J. R. Alger, in "Book of Abstracts: Society of Magnetic Resonance in Medicine Tenth Annual Meeting, San Francisco", vol. 2, p.592, Society of Magnetic Resonance in Medicine, Berkeley, 1991.

109. J. E. van Dijk, D. K. Bosman, R. A. F. M. Chamuleau, and W. M. M. J. Bovee, *Magn. Reson. Med.* **22**, 493 (1991).

110. T. L. Richards, *Invest. Radiol.* **24**, 955 (1989).

111. R. Reddy, V. H. Subramanian, and J. S. Leigh, in "Book of Abstracts: Society of Magnetic Resonanace in Medicine Ninth Annual Meeting, New York", vol. 1, p.447, Society of Magnetic Resonance in Medicine, Berkeley, 1990.

112. G. C. McKinnon, and P. Boesiger, in "Works in Progress: Society of Magnetic Resonance in Medicine Eighth Annual Meeting, Amsterdam", vol. 1, p.222, Society of Magnetic Resonance in Medicine, Berkeley, 1989.

113. B. A. Inglis, S. C. R. Williams, and K. D. Sales, in "Book of Abstracts: Society of Magnetic Resonance in Medicine Tenth Annual Meeting, San Francisco", vol. 1, p.426, Society of Magnetic Resonance in Medicine, Berkeley, 1991.

114. D. Spielman, T. Brosnan, G. Glover, and A. Macovski, in "In: Book of Abstracts, Society of Magnetic Resonance in Medicine, Tenth Annual Scientific Meeting", vol. 1, p.467, Society of Magnetic Resonance in Medicine, Berkeley, 1991.

115. P. S. Tofts, and S. Wray, *NMR Biomed.* **1**, 1 (1988).

116. R. Buchli, and P. Boesiger, *Magn. Reson. Med.* **30**, 552 (1993).

117. Z. Kovalikova, M. H. Hoehn-Berlage, K. Gersonde, R. Porschen, C. Mittermayer, and R.-P. Franke, *Radiology* **164**, 543 (1987).

118. H. Barkhuijsen, R. de Beer, W. M. M. J. Bovée, and D. van Ormondt, *J. Magn. Reson.* **61**, 465 (1985).

119. H. Barkhuijsen, R. de Beer, and D. van Ormondt, *J. Magn. Reson.* **73**, 553 (1987).

120. P. A. Bottomley, and C. J. Hardy, *Clin. Chem.* **35**, 392 (1989).

121. T. Michaelis, H. Bruhn, M. L. Gyngell, W. Hänicke, K. D. Merboldt, and J. Frahm, in "Book of Abstracts: Society of Magnetic Resonance in Medicine Tenth Annual Meeting, San Francisco", vol. 1, p.387, Society of Magnetic Resonance in Medicine, Berkeley, 1991.

122. P. B. Barker, S. J. Blackband, J. C. Chatham, V. P. Mathews, and R. N. Bryan, in "Book of Abstracts: Society of Magnetic Resonance in Medicine Tenth Annual Meeting, San Francisco", vol. 1, p.388, Society of Magnetic Resonance in Medicine, Berkeley, 1991.

123. R. E. Lenkinski, and T. J. Connick, in "Book of Abstracts: Society of Magnetic Resonance in Medicine Tenth Annual Meeting, San Francisco", vol. 1, p.451, Society of Magnetic Resonance in Medicine, Berkeley, 1991.

124. K. R. Thulborn, and J. J. H. Ackerman, *J. Magn. Reson.* **55**, 357 (1983).

125. J. R. Alger, S. C. Symko, A. Bizzi, S. Posse, D. J. DesPres, and M. R. Armstrong, *J. Comput. Assist. Tomogr.* **17**, 191 (1993).

126. W. Negendank, *NMR Biomed.* **5**, 303 (1992).

127. M. J. Kane, *Semin. Oncol.* **16**, 297 (1989).

128. S. M. Krane, and A. L. Schiller, in "Harrison's Principles of Internal Medicine" (J. D. Wilson, E. Braunwald, K. J. Isselbacher, R. G. Petersdorf, J. B. Martin, A. S. Fauci, and R. K. Root, Eds.), p.1944, McGRAW-HILL, Inc., New York, 1991.

129. R. A. Wood, P. Fosarelli, M. Kudak, A. Lake, and J. Modlin, "Pediatrics", J.B. Lippincott Co., Philadelphia, 1989.

130. F. R. Eiber, and G. Rosen, *Semin. Oncol.* **16**, 312 (1989).

131. E. F. McClay, *Semin. Oncol.* **16**, 264 (1989).

132. H.-J. S. Huang, J.-K. Yee, J.-Y. Shew, P.-L. Chen, R. Bookstein, T. Friedmann, E. Y.-H. P. Lee, and W.-H. Lee, *Science* **242**, 1563 (1988).

133. P.-L. Chen, Y. Chen, R. Bookstein, and W.-H. Lee, *Science* **250**, 1576 (1990).

134. B. L. Gallie, J. A. Squire, A. Goddard, J. M. Dunn, M. Canton, D. Hinton, X. Zhu, and R. A. Phillips, *Lab. Invest.* **62**, 394 (1990).

135. L. Michiels, and J. Merregaert, in "Osteosarcoma in Adolescents and Young Adults: New Developments and Controversies" (G. B. Humphrey, H. S. Koops, W. M. Molenaar, and A. Postma, Eds.), p.7, Kluwer Academic Publishers, Boston, 1993.

136. M. Friedman, and S. Carter, *J. Surg. Oncol.* **4**, 487 (1972).

137. N. Jaffe, and D. Paed, *Cancer* **30**, 1622 (1972).

138. N. Jaffe, H. Watts, E. Frei, D. Traggis, G. Vawter, and K. Fellows, *Recent Results Cancer Res.* **62**, 114 (1977).

139. L. L. Seeger, B. E. Widoff, L. W. Bassett, G. Rosen, and J. J. Eckardt, *AJR* **157**, 347 (1991).

140. S. L. Hanna, H. L. Magill, D. M. Parham, L. C. Bowman, and B. D. Flectcher, *Magn. Reson. Imaging* **8**, 669 (1990).

141. H. Pettersson, J. Eliasson, N. Egund, B. Rööser, Willén, A. Rydholm, N. O. Berg, and S. Holtås, *Skeletal Radiol.* **17**, 319 (1988).

142. D. Vanel, M.-J. Lacombe, D. Couanet, C. Kalifa, M. Spielmann, and J. Genin, *Radiology* **164**, 243 (1987).

143. S. P. Chawla, R. S. Benjamin, N. Jaffe, C. H. Carrasco, A. K. Raymond, A. Ayala, S. Wallace, T. Armen, N. E. J. Papadopoulos, C. Plager, and J. A. Murray, in "Adjuvant therapy of cancer", vol. 5 (S. E. Salmon, Ed.), p.701, Grune & Stratton, New York, 1987.

144. R. Erlemann, J. Sciuk, A. Bosse, J. Ritter, C. R. Kusnierz-Glaz, P. E. Peters, and P. Wuisman, *Radiology* **175**, 791 (1990).

145. R. B. Sanchez, S. F. Quinn, A. Walling, J. Estrada, and H. Greenberg, *Radiology* **174**, 237 (1990).

146. G. Pan, A. K. Raymond, C. H. Carrasco, S. Wallace, E. E. Kim, A. Shirkhoda, N. Jaffe, J. A. Murray, and R. S. Benjamin, *Radiology* **174**, 517 (1990).

147. S. L. Hanna, D. M. Parham, D. L. Fairclough, W. H. Meyer, A. H. Le, and B. D. Fletcher, *Invest. Radiol.* **27**, 367 (1992).

148. K. L. Verstraete, E. Achten, A. Dierick, J. Depoorter, D. Uyttendaele, H. Roels, H. Claessens, and M. Kunnen, in "Book of Abstracts: Society of Magnetic Resonance in Medicine Eleventh Annual Meeting", vol. 2, p.2609, Society of Magnetic Resonance in Medicine, Berkeley, 1992.

149. W. E. Reddick, S. L. Hanna, D. M. Parham, J. S. Taylor, and B. D. Fletcher, in "Book of Abstracts: Society of Magnetic Resonance in Medicine, Eleventh Annual Meeting", vol. 2, p.4230, Society of Magnetic Resonance in Medicine, Berkeley, 1992.

150. P. F. Daly, R. C. Lyon, P. F. Faustino, and J. S. Cohen, *J. Biol. Chem.* **262**, 14875 (1987).

151. A. L. Lehninger, "Principles of Biochemistry", Worth Publishers, Inc., New York, 1982.

152. R. J. T. Corbett, A. R. Laptook, and R. L. Nunnally, *Neurology* **37**, 1771 (1987).

153. B. Ross, J. T. Helsper, J. Cox, I. R. Young, R. Kempf, A. Makepeace, and J. Pennock, *Arch. Surg.* **122**, 1464 (1987).

154. W. Semmler, G. Gademann, P. Bachert-Baumann, H.-J. Zabel, W. J. Lorenz, and G. van Kaick, *Radiology* **166**, 533 (1988).

155. M. Spang-Thomsen, M. Clerici, S. A. Engelholm, and L. L. Vindelov, *Eur. J. Cancer Clin. Oncol.* **22**, 549 (1986).

156. R. E. Lenkinski, J. Listerud, M. A. Shinkwin, M. B. Zlatkin, H. Y. Kressel, R. G. Schmidt, and J. M. Daly, *Invest. Radiol.* **24**, 1006 (1989).

157. K. N. Scott, B. P. Croker, W. P. Kuan, H. Kang, and J. R. Fitzsimmons, in "Book of Abstracts: Society of Magnetic Resonance in Medicine Ninth Annual Meeting, New York", vol. 2, p.843, Society of Magnetic Resonance in Medicine, Berkeley, 1990.

158. K. N. Scott, B. P. Croker, H. Kang, and C. A. Sweeney, in "Book of Abstracts: Society of Magnetic Resonance in Medicine Tenth Annual Meeting, San Francisco", vol. 2, p.620, Society of Magnetic Resonance in Medicine, Berkeley, 1991.

159. A. C. Nidecker, S. Müller, W. P. Aue, J. Seelig, R. Fridrich, W. Remagen, H. Hartweg, and U. F. Benz, *Radiology* **157**, 167 (1985).

160. O. M. Redmond, J. P. Stack, P. A. Dervan, B. J. Hurson, D. N. Carney, and J. T. Ennis, *Radiology* **172**, 811 (1989).

161. B. D. Ross, *NMR Biomed.* **4**, 59 (1991).

162. O. M. Redmond, J. P. Stack, N. O'Connor, P. A. Dervan, D. N. Carney, and J. T. Ennis, in "Book of Abstracts: Society of Magnetic Resonance in Medicine Ninth Annual Meeting, New York", vol. 1, p.321, Society of Magnetic Resonance in Medicine, Berkeley, 1990.

163. J. A. Koutcher, D. Ballon, M. Graham, J. H. Healey, E. S. Casper, R. Heelan, and L. E. Gerweck, *Magn. Reson. Med.* **16**, 19 (1990).

164. T. C. Ng, W. T. Evanochko, R. N. Hiramoto, V. K. Ghanta, M. B. Lilly, A. J. Lawson, T. H. Corbett, J. R. Durant, and J. D. Glickson, *J. Magn. Reson.* **49**, 271 (1982).

165. J. L. Evelhoch, N. A. Keller, and T. H. Corbett, *Cancer Res.* **47**, 3396 (1987).

166. J. P. Wehrle, S.-J. Li, S. Rajan, R. G. Steen, and J. D. Glickson, *Ann. N.Y. Acad. Sci.* **508**, 200 (1987).

167. R. G. Steen, and M. M. Graham, *NMR Biomed.* **4**, 117 (1991).

168. O. M. Redmond, J. P. Stack, N. G. O'Connor, D. N. Carney, P. A. Dervan, B. J. Hurson, and J. T. Ennis, *Magn. Reson. Med.* **25**, 30 (1992).

169. G. Schröter, T. Auberger, K. Schick, H. Stern, M. Zafferani, E. Flierdt, H. R. Langhammer, and H. W. Pabst, in "Book of Abstracts: Society of Magnetic Resonance in Medicine Eleventh

Annual Scientific Meeting", vol. 1, p.57, Society of Magnetic Resonance in Medicine, Berkeley, 1992.

170. S. R. Smith, P. A. Martin, and R. H. T. Edwards, *Br. J. Radiol.* **64**, 923 (1991).

171. J. W. Pan, H. P. Hetherington, J. T. Vaughan, B. L. W. Chapman, P. M. Noa, J. W. A. H. Vermeulen, and G. M. Pohost, in "Book of Abstracts: Society of Magnetic Resonance in Medicine Tenth Annual Meeting, San Francisco", vol. 1, p.113, Society of Magnetic Resonance in Medicine, Berkeley, 1991.

172. J. Ruiz-Cabello, and J. S. Cohen, *NMR Biomed.* **5**, 226 (1992).

173. J. Kasimos, T. E. Merchant, L. W. Gierke, and T. Glonek, *Cancer Res.* **50**, 527 (1990).

174. O. S. Pettengill, T. J. Curphey, C. C. Cate, C. F. Flint, L. H. Maurer, and G. D. Sorenson, *Expl. Cell Biol.* **48**, 279 (1980).

175. M. Spang-Thomsen, N. Brünner, S. A. Engelholm, and L. L. Vindelov, in "Immune-Deficient Animals in Biomedical Reseach. 5th Int. Workshop on Immune-Deficient Animals, Copenhagen 1985" (J. Rygaard, N. Brünner, N. Græm, and M. Spang-Thomsen, Eds.), p.316, Karger, Basel, 1987.

176. J. Denekamp, *NMR Biomed.* **5**, 234 (1992).

177. Y. Ohnishi, K. Maruo, T. Normura, Y. Ueyama, M. Inaba, and J.-i Hata, in "Immune-Deficient Animals in Experimental Medicine. 6th Int. Workshop on Immune-Deficient Animals, Beijing, 1988" (B.-q Wu and J. Zheng, Eds.), p.329, Karger, Basel, 1989.

178. J. C. Romijn, C. F. Verkoelen, J. Trapman, and F. H. Schroeder, in "Immune-Deficient Animals in Biomedical Reseach. 5th Int. Workshop on Immune-Deficient Animals, Copenhagen 1985" (J. Rygaard, N. Brünner, N. Græm, and M. Spang-Thomsen, Eds.), p.194, Karger, Basel, 1987.

179. H. R. MacDonald, C. Blanc, R. K. Lees, and B. Sordat, in "Immune-Deficient Animals in Biomedical Reseach. 5th Int. Workshop on Immune-Deficient Animals, Copenhagen 1985" (J. Rygaard, N. Brünner, N. Græm, and M. Spang-Thomsen, Eds.), p.51, Karger, Basel, 1987.

180. S. Ikehara, R. Yasumizu, T. Nakamura, K. Sekita, E. Muso, H. Ohtsuki, M. Ogura, J. Toki, N. Inoue, K. Sugiura, H. Iwai, M. Shintaku, N. Ihara, Y. Hamashima, and R. A. Good, in "Immune-Deficient Animals in Biomedical Reseach. 5th Int. Workshop on Immune-Deficient Animals, Copenhagen 1985" (J. Rygaard, N. Brünner, N. Græm, and M. Spang-Thomsen, Eds.), p.69, Karger, Basel, 1987.

181. T. Kobayashi, M. Inaba, T. Tashiro, Y. Sakurai, and T. Nomura, in "Immune-Deficient Animals in Biomedical Reseach. 5th Int. Workshop on Immune-Deficient Animals, Copenhagen 1985" (J. Rygaard, N. Brünner, N. Græm, and M. Spang-Thomsen, Eds.), p.356, Karger, Basel, 1987.

182. M. Inaba, T. Kobayashi, T. Tashiro, and Y. Sakurai, *Jpn. J. Cancer Res.* **79**, 509 (1988).

183. M. Inaba, in "Immune-Deficient Animals in Experimental Medicine. 6th Int. Workshop on Immune-Deficient Animals, Beijing, 1988" (B.-q Wu and J. Zheng, Eds.), p.245, Karger, Basel, 1989.

184. K. Maruo, R. Emura, Y. Ohnishi, Y. Ueyama, T. Nomura, and M. Inaba, in "Immune-Deficient Animals in Experimental Medicine. 6th Int. Workshop on Immune-Deficient Animals" (B.-q Wu and J. Zheng, Eds.), p.277, Karger, Basel, 1989.

185. N. D. Reed, E. L. Newman, and B. O. Brooks, in "Immune-Dedficient Animals in Biomedical Research. 5th Int. Workshop on Immune-Deficient Animals, Copenhagen 1985" (J. Rygaard, N. Brünner, N. Græm, and M. Spang-Thomsen, Eds.), p.30, Karger, Basel, 1987.

186. R. E. Anderson, and I. Lifkovits, *Expl. Cell Biol.* **48**, 255 (1980).

187. F. Blommaert, W. F. Cassano, and B. P. Croker, *Clin. Immunol. and Immunopath.* **60**, 430 (1991).

188. S. K. Wixson, W. J. White, H. C. Hughes, C. M. Lang, and W. K. Marshall, *Lab. Anim. Sci.* **37**, 726 (1987).

189. S. K. Wixson, W. J. White, H. C. Hughes, C. M. Lang, and W. K. Marshall, *Lab. Anim. Sci.* **37**, 736 (1987).

190. S. K. Wixson, W. J. White, H. C. J. Hughes, C. M. Lang, and W. K. Marshall, *Lab. Anim. Sci.* **37**, 743 (1987).

191. J. A. Hanley, and B. J. McNeil, *Radiology* **143**, 29 (1982).

192. C. E. Metz, *Semin. Nucl. Med.* **8**, 283 (1978).

193. P. J. Chang, *AJR* **152**, 721 (1989).

194. C. E. Metz, *Invest. Radiol.* **24**, 234 (1989).

195. D. D. Dorfman, and E. Alf Jr., *J. Math. Psych.* **6**, 487 (1969).

196. D. R. Grey, and B. J. T. Morgan, *J. Math. Psych.* **9**, 128 (1972).

197. K. T. Brunner, J. Mauel, J. C. Cerottini, and B. Chapuis, *Immunology* **14**, 181 (1968).

198. R. G. Steen, D. A. Wilson, C. Browser, J. P. Wehrle, J. D. Glickson, and S. S. Rajan, *NMR Biomed.* **2**, 87 (1989).

199. D. C. Johnson, M. Nishimura, P. Okunieff, H. Kazemi, and B. Hitzig, *Appl. Physiol.* **67**, 2527 (1989).

200. J. R. Griffiths, Z. Bhujwalla, R. C. Coombes, R. J. Maxwell, C. J. Midwood, R. J. Morgan, A. H. W. Nias, P. Perry, M. Prior, R. A. Prysor-Jones, L. M. Rodrigues, M. Stubbs, and G. M. Tozer, *Ann. N.Y. Acad. Sci.* **508**, 183 (1987).

201. P. Okunieff, E. Rummeny, P. Vaupel, S. Skates, C. Willett, L. J. Neuringer, and H. D. Suit, *Radiat. Res.* **115**, 361 (1988).

202. B. M. Fenton, R. F. Raubertas, and R. M. Sutherland, *NMR Biomed.* **4**, 137 (1991).

203. S. J. Karlik, J. Fuller, and A. W. Gelb, *Acta. Radiol. Suppl. Stockh.* **369**, 500 (1986).

204. J. C. M. Bremner, C. J. R. Counsell, G. E. Adams, I. J. Stratford, P. J. Wood, J. F. Dunn, and G. K. Radda, *Br. J. Cancer* **64**, 862 (1991).

205. S. K. Wixson, W. J. White, H. C. Hughes, W. K. Marshall, and C. M. Lang, *Lab. Anim. Sci.* **37**, 731 (1987).

206. G. J. Kost, *Magn. Reson. Med.* **14**, 496 (1990).

207. R. B. Reeves, *Respir. Physiol.* **14**, 219 (1972).

208. R. B. Reeves, *J. Appl. Physiol.* **40**, 752 (1976).

209. A. Roos, and W. F. Boron, *Physiol. Rev.* **61**, 296 (1981).

210. F. N. White, and G. Somero, *Physiol. Rev.* **62**, 40 (1982).

211. J. A. Swain, T. J. McDonald, R. C. Robbins, and R. S. Balaban, *Am. J. Physiol.* **260**, H1640 (1991).

212. T. Binzoni, G. Ferretti, F. Barbalat, and P. Cerretelli, *Respir. Physiol.* **82**, 137 (1990).

213. R. Kries, and B. D. Ross, *Radiology* **184**, 123 (1992).

214. C. E. Wright, H. H. Tallan, and Y. Y. Lin, *Ann. Rev. Biochem.* **55**, 427 (1986).

215. W. T. Evanochko, T. T. Sakai, T. C. Ng, N. R. Krishna, H. D. Kim, R. B. Zeidler, V. K. Ghanta, R. W. Brockman, L. M. Schiffer, P. G. Braunschweiger, and J. D. Glickson, *Biochim. Biophys. Acta* **805**, 104 (1984).

216. D. C. Shungu, Z. M. Bhujwalla, S.-J. Li, L. M. Rose, J. P. Wehrle, and J. D. Glickson, *Magn. Reson. Med.* **28**, 105 (1992).

217. A. Moreno, M. Rey, J. M. Montane, J. Alonso, and C. Arús, *NMR Biomed.* **6**, 111 (1993).

218. F. Podo, G. Carpinelli, M. Di Vito, M. Giannini, E. Proietti, W. Fiers, I. Gresser, and F. Belardelli, *Cancer Res.* **47**, 6481 (1987).

219. B. N. Milestone, and R. E. Lenkinski, in "Book of Abstracts: Society of Magnetic Resonance in Medicine Ninth Annual Meeting, New York", vol. 2, p.813, Society of Magnetic Resonance in Medicine, Berkeley, 1990.

220. P. Bachert, M. E. Bellemann, G. Layer, T. Koch, W. Semmler, and W. J. Lorenz, *NMR Biomed.* **5**, 161 (1992).

221. C. Arús, and M. Bárány, *J. Magn. Reson.* **57**, 519 (1984).

222. C. Arús, M. Bárány, W. M. Westler, and J. L. Markley, *FEBS Lett.* **165**, 231 (1984).

223. J. S. Beech, S. C. R. Williams, R. D. Cohen, and R. A. Iles, in "Book of Abstracts: Society of Magnetic Resonance in Medicine Tenth Annual Meeting, San Francisco", vol. 2, p.528, Society of Magnetic Resonance in Medicine, Berkeley, 1991.

224. S. R. Williams, D. G. Gadian, E. Proctor, D. B. Sprague, D. F. Talbot, I. R. Young, and F. F. Brown, *J. Magn. Reson.* **63**, 406 (1985).

225. H. Bruhn, J. Frahm, M. L. Gyngell, K. D. Merboldt, W. Hänicke, and R. Sauter, *Magn. Reson. Med.* **17**, 82 (1991).

226. D. G. Gadian, E. Proctor, and S. R. Williams, *Ann. N.Y. Acad. Sci.* **508**, 241 (1987).

227. E. R. Andrew, G. Bydder, J. Griffiths, R. Iles, and P. Styles, "Clinical Magnetic Resonance Imaging and Spectroscopy", John Wiley & Sons, Ltd., Chichester West Sussex, England, 1990.

228. D. L. Arnold, and J. G. Villemure, in "Book of Abstracts: Society of Magnetic Resonance in Medicine Ninth Annual Meeting, New York", vol. 2, p.990, Society of Magnetic Resonance in Medicine, Berkeley, 1990.

229. J. A. Frank, J. R. Alger, A. Bizzi, M. Fulham, S. W. Inscoe, J. L. Black, P. Van Zijl, C. T. W. Moonen, B. X. Desouza, and G. Di Chiro, in "Book of Abstracts: Society of Magnetic Resonance in Medicine Ninth Annual Meeting, New York", vol. 1, p.102, Society of Magnetic Resonance in Medicine, Berkeley, 1990.

230. D. Ott, T. Ernst, and J. Hennig, in "Book of Abstracts: Society of Magnetic Resonance in Medicine Ninth Annual Meeting, New York", vol. 1, p.105, Society of Magnetic Resonance in Medicine, Berkeley, 1990.

231. H. Kugel, W. Heindel, R.-I. Ernestus, J. Bunke, and G. Friedmann, in "Book of Abstracts: Society of Magnetic Resonance in Medicine Tenth Annual Meeting, San Francisco", vol. 2, p.589, Society of Magnetic Resonance in Medicine, Berkeley, 1991.

232. A. Madden, M. O. Leach, J. C. Sharp, D. J. Collins, and D. Easton, *NMR Biomed.* **4**, 1 (1991).

233. H. Bruhn, T. Michaelis, K. D. Merboldt, W. Hänicke, M. L. Gyngell, C. Hamburger, and J. Frahm, *NMR Biomed.* **5**, 253 (1992).

234. R. C. Weast, D. R. Lide, M. J. Astle, and W. H. Beyer, "CRC Handbook of Chemistry and Physics", CRC Press, Inc., Boca Raton, 1989.

235. M. L. Gyngell, M. Hoehn-Berlage, O. Kloiber, T. Michaelis, R.-I. Ernestus, D. Hörstermann, and J. Frahm, *NMR Biomed.* **5**, 335 (1992).

236. J. W. Prichard, *NMR Biomed.* **4**, 99 (1991).

237. H. D. Sostman, H. C. Charles, S. Rockwell, K. Leopold, C. Beam, D. Madwed, M. Dewhirst, G. Cofer, D. Moore, R. Burn, and J. Oleson, *Radiology* **176**, 837 (1990).

238. D. Spielman, T. Brosnan, G. Glover, A. Macovski, in "Book of Abstracts: Society of Magnetic Resonance in Medicine Tenth Annual Meeting, San Francisco", vol. 1, p.467, Society of Magnetic Resonance in Medicine, Berkeley, 1991.

239. J. Murphy-Boesch, and A. P. Koretsky, *J. Magn. Reson.* **54**, 526 (1983).

240. G. D. Zanelli, P. B. Lucas, and J. F. Fowler, *Br. J. Cancer* **32**, 380 (1975).

241. W. Roser, I. Mader, G. Hagberg, L. Kappos, E. W. Radü, and J. Seelig, in "Proceedings of the Society of Magnetic Resonance in Medicine, Twelfth Annual Scientific Meeting, New York", vol. 1, p.278, Society of Magnetic Resonance in Medicine, Berkeley, 1993.

242. O. A. C. Petroff, T. Ogino, and J. R. Alger, *J. Neurochem.* **51**, 163 (1988).

243. T. Michaelis, K.-D. Merboldt, W. Hänicke, M. L. Gyngell, H. Bruhn, and J. Frahm, *NMR Biomed.* **4**, 90 (1991).

244. W. M. M. J. Bovée, *NMR Biomed.* **4**, 81 (1991).

245. R. Wood, "Tumor Lipids: Biochemistry and Metabolism", The American Oil Chemists' Society, Champaign, 1973.

246. H. Bongers, F. Schick, M. Skalej, W.-I. Jung, and A. Stevens, *Magn. Reson. Imaging* **10**, 957 (1992).

247. D. L. Arnold, P. M. Matthews, and G. K. Radda, *Magn. Reson. Med.* **1**, 307 (1984).

248. W. B. Mackinnon, M. Dyne, K. T. Holmes, C. E. Mountford, and R. S. Gupta, *NMR Biomed.* **2**, 161 (1989).

249. A. C. Kuesel, G. R. Sutherland, W. Halliday, and I. C. P. Smith, *NMR Biomed.* **7**, 149 (1994).

250. A. Bergman, T. Victor, and R. Knop Analysis of the degree of unsaturation of fatty acids present in normal and cancerous living human breast tissue as detected by high field ^{13}C NMR. Poster #246, presented at the 34th Experimental Nuclear Magnetic Resonance Conference, St. Louis, MI.

251. N. R. Hertzer, *Circulation* **83[suppl I]**, I12 (1991).

252. R. Ekroth, A.-G. Dahllöf, B. Gundevall, J. Holm, and T. Scherstén, *Surgery* **84**, 640 (1978).

253. W. R. Hiatt, J. G. Regensteiner, M. E. Hargarten, E. E. Wolfel, and E. P. Brass, *Circulation* **81**, 602 (1990).

254. J. S. Skinner, and D. E. J. Strandness, *Circulation* **36**, 23 (1967).

255. M. J. Belman, and G. A. Gaesser, *Med. Sci. Sports Exerc.* **23**, 562 (1991).

256. L. K. Marburger, *Effects of low-intensity, pain-free exercise on muscle metabolism in patients with peripheral vascular disease evaluated by ^{31}P-NMR spectroscopy*, M.S. Thesis (University of Florida, Gainesville, 1992)

257. A. W. Gardner, J. S. Skinner, B. W. Cantwell, and L. K. Smith, *Med. Sci. Sports Exerc.* **24**, 163 (1992).

258. H. Leinonen, S. Salminen, and P. Peltokallio, *Scand. J. Clin. Lab. Invest.* **38**, 223 (1978).

259. J. O. Holloszy, and F. W. Booth, *Annu. Rev. Physiol.* **18**, 273 (1976).

260. I. Kjellmer, I. Lindbjerg, I. Prerovsky, and H. Tonnesen, *Acta Physiol. Scand.* **69**, 69 (1967).

261. M. H. Laughlin, R. J. Korthuis, W. L. Sexton, and R. B. Armstrong, *J. Appl. Physiol.* **64**, 2420 (1988).

262. J. A. Kent-Braun, K. K. McCully, and B. Chance, *J. Appl. Physiol.* **69**, 1165 (1990).

263. P. D. Gollnick, R. B. Armstrong, B. Saltin, C. W. Saubert, W. L. Sembrowich, and R. E. Shepherd, *J. Appl. Physiol.* **34**, 107 (1973).

264. G. A. Dudley, W. M. Abraham, and R. L. Terjung, *J. Appl. Physiol.* **53**, 844 (1982).

265. J. Holm, P. Björntorp, and T. Scherstén, *Europ. J. Clin. Invest.* **2**, 321 (1972).

266. A.-C. Bylund, J. Hammarsten, J. Holm, and T. Scherstén, *Europ. J. Clin. Invest.* **6**, 425 (1976).

267. A. Elander, J.-P. Idström, T. Schersén, and A.-C. Bylund-Fellenius, *Am. J. Physiol.* **249**, E63 (1985).

268. A. Elander, J.-p Idström, S. Holm, T. Scherstén, and A.-C. Bylund-Fellenius, *Am. J. Physiol.* **249**, E70 (1985).

269. L. Kaijser, C. J. Sundberg, O. Eiken, A. Nygren, M. Esbjörnsson, C. Sylvén, and E. Jansson, *J. Appl. Physiol.* **69**, 785 (1990).

270. D. Sorlie, and K. Myhre, *Scand. J. Clin. Lab. Invest.* **38**, 217 (1978).

271. L. A. Carlson, and B. Pernow, *Acta Med. Scand.* **164**, 39 (1959).

272. G. K. Radda, B. Rajagopalan, and D. J. Taylor, *Magnetic Resonance Quarterly* **5**, 122 (1989).

273. B. Chance, and G. R. Williams, *J. Biol. Chem.* **217**, 383 (1955).

274. B. Chance, J. S. Leigh, J. Kent, K. McCully, B. J. Clark, J. M. Maris, and T. Graham, *Proc. Natl. Acad. Sci. USA* **83**, 9458 (1986).

275. R. W. Barnes, *Circulation* **83[suppl I]**, I20 (1991).

276. P. R. Luyten, J. P. Groen, J. W. A. H. Vermeulen, and J. A. den Hollander, *Magn. Reson. Med.* **11**, 1 (1989).

277. C. J. Threlfall, and H. B. Stoner, *Biochem. J.* **79**, 553 (1961).

278. S. Bellman, and S. Jetterquist, *Acta Chir. Scand.* **132**, 43 (1966).

279. D. M. Mancini, E. Coyle, A. Coggan, J. Beltz, N. Ferraro, S. Montain, and J. R. Wilson, *Circulation* **80**, 1338 (1989).

280. D. M. Mancini, G. Walter, N. Reichek, R. Lenkinski, K. K. McCully, J. L. Mullen, and J. R. Wilson, *Circulation* **85**, 1364 (1992).

281. H. Drexler, *Eur. Heart J.* **12 (Supplement C)**, 21 (1991).

282. L. Arnolda, J. Brosnan, B. Rajagopalan, and G. Radda, *Am. J. Physiol.* **261**, H434 (1991).

283. P. Kosolcharoen, J. Nappi, P. Peduzzi, A. Shug, A. Patel, T. Filipek, and J. H. Thomsen, *Curr. Ther. Res.* **30**, 753 (1981).

284. T. Kamikawa, Y. Suzuki, A. Kobayashi, H. Hayashi, Y. Masumura, K. Nishihara, M. Abe, and N. Yamazaki, *Jpn. Heart J.*, 587 (1984).

285. C. Canale, V. Terrachini, A. Biagini, A. Vallebona, M. A. Masperone, S. Valice, and A. Castellano, *Int. J. Clin. Pharmacol. Ther. Toxicol.* **26**, 221 (1988).

286. G. Brevetti, M. Chiariello, G. Ferulano, A. Policicchio, E. Nevola, A. Rossini, T. Attisano, G. Ambosio, N. Siliprandi, and C. Angelini, *Circulation* **77**, 767 (1988).

287. G. Brevetti, C. Angelini, M. Rosa, R. Carrozzo, S. Perna, M. Corsi, A. Matarazzo, and A. Marcialis, *Circulation* **84**, 1490 (1991).

288. B. Quistorff, S. Nielsen, C. Thomsen, K. E. Jensen, and O. Henriksen, *Magn. Reson. Med.* **13**, 444 (1990).

289. T. Allman, G. A. Holland, R. E. Lenkinski, and H. C. Charles, *Magn. Reson. Med.* **7**, 88 (1988).

290. R. A. Kramer, J. Zakher, and G. Kim, *Science* **241**, 694 (1988).

291. R. F. Ozols, K. G. Louie, J. Plowman, B. C. Behrens, R. L. Fine, D. Dykes, and T. C. Hamilton, *Biochem. Pharmacol.* **36**, 147 (1987).

292. J. A. Green, D. T. Vistica, R. C. Young, T. C. Hamilton, A. M. Rogan, and R. F. Ozols, *Cancer Res.* **44**, 5427 (1984).

293. T. C. Hamilton, M. A. Winker, K. G. Louie, G. Batist, B. C. Behrens, T. Tsuruo, K. R. Grotzinger, W. M. McKoy, R. C. Young, and R. F. Ozols, *Biochem. Pharmacol.* **34**, 2583 (1985).

294. L. Ott, "An Introduction To Statistical Methods And Data Analysis", PWS-KENT Publishing Company, Boston, 1988.

BIOGRAPHICAL SKETCH

James Ray Ballinger attended the University of South Florida where he graduated in 1973 with a B.A. degree with honors in natural science. While an undergraduate, he received the Dr. Sylvan Myers Award for Highest Achievement in Physics and Mathematics by Pre-Medical Students at the University of South Florida (1972). He then attended the University of Miami, School of Medicine and graduated in 1976. Medical school was followed by an internship in internal medicine for one year, and a residency and fellowship in diagnostic radiology and nuclear medicine. Board certification in diagnostic radiology with special competency in nuclear radiology was awarded in June 1982. Dr. Ballinger worked in private practice radiology for five years in the Tampa Bay area and started at the University of Florida in January 1989 in the medical physics program. In April 1992, he was awarded a Physician Scientist Award from the National Cancer Institute of the National Institutes of Health to fund his research training.

I certify that I have read this study and that in my opinion it conforms to acceptable standards of scholarly presentation and is fully adequate, in scope and quality, as a dissertation for the degree of Doctor of Philosophy.

K N Scott

Katherine N. Scott, Chairman
Professor of Nuclear Engineering Sciences

I certify that I have read this study and that in my opinion it conforms to acceptable standards of scholarly presentation and is fully adequate, in scope and quality, as a dissertation for the degree of Doctor of Philosophy.

E R Andrew

E. Raymond Andrew
Graduate Research Professor of Physics

I certify that I have read this study and that in my opinion it conforms to acceptable standards of scholarly presentation and is fully adequate, in scope and quality, as a dissertation for the degree of Doctor of Philosophy.

Richard W. Briggs

Richard W. Briggs
Associate Professor of Biochemistry and Molecular Biology

I certify that I have read this study and that in my opinion it conforms to acceptable standards of scholarly presentation and is fully adequate, in scope and quality, as a dissertation for the degree of Doctor of Philosophy.

Jeffrey R. Fitzsimmons

Jeffrey R. Fitzsimmons
Associate Professor of Radiology

I certify that I have read this study and that in my opinion it conforms to acceptable standards of scholarly presentation and is fully adequate, in scope and quality, as a dissertation for the degree of Doctor of Philosophy.

David E. Hintenlang
Assistant Professor of Nuclear Engineering Sciences

This thesis was submitted to the Graduate Faculty of the College of Engineering and to the Graduate School and was accepted as partial fulfillment of the requirements of the degree of Doctor of Philosophy.

August, 1994

Winfred M. Phillips
Dean, College of Engineering

Karen A. Holbrook
Dean, Graduate School